ELSEVIER

Physica C 367 (2002) 260–266

PHYSICA C

www.elsevier.com/locate/physc

Current transport in interface-engineered high-T_c Josephson junctions

J. Yoshida *, H. Katsuno, S. Inoue, T. Nagano

Advanced Materials and Devices Laboratory, Corporate Research and Development Center, Toshiba Corporation, 1 Komukai, Toshiba-cho, Saiwai-ku, Kawasaki 212-8582, Japan

Abstract

The mechanisms of current transport in interface-engineered junctions (IEJs) were investigated based on more than 400 junctions fabricated under various process conditions. We confirmed that the I_cR_n values of IEJs scaled with the square root of the Josephson critical current density (J_c) universally, as long as the junctions had a low critical current density of less than 1×10^4 A/cm^2 at 4.2 K. These low-J_c junctions exhibited dI/dV profiles peculiar to inelastic tunneling via two or less localized states with some remnant of a smeared superconducting gap. In contrast, we could not observe a universal scaling relation between I_cR_n and J_c among higher-J_c junctions. The maximum I_cR_n values of IEJs having J_c ranging from 10^4 to 10^6 A/cm^2 were limited to 2–3 mV at 4.2 K. The dI/dV profiles of these high-J_c junctions differed considerably from those of low-J_c junctions, and were characterized by a highly smeared-out superconducting gap with a reproducible sub-gap structure. The differential conductance at high bias voltages increased slightly with decreasing temperature. These results indicate that a simple tunneling picture is inadequate to describe IEJs with high-J_c values.

PACS: 74.50.+r; 74.25.Fy; 74.76.Bz

Keywords: Josephson junction; Interface-engineered junction; Transport mechanisms; Andreev reflection; Micro-constriction

1. Introduction

Interface-engineered junctions (IEJs) are regarded as the most promising candidates for the construction of high-T_c digital circuits because they are superior to other high-T_c Josephson junctions in terms of uniformity and reproducibility. The basic concept of an IEJ is to create a thin barrier layer by altering the structure or chemistry of the base-electrode layer only at the surfaces [1]. Even a conventional ion-milling process to form a ramp-edge structure in base electrodes followed by a counter-electrode deposition in an appropriate condition was confirmed to be sufficient to form an interface barrier for Josephson junctions [2]. The spread in the Josephson critical current (I_c) of this type of junction was reported to be as low as 6.6% for a 100-junction array [3], and was 10% even for 1000 junctions [2].

The structure and the chemical composition of the barrier at the interface as well as the current transport mechanism in the junctions, however, are still the subject of intensive investigations. Although transmission electron microscopy stud-

* Corresponding author. Tel.: +81-44-549-2110; fax: +81-44-520-1801.

E-mail address: jiro-yoshida@arl.rdc.toshiba.co.jp (J. Yoshida).

0921-4534/02/$ - see front matter
PII: S0921-4534(01)01048-6

ies have revealed a well-crystallized material with pseudo-cubic symmetry of around 2–3 nm in thickness continuously covering the ramp-edge surface, at least for IEJs with a relatively low Josephson critical current density (J_c) [4,5], such a barrier seems to disappear in high-J_c junctions [3]. These results indicate that the structure of the interface barrier may be process dependent. Therefore, there is a possibility that various current transport mechanisms coexist within the junction, and the relative importance of the individual mechanism depends on the fabrication process. In fact, some authors have already pointed out that resonant tunneling of quasiparticles plays an important role in low-J_c junctions while a metallic channel dominates the Josephson current in high-J_c junctions [6,7].

In this paper, we report an intensive study of the current transport mechanisms in IEJs based on more than 400 junctions we have fabricated so far, under various process conditions.

2. Junction fabrication

IEJs with either $YBa_2Cu_3O_{7-x}$ (YBCO) or $YbBa_2Cu_3O_{7-x}$ (YbBCO) as the counter-electrode material were fabricated on ramp edges formed in YBCO base-electrode layers. An epitaxial $SrTiO_3$ or CeO_2 film was used for the interlayer isolation. All the films used in the present work were grown on $SrTiO_3$(1 0 0) substrates using an off-axis sputtering system. The advantage of YbBCO as the counter-electrode material compared with the conventional YBCO lies in the fact that it can grow with complete c-axis orientation in a far wider temperature range than is possible with other 123 compounds [8]. This enables us to investigate the dependence of the junction characteristics on the substrate temperature for the counter-electrode deposition in a wide range without sacrificing the quality of the counter-electrode layer. Details of our thin-film growth technique have been published elsewhere [6,9].

Ramp-edge structures were produced using a photoresist mask reflowed after patterning, together with Ar-ion milling with substrate rotation during etching. The resultant ramp edges had a taper of 20° independent of the edge orientation in a wafer. After etching, the samples were heated to the temperature for the subsequent layer deposition and maintained at that temperature for 10 min. An activated oxygen flux from an ECR plasma source was supplied during the annealing process. The junction width was fixed at 4 μm throughout the present work.

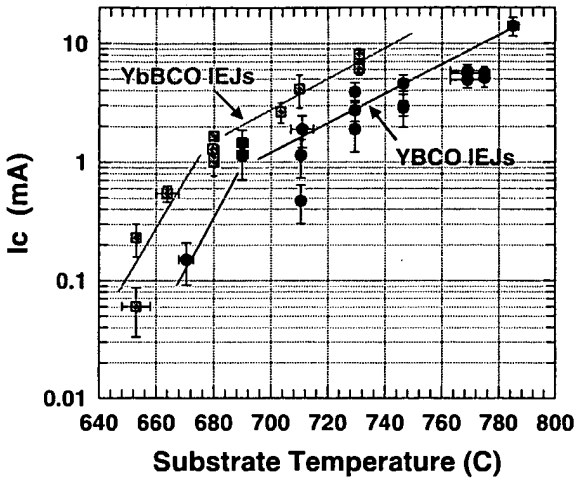

Fig. 1. Critical current at 4.2 K averaged over 16 junctions in a chip versus substrate temperature obtained for two types of interface-engineered junctions with either YBCO or YbBCO as the counter-electrode material. The solid lines are drawn by eye as guides.

Fig. 1 summarizes the substrate temperature dependence of I_c at 4.2 K averaged over 16 junctions in a chip, for the two different counter-electrode materials. In either case, the I_c values increase with increasing substrate temperature, but the substrate temperature at which a given I_c value is obtained differs by about 20–40 °C between the two types of junctions. This implies that the difference in the counter-electrode materials has some influence on the interface-barrier formation, though we could not observe any significant difference in the junction characteristics between YBCO and YbBCO junctions with a similar I_c value. Another interesting point to note in Fig. 1 is that, in both cases, the dependence of I_c on the substrate temperature becomes stronger in the low-temperature region. This may indicate the existence of some threshold in the thermodynamics in the interface-barrier formation. Unfortunately,

however, we do not fully understand the details yet.

3. Junction characteristics

Fig. 2 shows the I_cR_n values as a function of J_c obtained for junctions on various wafers processed at various substrate temperatures. Similar data reported by two other research groups [3,10] are also plotted in the same figure for comparison. We can see that the experimental data from three independent research groups roughly coincides, implying that Fig. 1 depicts the general features of IEJs. An interesting feature seen in Fig. 1 is that the I_cR_n values approximately scale with the square root of J_c in the J_c region below 10^4 A/cm^2, and then seem to saturate at around 3 mV at higher J_c. However, we noticed that the I_cR_n values in the high-J_c region often exhibited similar square-root behavior as long as the junctions were on the same wafer, i.e., processed under the same conditions.

The scaling of I_cR_n with the square root of J_c has been confirmed for grain boundary junctions as well as for PBCO barrier junctions, and is ascribed to the existence of different transport channels for Cooper pairs and quasiparticles; that is, Cooper pairs transfer by direct tunneling while quasiparticles can also flow by resonant tunneling [11–13]. The existence of similar scaling behavior seems to indicate that the current transport in IEJs can be understood within the same theoretical framework. We have confirmed that this is actually the case for IEJs in the low-J_c region, as described below.

Fig. 3 shows differential conductance versus voltage (dI/dV–V) characteristics observed for an IEJ with J_c of 3.4×10^3 A/cm^2 at various temperatures ranging from 4.2 to 60 K. The dI/dV profiles can be characterized by a slightly nonlinear increase in the conductance at high bias voltages, which is essentially independent of the temperature, and a temperature-dependent symmetrical dip with its minimum at zero voltage. We found that the nonlinear behavior at high voltages was fit quite well by $V^{4/3}$, as shown by the dotted line in the figure. This indicates that inelastic tunneling via two localized states in the barrier certainly plays a part in the quasiparticle current transport in the junction at high voltages [14]. We think this

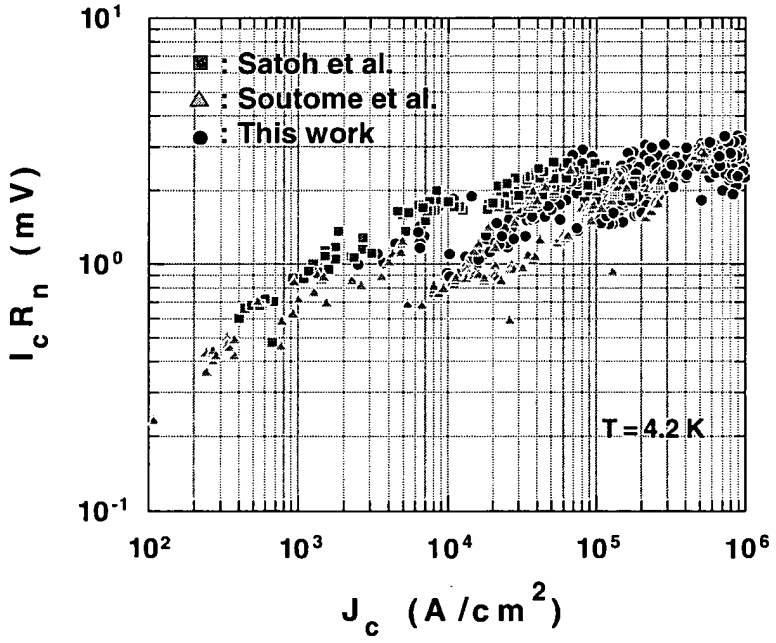

Fig. 2. I_cR_n product values as a function of J_c obtained for interface-engineered junctions processed under various conditions.

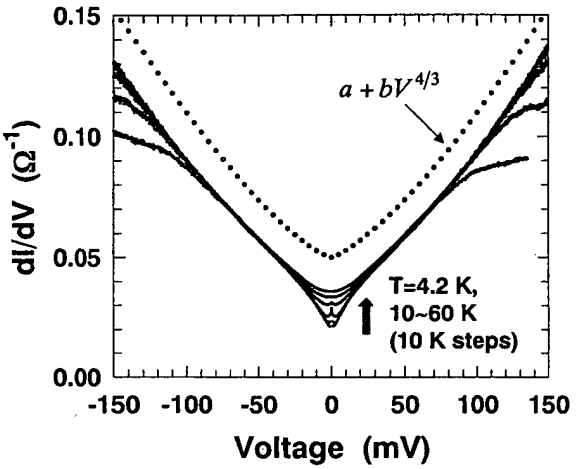

Fig. 3. Differential conductance versus voltage characteristics observed at various temperatures ranging from 4.2 to 60 K for an interface-engineered junction with $J_c = 3.4 \times 10^3$ A/cm^2.

offers strong evidence that IEJs with low J_c are tunnel junctions with an insulative barrier containing a high density of localized states in it. The symmetrical dip around zero voltage would be a remnant of a superconducting gap structure smeared out by a thin normal conducting or a reduced-T_c layer adjacent to the tunnel barrier.

The dI/dV profile of IEJs having J_c exceeding 10^4 A/cm^2 differs considerably from that of low-J_c junctions. Fig. 4 depicts the temperature dependence of the dI/dV profile observed for a junction with J_c of 5.5×10^4 A/cm^2 at 4.2 K. The differential conductance does not exhibit a rapid increase at high voltages. Moreover, the differential conductance at high voltages increases gradually with decreasing temperature. Such behavior is certainly beyond the scope of a tunneling picture, and indicates the presence of a metallic channel within the junction. Another feature seen in Fig. 4 is the existence of fine structures in the superconducting gap region. The structure is reproducible, as shown in Fig. 5, as magnified differential resistance profiles for three different specimens.

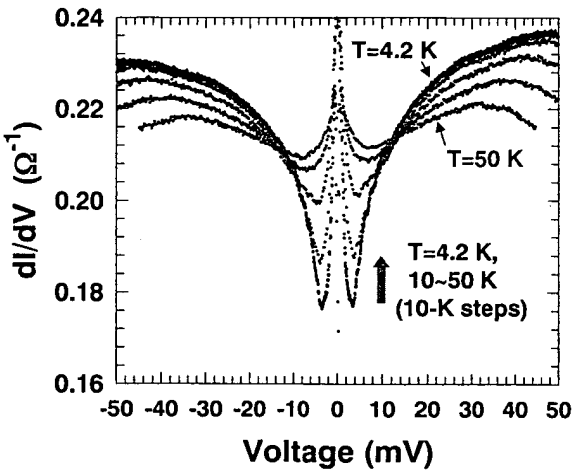

Fig. 4. Differential conductance versus voltage characteristics observed at various temperatures ranging from 4.2 to 50 K for an interface-engineered junction with $J_c = 5.5 \times 10^4$ A/cm^2.

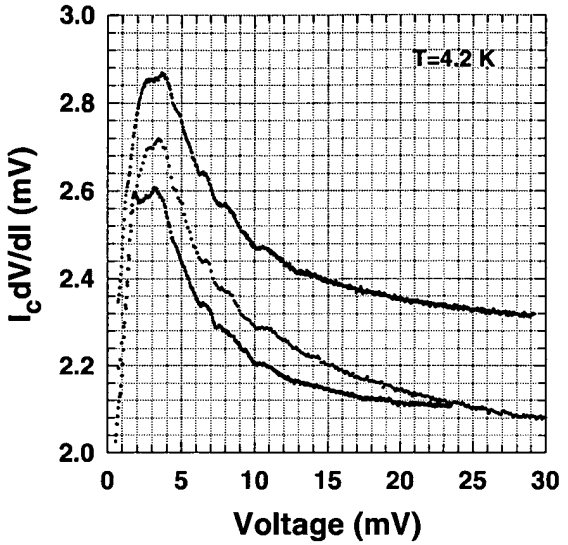

Fig. 5. dV/dI characteristics in the sub-gap region at 4.2 K for three different specimens.

We can find two plausible explanations in the literature for the fine structure in the sub-gap region. One is the Andreev levels formed in a clean superconductor–normal–superconductor (SNS) junction [15]. The Andreev levels are formed due to the interference of wave functions of quasiparticles in the N region which are Andreev reflected at the SN interfaces. Although the energy of the Andreev levels is usually dependent on the phase difference between the two superconducting banks, the presence of a point impurity having a large reflection coefficient in the SNS channel makes them almost phase insensitive [16]. Such levels could be observed as nearly equidistant

singularities in dI/dV profiles. The spacing between the Andreev levels is approximately given as $\Delta E \approx \pi\hbar v_F/d$, where v_F is the Fermi velocity in the N-layer and d is the length of the N-layer. A serious problem concerning the interpretation of the experimentally observed fine structure as the Andreev levels is its small spacing between singularities amounting to 3–5 mV. This requires an anomalously small v_F/d value, which does not seem to be valid when we take into account the short mean-free path in high-T_c superconductors.

A more plausible explanation would be the so-called "sub-harmonic gap structure (SGS)" originating from the process of multiple Andreev reflections in short SNS junctions [17]. The SGS appears as singularities at voltages $V_n = 2\Delta/en$, $n = 1, 2, 3, \ldots$, where Δ is the superconducting gap of the junction electrodes. The major structure below 10 mV seen in Fig. 5 may be assigned as the SGS with $n \geqslant 3$ for $2\Delta \approx 30$ meV. This interpretation, however, requires another explanation for the lack of the structure corresponding to $n = 1$ and 2. Moreover, the experimental profiles below 10 mV seem to include more complicated structures than that expected from this simple SGS model. One possible solution to this apparent discrepancy may be the introduction of a more complex SNcNS (here c denotes the constriction) model in which the proximity effect in the SN bilayers is taken into account. Aminov has shown that, in the case of an SNcNS structure, new resonances appear at $V_n = (\Delta_S - \Delta_N)/en$, $V_n = 2\Delta_N/en$, and $V_n = (\Delta_S + \Delta_N)/en$, due to the multiple Andreev reflections within the junction, where Δ_S and Δ_N are superconducting gaps in the S- and N-layer, respectively [18]. The relative importance of each process, and, thereby, the amplitude of resonance peaks in dI/dV profiles depends on the structure of individual junctions. Unfortunately, this makes it difficult to conclude specifically whether the fine structure seen in our dI/dV profiles can be assigned as the SGS in SNcNS junctions or not.

4. Unsolved problems

The universal scaling of I_cR_n with the square root of J_c, and the nonlinear differential conductance which fits well with $V^{4/3}$ in IEJs with J_c less than 10^4 A/cm^2, forces us to think that the junctions in this regime can be classified as SIS or SNINS junctions with localized states in the barrier, and that Cooper pairs in the junctions transfer by direct tunneling while the quasiparticle current is dominated by resonant tunneling. This simple picture, however, does not seem to coincide with the quasilinear temperature dependence of I_c, as seen in Fig. 6 (two figures at the bottom). The nonexponential dependence of I_c on temperature,

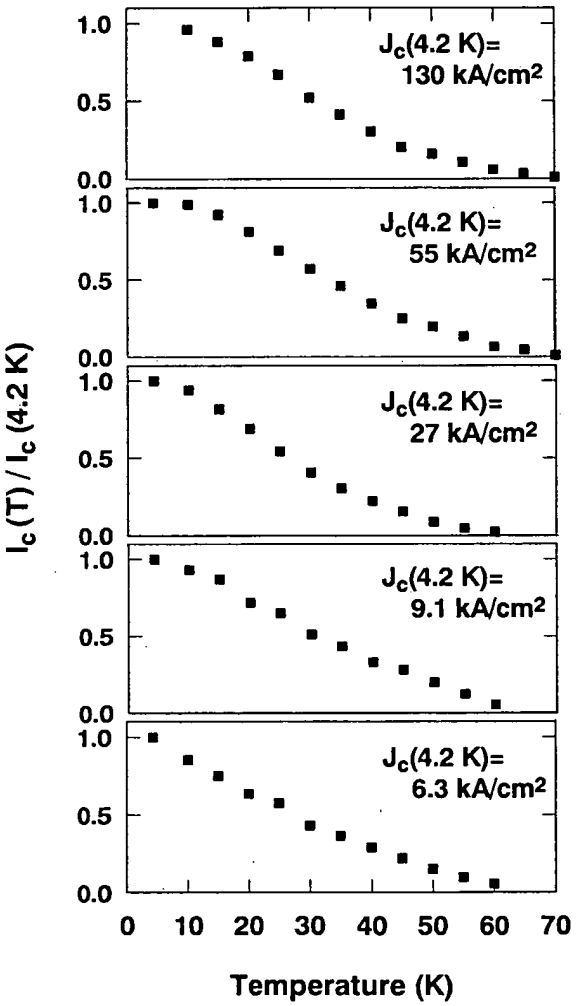

Fig. 6. Temperature dependences of I_c observed for interface-engineered junctions with various Josephson critical current densities at 4.2 K ranging 1.3×10^5–6.3×10^3 A/cm^2.

at high temperatures, and the lack of a saturation tendency in the low-temperature region are certainly beyond the scope of the SNINS model, and remind us of dirty point contacts [19]. However, if the Josephson current in these junctions is actually dominated by point contacts within an insulating barrier, we have to seek another rational explanation for the peculiar scaling relationship between I_cR_n and J_c.

The temperature dependence of I_c in IEJs in the high-J_c regime is more SNINS-like, as seen in the top three figures in Fig. 6. This does not conflict with the SNcNS model with a low transmission probability in the metallic channels. One curious aspect with high-J_c IEJs is that they often exhibit a scaling behavior in their I_cR_n versus J_c characteristics, similar to that observed for low-J_c junctions. Such scaling has been observed only among junctions fabricated simultaneously on the same wafer. In this sense, this scaling behavior is not universal, but, here again, we are required to consider a rational explanation other than that of the direct- and resonant-tunneling framework.

The mechanism of J_c variation in the high-J_c region due to process conditions is not clear at present. We can think of three possible reasons; variations in the N-layer thickness and in transmission probability of metallic channels, and the change in the number of the metallic channels within the junction area. A slight increase in the maximum I_cR_n values with J_c may be a consequence of the N-layer thickness variation, but this does not seem to dominate the J_c variation over the two orders of magnitude seen in Fig. 2. It is not easy to distinguish the other two mechanisms from each other. One possibility would be to observe the change in dI/dV profiles with an increase in the J_c values. Unfortunately, we have not succeeded in observing the dI/dV profile of high-J_c junctions in a wide voltage range because of the breakdown of superconductivity in the electrodes due to the large current flowing in the junction.

5. Summary

We investigated the current transport mechanism in interface-engineered junctions. We found that the junction characteristics can be classified into two groups in accordance with their J_c values. The borderline between the low-J_c group and the high-J_c group lies at around $J_c = 1 \times 10^4$ A/cm^2. In the low-J_c region, I_cR_n values scaled universally with the square root of J_c, and the contribution of elastic and inelastic tunneling processes, at least to the quasiparticle currents, was confirmed through the measurement of dI/dV profiles. However, some questions still remain concerning the transport of Cooper pairs in this region.

In the high-J_c region, an SNcNS model with low transmission probability of metallic channels seems to be most appropriate to account for the overall features of experimentally observed junction characteristics. Further investigations, however, are definitely required to identify the origins of the fine structure appearing in the dI/dV profiles as well as of the variation in J_c values over two orders of magnitude, due to process conditions.

Acknowledgements

This work was supported by the New Energy and Industrial Technology Development Organization (NEDO) through the International Superconductivity Technology Center (ISTEC).

References

[1] B.H. Moeckly, K. Char, Appl. Phys. Lett. 71 (1997) 2526.
[2] T. Satoh, M. Hidaka, S. Tahara, IEEE Trans. Appl. Supercond. 9 (1999) 3141.
[3] Y. Soutome, R. Hanson, T. Fukazawa, K. Saitoh, A. Tsukamoto, Y. Tarutani, K. Takagi, IEEE Trans. Appl. Supercond. 11 (2001) 163.
[4] Y. Huang, K.L. Merkle, B.H. Moeckly, K. Char, Physica C 314 (1999) 36.
[5] J.G. Wen, N. Koshizuka, S. Tanaka, T. Satoh, M. Hidaka, S. Tahara, Appl. Phys. Lett. 75 (1999) 2470.
[6] J. Yoshida, S. Inoue, H. Sugiyama, T. Nagano, IEEE Trans. Appl. Supercond. 11 (2001) 784.
[7] J.K. Heinsohn, R. Dittmann, J. Rodriguiez Contreras, J. Scherbed, A. Klushin, M. Siegel, IEEE Trans. Appl. Supercond. 11 (2001) 795.
[8] K. Yamaguchi, I. Hirabayashi, Jpn. J. Appl. Phys. 39 (2000) 452.

[9] H. Katsuno, S. Inoue, T. Nagano, J. Yoshida, Ext. Abst. ISEC'01 Paper JP-5, Osaka, 2001.
[10] T. Satoh, J.G. Wen, M. Hidaka, S. Tahara, N. Koshizuka, S. Tanaka, Supercond. Sci. Technol. 13 (2000) 88.
[11] R. Gross, L. Alff, A. Beck, O.M. Froehlich, D. Koelle, A. Marx, IEEE Trans. Appl. Supercond. 7 (1997) 2929.
[12] J. Yoshida, T. Nagano, Phys. Rev. B 55 (1997) 11860.
[13] J. Yoshida, S. Inoue, H. Sugiyama, T. Nagano, Physica C 335 (2000) 226.
[14] L.I. Glazman, K.A. Matveev, Sov. Phys. JETP 67 (1988) 1276.
[15] I.O. Kulik, Sov. Phys. JETP 30 (1970) 944.
[16] P.F. Bagwell, Phys. Rev. B 46 (1992) 12573.
[17] T.M. Klapwijk, G.E. Blonder, M. Tinkham, Physica 109/110B (1982) 1657.
[18] B.A. Aminov, A.A. Golubov, M.Yu. Kupriyanov, Phys. Rev. B 53 (1996) 365.
[19] I.O. Kulik, A.N. Omel'yanchuk, JETP Lett. 21 (1975) 96.

Characteristics of interface-engineered Josephson junctions using a $YbBa_2Cu_3O_y$ counterelectrode layer

H. Katsuno,[a] S. Inoue, T. Nagano, and J. Yoshida
Advanced Materials & Devices Laboratory, Corporate Research and Development Center, Toshiba Corporation, 1, Komukai Toshiba-cho, Saiwai-ku, Kawasaki 212-8582, Japan

(Received 30 July 2001; accepted for publication 13 October 2001)

We have fabricated interface-engineered junctions with $YbBa_2Cu_3O_y$ as the counterelectrode. The junctions fabricated on $YBa_2Cu_3O_y$ base electrodes exhibited excellent Josephson characteristics with the 1σ-spread in I_c as low as 5.4% for 16 junctions with an average I_c of around 1 mA. We also confirmed that the 1σ in I_c correlates with the surface morphology of the base-electrode layer, indicating that further improvements in 1σ would be possible by advancing the thin-film growth technology. © *2001 American Institute of Physics.* [DOI: 10.1063/1.1428115]

The interface-engineering technique proposed by Moeckly and Char[1] is regarded as the most promising method for fabricating high-temperature superconductor Josephson junctions for digital circuit applications, because of the resultant high uniformity in junction characteristics.[2,3] The basic concept of the interface engineering is to create a thin barrier layer by damaging the base-electrode surface using ion bombardment and then recrystallizing it during the subsequent counterelectrode deposition process. Even a conventional ion-milling process to form a ramp-edge structure in the base-electrode layer was confirmed to be sufficient to form an interface barrier.[2]

The electrical properties of interface-engineered junctions (IEJs) are known to be extremely sensitive to the substrate temperature and the oxygen atmosphere during the annealing process prior to the counterelectrode deposition. In the previous paper,[4] we demonstrated that annealing in an electron-cyclotron-resonance (ECR) activated oxygen flux and subsequent deposition of $YBa_2Cu_3O_7$ (YBCO) counterelectrodes by sputtering were advantageous in that they resulted in weaker substrate-temperature dependence of junction critical current (I_c) than was possible by other methods. Unfortunately, however, the I_c value appropriate for the fabrication of single flux quantum (SFQ) circuits could be obtained only at a relatively low substrate temperature range, which conflicted with the complete c-axis oriented growth of the counterelectrode layer.

The operation of a SFQ circuit is based on the transmission and storage of a single flux quantum by superconducting loops, which are connected in series or in parallel.[5] This operation principle results in the inductance L of the superconducting loops in SFQ circuits being restricted according to the inequality $0.5\Phi_0 < LI_c < 1.5\Phi_0$, where Φ_0 denotes the flux quantum ($h/2e$), and this limits the maximum I_c of Josephson junctions in practical circuits. For the reliable operation of a SFQ circuit at high temperatures, I_c must be sufficiently large compared with the thermal fluctuation current $I_T = (2\pi/\Phi_0)k_BT$. The inclusion of even a small amount of a-axis oriented grains in the counterelectrode YBCO film results in a significant increase in L, which makes it impossible to operate a SFQ circuit correctly at a desired temperature.

The trade-off problem between I_c and L we encountered for the sputter-deposited YBCO counterelectrode layer could be solved if we adopted $YbBa_2Cu_3O_7$ (YbBCO) as the counterelectrode, because it can grow with complete c-axis orientation in a far wider temperature range than is possible with YBCO.[6–8] This letter reports our successful fabrication of IEJs with YbBCO as the counterelectrode.

The YbBCO and YBCO films used in the present work were grown on $SrTiO_3$(100) (STO) substrates using an off-axis sputtering system. Both films were deposited in a 200 mTorr mixture of 70% Ar and 30% O_2. Figure 1 shows the volume fractions of a-axis oriented grains in the films as functions of the substrate temperature. The volume fractions were estimated from the x-ray (200) diffraction intensity relative to (004). It is apparent that the curve for YbBCO shifts to the lower temperature side by approximately 100 °C compared with that for YBCO, indicating that by adopting YbBCO as the counterelectrode the substrate temperature can be reduced significantly while maintaining the quality of the wiring layer.

Ramp-edge structures were produced on the bilayer composed of the STO insulation layer and 200-nm-thick YBCO base-electrode layer by the two-step etching technique for a clean surface.[9] The STO layer was patterned using a reflowed resist mask together with Ar ion milling,

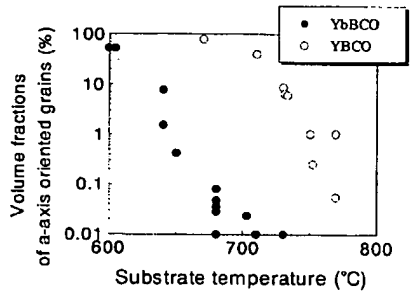

FIG. 1. The volume fractions of a-axis oriented grains in the films as functions of the substrate temperature for the counterelectrode deposition. The dot plots are results of junctions using YbBCO counterelectrodes and the circle plots are results of all-YBCO junctions.

[a]Electronic mail: hiroshi.katsuno@toshiba.co.jp

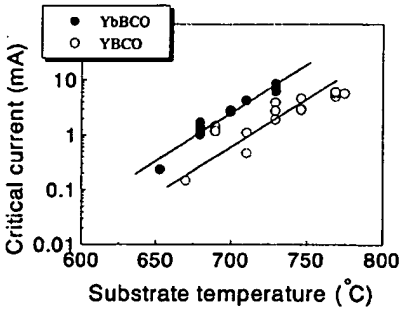

FIG. 2. The junction critical currents averaged over 16 junctions as functions of the substrate temperature for the counterelectrode deposition. The counterelectrodes of these junctions were fabricated by YbBCO (dots) and YBCO (circles), respectively.

while rotating the substrate. The Ar-ion beam was applied to the substrate surface vertically. After removing the resist, the remaining STO layer and the YBCO base-electrode layer were etched with 30° tilting. The resultant ramp-edge angles were formed at about 20°.

The samples were heated to the deposition temperature which ranged from 650 to 730 °C for the fabrication of the counterelectrode layer in the sputtering chamber, and annealed for 10 min in an activated oxygen flux from an ECR plasma source at 2.1 mTorr. The ramp-edge surface of the YBCO base electrode became the barrier as samples were annealed. Successively, a 300-nm-thick YbBCO counterelectrode layer was deposited *in situ*. The YbBCO layer was patterned as the counterelectrode after covering the wafer surface with a 1-μm-thick Au film for contact pads. The junction width was fixed at 4 μm throughout this study. Then, the samples were annealed at 400 °C in O_2 for 24 h. The critical temperatures (T_c) of each electrode were exceeding 80 K.

Figure 2 compares the substrate temperature (T_{sub}) dependence of I_c observed for junctions using a YbBCO counterelectrode with that for all-YBCO junctions. Each circle in Fig. 2 represents the I_c value at 4.2 K averaged over 16 junctions on a chip. Both types of junctions exhibited nearly exponential dependence of I_c on the substrate temperature, with a similar increasing ratio of approximately 3%/° C. An interesting point to note is that the I_c vs T_{sub} curve for YbBCO junctions seems to shift to the lower temperature side by approximately 30 °C compared with that for YBCO junctions. This implies that the characteristics of IEJs are influenced not only by the process conditions but also by the counterelectrode material itself. Unfortunately, we do not understand the details of this phenomenon.

The maximum I_c value of Josephson junctions usable in high-T_c SFQ circuits is estimated to be 0.4–0.5 mA at 30–40 K because of the restriction arising from inductance design.[10] Since the I_c value of IEJs at 4.2 K is approximately twice that at 30–40 K, the I_c value around 1 mA at 4.2 K is particularly important for SFQ circuit applications. Figure 2 indicates that such a junction can be obtained at T_{sub} of around 680 and 710 °C for YbBCO and YBCO junctions, respectively. The former temperature is high enough to obtain YbBCO films with negligible inclusion of *a*-axis oriented grains, as seen in Fig. 1, while the latter is far too low to obtain YBCO films with similar quality.

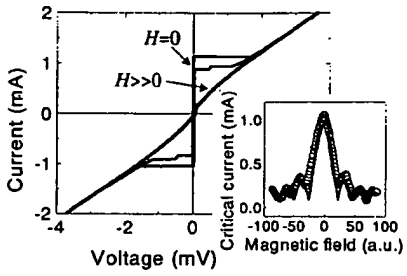

FIG. 3. The $I-V$ characteristics at 4.2 K using the YbBCO counterelectrode fabricated at 680 K. The inset shows the magnetic field modulation of I_c. The solid line in the inset is a fit to the Fraunhofer pattern.

Figure 3 shows the $I-V$ characteristics at 4.2 K and the Fraunhofer pattern observed for a YbBCO junction fabricated at 680 °C showing complete *c*-axis orientation in the counterelectrode. The junction exhibited excellent Josephson characteristics with the magnetic field modulation of I_c exceeding 90% and the I_cR_n product of the junctions exceeding 2 mV. The curve included a weak hysteretic behavior with a small bump structure probably due to the parasitic LC resonance peculiar to a ramp-edge structure.[3] These characteristics were not different from those of YBCO junctions. It was confirmed that the weak hysteresis seen in the $I-V$ curve diminished at 30–40 K.

The I_cR_n product gradually increased with an increase in I_c and ranged from 1 to 3 mV at 4.2 K in I_c ranging from 0.1 to 10 mA as seen in Fig. 4. The whole feature of Fig. 4 showed the I_cR_n products had slightly weak dependence on I_c and scaled approximately with I_c^P where P ranged from 0.2 to 0.3.[2,11] The normal-state resistance R_n was also essentially independent of the temperature. These behaviors are different from Co-doped PBCO barrier junctions which are based on the localized states in the barrier,[10] which may imply the lesser barrier thickness or the smaller density of the localized states.

The temperature dependence of I_c was considerably different from that of superconductor–insulator–superconductor junctions. The critical current was proportional to $(1-T/T_c)^2$ in the vicinity of T_c. With decreasing temperature, the I_c value showed the saturation behavior. Such behavior is a typical tendency of superconductor–normal metal–insulator–normal metal–superconductor junctions.[12]

The uniformity and reproducibility of the junction characteristics were investigated for 16 junctions, as seen in Fig.

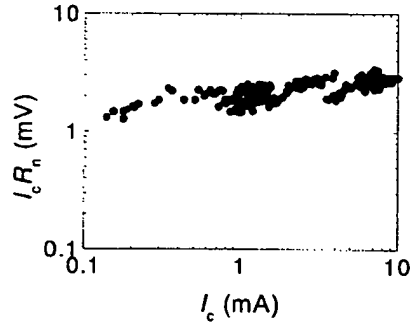

FIG. 4. The relation between I_c and the I_cR_n product for junctions with YbBCO counterelectrodes at 4.2 K.

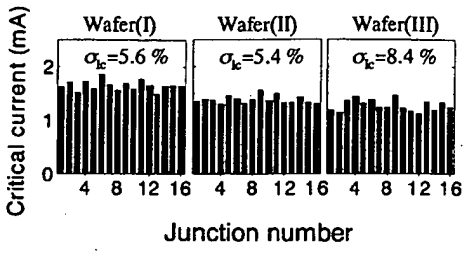

FIG. 5. These graphs show the uniformity in three wafers at 4.2 K independently fabricated under the same process condition (T_{sub}= 680 °C). The $\langle I_c \rangle$ values of each chip averaged over 16 junctions are estimated as 1.65, 1.39, and 1.28 mA, respectively.

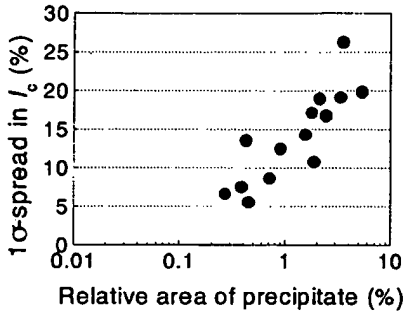

FIG. 6. The relation between the 1 σ-spread in I_c and the relative area of precipitate observed on the surface of the isolation layer.

5. These chips were independently fabricated under the same process condition and were located at the same place in each wafer. We confirmed good reproducibility in I_c between wafers. The best uniformity obtained so far was a 1 σ-spread in I_c of 5.4%. This value was reproducible as long as the junctions were fabricated on a YBCO base-electrode layer of high quality. We found that the 1 σ-spread correlated strongly with the surface morphology of the isolation/base-electrode bilayers. Figure 6 shows the relation between the 1 σ-spread in I_c and the relative area of precipitate observed on the surface of the isolation layer by a scanning electron microscope prior to the fabrication of a ramp-edge structure. According to the deposition condition, there were small precipitates (0.1–1 μm in diameter), which could not be detected by x-ray diffraction, on the bilayer. As a result of Auger electron spectroscopy, these precipitates are thought to originate mainly from the slight deviation of the atomic composition from stoichiometry in the YBCO base-electrode layer located underneath the isolation layer. It was shown that the 1 σ-spread in I_c is affected strongly by the quality of the base-electrode layer. In other words, there is an opportunity to reduce the 1 σ-spread further by improving the quality of the base-electrode layer.

In summary, we have fabricated interface-engineered junctions suitable for the construction of SFQ circuits based on high-temperature superconductors by adopting YbBCO as the counterelectrode. The junctions exhibited excellent Josephson characteristics together with the 1 σ-spread in I_c as low as 5.4%. Further reduction in 1 σ would be possible by improving the quality of the base-electrode layer.

This work was supported by the New Energy and Industrial Technology Development Organization (NEDO) as Collaborative Research and Development of Technologies for Superconductivity Applications.

[1] B. H. Moeckly and K. Char, Appl. Phys. Lett. **71**, 2526 (1997).
[2] T. Satoh, J. G. Wen, M. Hidaka, S. Tahara, N. Koshizuka, and S. Tanaka, IEEE Trans. Appl. Supercond. **11**, 770 (2001).
[3] Y. Soutome, R. Hanson, T. Fukazawa, K. Saitoh, A. Tsukamoto, Y. Tarutani, and K. Takagi, IEEE Trans. Appl. Supercond. **11**, 163 (2001).
[4] J. Yoshida, S. Inoue, H. Sugiyama, and T. Nagano, IEEE Trans. Appl. Supercond. **11**, 784 (2001).
[5] K. K. Likharev and V. K. Semenov, IEEE Trans. Appl. Supercond. **1**, 3 (1991).
[6] M. Kawasaki, S. Nagata, Y. Sato, M. Funabashi, T. Hasegawa, K. Kishio, K. Kitazawa, K. Fueki, and H. Koinuma, Jpn. J. Appl. Phys., Part 2 **26**, L738 (1987).
[7] K. Osamura and W. Zhang, Z. Metaqallkd. **84**, 522 (1993).
[8] K. Yamagiwa and I. Hirabayashi, Jpn. J. Appl. Phys., Part 1 **39**, 452 (2000).
[9] T. Satoh, M. Hidaka, and S. Tahara, IEEE Trans. Appl. Supercond. **7**, 3001 (1997).
[10] J. Yoshida, IEICE Trans. Electron. **E83-C**, 49 (2000).
[11] B. H. Moeckly, K. Char, Y. Huang, and K. L. Merkle, IEEE Trans. Appl. Supercond. **9**, 3358 (1999).
[12] A. A. Golubov, E. P. Houwman, J. G. Gijsbertsen, V. M. Krasnov, J. Flokstra, and H. Rogalla, Phys. Rev. B **51**, 1073 (1995).

INSTITUTE OF PHYSICS PUBLISHING SUPERCONDUCTOR SCIENCE AND TECHNOLOGY
Supercond. Sci. Technol. 14 (2001) 1056–1059 PII: S0953-2048(01)27288-1

Interface-modified YBCO ramp-edge Josephson junctions by deionized water

Jeong-Il Kye, Hong-Seok Choi, Joon-Hyung Ahn, Ju-Hwan Yun, Seung-Hyun Moon and Byung-Du Oh

LG Electronics Institute of Technology, Seoul 137-724, Korea

Received 25 July 2001
Published 21 November 2001
Online at stacks.iop.org/SUST/14/1056

Abstract

We have investigated $YBa_2Cu_3O_{7-x}$ (YBCO) ramp-edge Josephson junctions by reacting the ramp-edge interface with deionized water. $YBa_2Cu_3O_{7-x}/PrBa_2Cu_3O_x$ (YBCO/PBCO) films were deposited on $SrTiO_3$(1 0 0) by on-axis KrF laser deposition. After patterning the bottom YBCO/PBCO layer, the ramp edge was cleaned by Br-in-ethanol and then reacted with deionized water. The top YBCO/PBCO layer was deposited and patterned by photolithography and ion milling. We measured the current–voltage (I–V) characteristics, magnetic field modulation of the critical current and microwave response at 10 GHz. The 20-minute water-immersed junction showed resistively shunted junction (RSJ)-type I–V characteristics, while others exhibited flux-flow behaviour. The average values of I_c, R_n and I_cR_n of these RSJ-type junctions were 4 mA, 0.1 Ω and 400 μV, respectively, and Shapiro steps were fitted well by the microwave characteristic parameter $\Omega\ (= hf/2eI_cR_n) = 0.18$.

1. Introduction

For the manufacture of electronic devices based on high-temperature superconductors (HTSC) there have been a great number of efforts to establish a reliable Josephson junction (JJ) fabrication process. Due to the extremely short coherence length of HTSC the control of the interface on this length scale is crucial. Since the coherence length in the *ab*-plane is longer than that in the direction of the *c*-axis in $YBa_2Cu_3O_{7-x}$ (YBCO), the JJ of this material has usually been made in the *ab*-direction using the ramp-edge geometry. Attempts to create artificial-layered tunnel barriers have not been very successful.

Several years ago Moeckly and Char fabricated interface-modified ramp-edge type HTSC JJ without depositing any artificial barrier [1]. The main idea is that the YBCO surface can be modified into a non-superconducting material after being exposed to appropriate ion damage. Since this study, there has been a great deal of research on interface-modified ramp-edge-type HTSC JJ using various methods for interface modification, such as plasma treatment [1–3], ion beam damage [4–7], chemical treatment [7] and base electrode doping [9]. Wen *et al* argued that the barrier layer, composed of Ba-based cubic perovskite phase, is certainly a derivative compound of YBCO [10]. On the other hand, Huang *et al* reported that the barrier layer of plasma-treated junctions consists of a cation-disordered non-superconducting cubic structure [11].

In addition, the reproducibility of ramp-edge-type HTSC JJ is still under debate, hence Schoop *et al* have carried out a detailed study of ramp formation by ion beam techniques [12]. Moeckly recently succeeded in producing a *c*-axis trilayer interface-engineered JJ [13]. However, the reproducibility is still in question.

It has been shown that YBCO decomposes in water to CuO, $Ba(OH)_2$, Y_2BaCuO_5 and evolving oxygen [14, 15]. Therefore, in this study we have tried to make JJ using the barrier formed by this chemical reaction instead of by physical damage.

2. Fabrication

Josephson junctions were fabricated using thin films deposited by pulsed laser ablation. The optimized parameters for pulsed laser deposition of YBCO thin films were as follows: oxygen partial pressure = 750 mT, substrate temperature = 800 °C and laser energy density = 1.4 J cm^{-2}. The zero-resistance critical temperature was ~90 K with transition width smaller than 1 K [16]. The deposition parameters for $PrBa_2Cu_3O_x$ (PBCO) thin film were the same as those for YBCO. YBCO (220 nm)/PBCO (100 nm) bilayers are deposited onto single-crystal

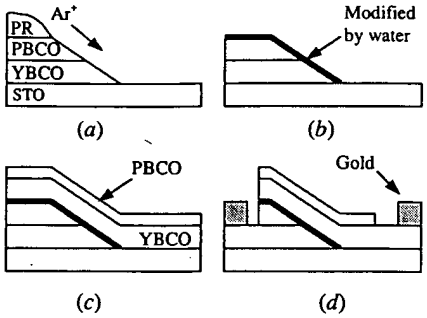

Figure 1. Schematic diagrams of the overall junction fabrication process: (*a*) formation of the ramp edge, (*b*) ramp-edge modification by water, (*c*) deposition of counter-electrode and (*d*) lift-off of gold contact pads.

$SrTiO_3(100)$ substrates. After conventional photolithography for the base electrode, Ar-ion milling was performed using a Kaufmann-type ion source at an incident angle of 65° to obtain ramp edges with small angles. The energy of the ion beam was 400 eV and the current density was 1.0 mA cm^{-2}. After edge formation, the dead surface layer was removed by a subsequent 0.2% in volume Br-in-ethanol cleaning for 20 s [17]. We then immersed it in deionized water at room temperature (RT) after rinsing it with methanol and acetone several times. The resistivity of the deionized water was 16 MΩcm. Base electrodes with modified edges were immediately attached onto a heater block and transferred to a deposition chamber. The counter-electrode YBCO (220 nm)/ PBCO (40 nm) thin films were deposited using the same parameters as for the base electrode. The samples were patterned into structures of ramp-edge-type junctions by using

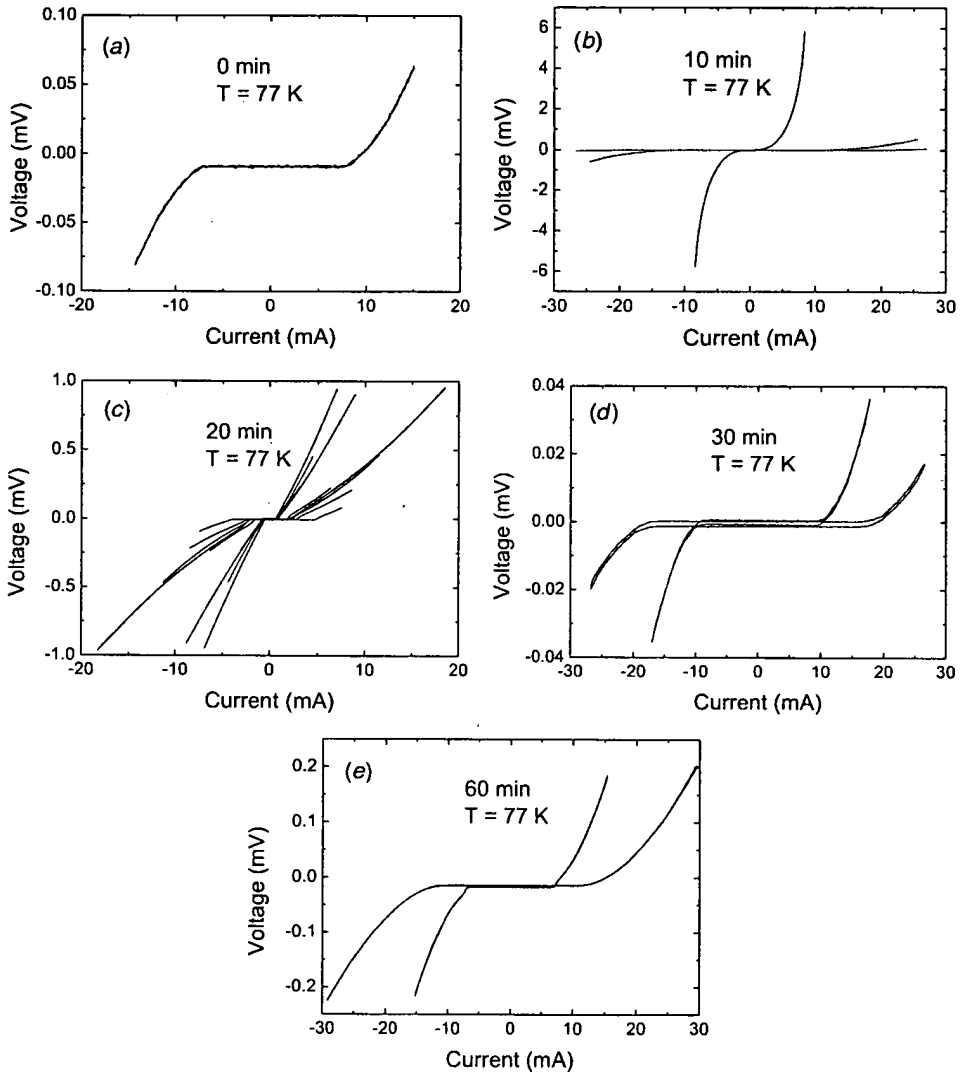

Figure 2. Current–voltage characteristics of junctions at 77 K for different water immersion times: (*a*) 0 minute, (*b*) 10 minutes, (*c*) 20 minutes, (*d*) 30 minutes and (*e*) 60 minutes.

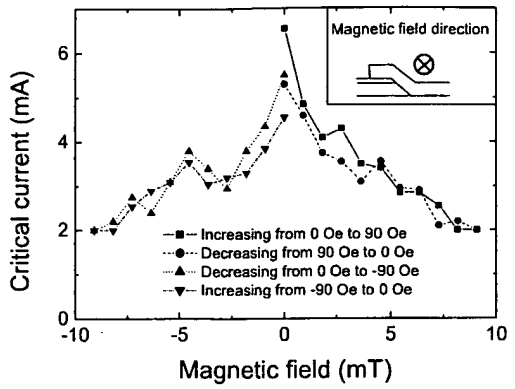

Figure 3. Magnetic field modulation of the critical current of an RSJ-type junction at 77 K.

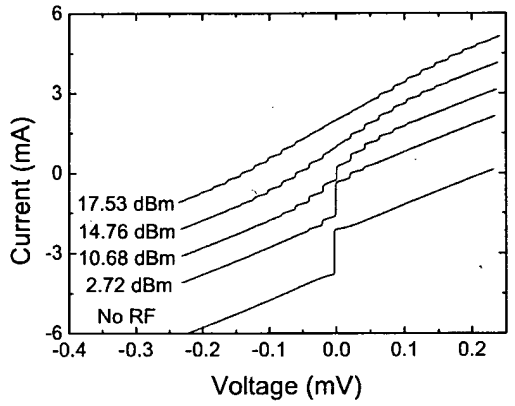

Figure 4. Current–voltage curves for the same junction in figure 3 exposed to a 10-GHz signal at various power levels.

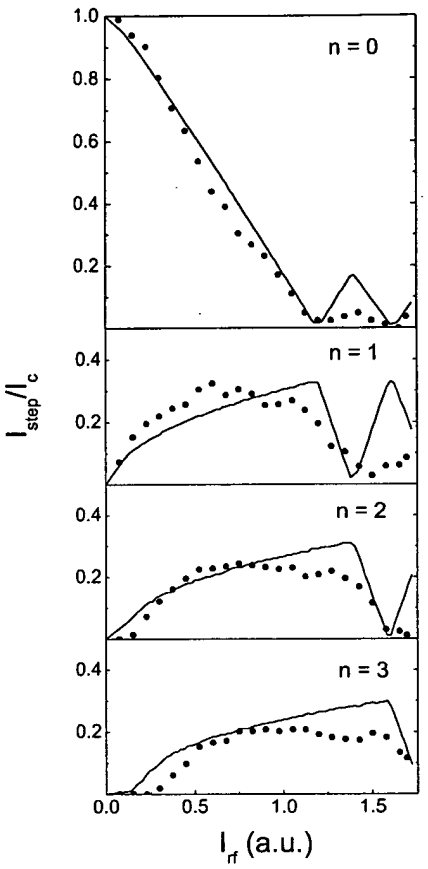

Figure 5. Dependence of the normalized Shapiro-step heights on the microwave current for $n = 0, 1, 2$ and 3 of the same previous junction. The lines show the RSJ simulation results with $\Omega = 0.18$.

photolithography and Ar-ion milling. Finally, gold contact pads were formed by the conventional lift-off process. The process sequence is shown schematically in figure 1. Typically, we have annealed our junctions at 450 °C for 30 min with oxygen flow 50 sccm in the chamber.

Each chip of 10 mm × 10 mm size contains nine sectors, each of which is composed of 22 junctions with a junction width of 4 μm. To check the transport properties of each electrode, four-probe test patterns of micro-bridge type were also included in both the bottom and the top layers. We measured the current–voltage (I–V) characteristics, magnetic field dependence of the critical current and Shapiro steps by dipping samples in liquid nitrogen.

3. Results

The immersion time in the deionized water was varied as 0, 10, 20, 30, 40 and 60 min. Figures 2(*a*)–(*e*) show the I–V characteristics for each chip. The 20-minute junctions showed RSJ-like I–V characteristics at 77 K as in figure 2(*c*), which still have excess currents. The average values of I_c, R_n, and I_cR_n of 10 junctions are 4 mA, 0.1 Ω and 400 μV, respectively. Most of the other junctions, with either shorter or longer immersion time, showed flux-flow-type with J_c between 1×10^6 and 2×10^6 A cm^{-2}, which implies that there exists little barrier between two YBCO electrodes. The resistance grows from 0.01 Ω for the 0-minute junction to 0.1 Ω for the 20-minute junction and suddenly returns to 0.01 Ω again for the 30-minute junction. Then the resistance grows slowly again as the immersion time increases. The critical current behaves in the opposite way. We will discuss this behaviour in more detail later.

The magnetic field dependence of the critical current of a typical RSJ-type junction is plotted in figure 3, where the first minimum is found at about 3 mT. As Heinsohn *et al* pointed out [18], junctions with an excess current do not show a clear Fraunhofer-like pattern. Assuming that the junction width (which, in this case, is the thickness t of the bottom film as indicated in the inset of figure 3) is shorter than the Josephson penetration depth $\lambda_J = [h/4\pi\mu_0 eJ_c(d + 2\lambda_L)]^{1/2}$ we can roughly estimate the penetration depth $\lambda_L \approx \Phi_0/(2tH_{\min}) \approx 1.6$ μm, which is somewhat larger than the literature value of YBCO at 77 K, i.e. $\lambda_{ab} \approx 0.16$ μm, or $\lambda_c \approx 1.1$ μm [19].

Figure 4 shows the microwave (10 GHz) responses of the same JJ of figure 3. We can observe current steps at $V = nV_0$ where $V_0 = hf/2e = 20.7$ μV. The Shapiro step amplitude is plotted as a function of microwave current in figure 5. The theoretical value was found from the RSJ current source

model [20]. The fitting parameter $\Omega = hf/2eI_cR_n$ varies from 0.10 to 0.90. As Ω grows, the first maxima for $n > 0$ increases so that it is easy to find the optimal fitting value of Ω by matching the first maximum. The most probable value of Ω was 0.18, which is inconsistent with the calculated value from the *I–V* characteristics in figure 4 where $\Omega = hf/2eI_cR_n = V_0/I_cR_n = 20.7\ \mu V/61.5\ \mu V = 0.34$. This results from the excess current, which has not been considered in the RSJ model. Heinsohn *et al* have also observed this kind of inconsistency in their interface-engineered JJ; when the temperature was lowered the excess current became significant [18].

4. Discussions and summary

What happened to the YBCO surface on immersion in water? After decomposition of the YBCO surface by water, the reaction product $Ba(OH)_2$ dissolves easily. The other products, i.e. CuO and Y_2BaCuO_5 remain as a barrier for JJ. However, when the etching time in deionized water is too long, we speculate that the original YBCO phase was exposed to the surface again as the barrier materials were washed away. This results in high critical currents of the flux-flow-type junctions etched in deionized water for more than 30 minutes.

In summary, we have made ramp-edge JJs using the barrier obtained from YBCO and water reaction. The optimum time for immersing in water is about 20 minutes, and this JJ showed RSJ-like behaviour with an excess current. We have measured the *I–V* characteristics, magnetic field modulation of the critical current and microwave response. However, there are still many problems which must be overcome before reproducible and controllable JJs can be achieved by this method.

Acknowledgments

The authors thank Joo-Do Park and Ki-Young Lee for assistance with photolithography and ion milling. This work was supported by the National Research Laboratory Program of the Korean Ministry of Science and Technology.

References

[1] Moeckly B H and Char K 1991 *Appl. Phys. Lett.* **71** 2526
[2] Horibe M, Inagaki Y, Yoshida K, Mtsuda G, Hayashi N, Fujimaki A and Hayakawa H 2000 *Japan. J. Appl. Phys.* **39** L284
[3] Makita T, Toma K, Ishikawa K, Zama H, Tano H and Tanabe K 2000 *Japan. J. Appl. Phys.* **39** L730
[4] Satoh T, Hidaka M and Tahara S 1999 *IEEE Trans. Appl. Supercond.* **9** 3141
[5] Fujimaki A, Kawai K, Hayashi N, Horibe M, Murayama M and Hayakawa H 1999 *IEEE Trans. Appl. Supercond.* **9** 3436
[6] Heinsohn J-K, Hadfield R H and Dittmann R 1999 *Physica* C **326–327** 157
[7] Hunt B D, Forrester M G, Talvacchio J andYoung R M 1999 *IEEE Trans. Appl. Supercond.* **9** 3362
[8] Soutome Y, Hanson R, Fukazawa T, Saitoh K, Tsukamoto A, Tarutani Y and Takagi K 2001 *IEEE Trans. Appl. Supercond.* **11** 163
[9] Schneider C W, Schulz R R, Goetz B, Schmehl A, Bielefeldt H, Hilgenkamp H and Mannhart J 1999 *Appl. Phys. Lett.* **75** 850
[10] Wen J G, Koshizuka N, Tanaka S, Satoh T, Hidaka M and Tahara S 1999 *Appl. Phys. Lett.* **75** 2470
[11] Huang Y, Merkle K L, Moeckly B H and Char K 1999 *Physica* C **314** 36
[12] Schoop U, Schonecke M, Thienhaus S, Schymon S, Alff L and Gross R 2001 *Physica* C **351** 200
[13] Moeckly B H 2001 *Appl. Phys. Lett.* **78** 790
[14] Yan M F, Barns R L, O'Bryan Jr H M, Gallagher P K, Sherwood R C and Jin S 1987 *Appl. Phys. Lett.* **51** 532
[15] Bertsche G, Clauss W, Prins F E and Kern D P 1998 *Vac. Sci. Technol.* B **16** 2833
[16] Park W K, Lee H J, Kye J I, Yun J H, Lee S-M, Moon S H and Oh B 2001 *IEEE Trans. Appl. Supercond.* **11** 147
[17] Yeh N C, Chen C T , Hammerl G, Mannhart J, Tajima S, Yoshida K, Schmehl A and Schulz R R 2001 *Preprint* cond-mat/0103205
[18] Heinsohn J-K, Dittmann R, Contreras J Rodríguez, Scherbel J, Klushin A, Siegel M, Jia C L, Golubov S and Kupryanov M Yu 2001 *J. Appl. Phys.* **89** 3852
[19] Van Duzer T V and Turner C W 1999 *Principles of Superconductive Devices and Circuits* (Englewood Cliffs, NJ: Prentice-Hall) p 123
[20] Barone A 1982 *Physics and Applications of the Josephson Effect* (New York: Wiley) p 305

Supercond. Sci. Technol. 12 (1999) L5–L7. Printed in the UK PII: S0953-2048(99)05231-8

RAPID COMMUNICATION

'Interface-engineered' high-T_c Josephson junctions: a possible mechanism of operation

S S Tinchev

Institute of Electronics, Bulgarian Academy of Sciences, Tzarigradsko Chausse 72, Sofia 1784, Bulgaria

Received 16 June 1999

Abstract. The mechanism of operation of the 'interface-engineered' high-T_c Josephson junctions with ion-modified barrier has been discussed. The analysis is performed for a YBaCuO base electrode modified by Ar^+ and O^+ ions. Using the diffusion coefficients of each YBaCuO component it is shown that at the counter-electrode deposition temperature (about 780 °C) the O and Cu defects anneal out and the Ba and Y sublattice disorder remains the only factor to play an important role in YBaCuO interface modification. The nature of the barrier in these devices seems to be very complicated, probably 'insulator/normal conductor/superconductor with reduced critical temperature' and the junctions can be described as S–I–N–S′–S.

Ramp-type Josephson junctions fabricated without any deposited interlayer and in which the barrier is created by an interface modification have attracted great attention recently [1–4]. In this method of fabrication a YBaCuO ramp (the base electrode) is treated with Ar^+ or O^+ ions and subsequently annealed prior to the deposition of the top electrode. These devices appear to be reproducible and with I–V characteristics well described by the resistive shunted junction (RSJ) model. The modulation of the critical current with an external magnetic field indicates the formation of a homogeneous barrier layer at the interface. The temperature dependences of the critical current and of the normal resistance suggest the existence of a non-superconducting barrier. However, the nature of the barrier is still under debate and the mechanism of operation of these junctions is unclear.

Recently [5] we have made an attempt to shed light on the nature of the interface-engineered junctions. We supposed that these devices can be described as S–N–S devices, where the normal region is created by ion modification similarly to our e-beam-modified or oxygen-ion-modified weak links [6–10]. The thickness of the modified region in the layer was calculated for a typical experimental ion energy of 500 eV and it was found to be only 2–3 nm. Obviously the plasma treatment creates a barrier region only a few YBaCuO unit cells thick. This extremely thin layer actually determines the length of the created weak link and is responsible for the excellent properties of these junctions. Such a barrier thickness is consistent with the recent observation [11] by transmission electron microscopy of a 2–3 nm thin region at the YBCO interface with a different structure.

However, there is still a problem that has to be solved precisely. During the deposition of the top YBaCuO layer a thermal annealing occurs at a temperature of about 780 °C. We suggested [5] that the displacement of oxygen ions alone is important for the depressing of T_c and during the high-temperature treatment a significant part, but not all of the induced oxygen defects will be annealed out. A rough estimation using the value of the activation energy for oxygen diffusion was made [5] leading to a reasonable agreement with the experimental data. However, recently some strong indications have been given that not the oxygen sublattice disorder, but rather the cation disorder is probably the primary cause of the Josephson effect in these devices [11]. The authors stated that these junctions are stable under high temperature oxygen anneals for several hours, which means that the oxygen diffusion at 780 °C probably cannot play the major role in these devices. In this communication we try to present a more accurate analysis of this still open question, taking into account also the created cation defects.

The well known Monte Carlo code TRIM [12] can be used for this purpose, similarly to our previous work [5, 13]. The profiles of the total ion energy loss together with the energy absorbed by each YBaCuO component are plotted in figure 1 in the case of 500 eV argon ion modification. The YBaCuO critical temperature reduction is related to the total energy losses of the ions and thus to the average number of defects produced, as already shown

0953-2048/99/090005+03$30.00

Table 1. Averaged critical temperatures calculated for 100 nm YBaCuO film irradiated with 200 keV O^+ compared to the experimental data [15].

Dose (ions cm^{-2})	T_c (K) calculated using energy losses of all YBaCuO elements	T_c (K) calculated using energy losses of only Y, Ba and Cu	T_c (K) experimental [15] (middle of transition)
1×10^{13}	81	84.5	81
2×10^{13}	75	81.5	80
4×10^{13}	62.5	75	74
6×10^{13}	50	68.5	67
8×10^{13}	38	62.5	62.5

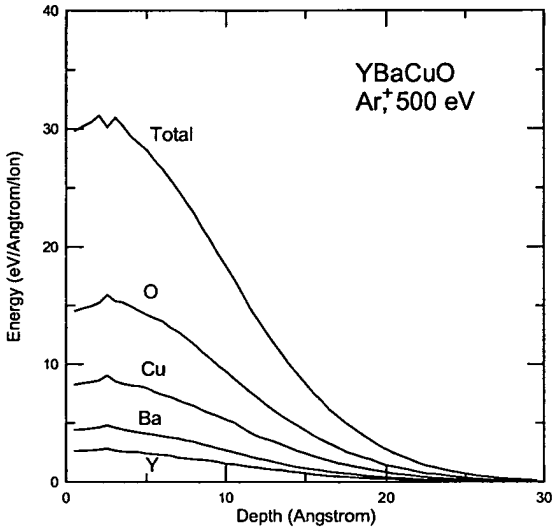

Figure 1. Calculated total energy losses and energy losses for each component in YBaCuO film for modification by argon ions with energy of 500 eV.

by Summers *et al* [14]. As seen in figure 1 about one half of created defects are oxygen defects. They probably annealed out almost completely [15] as early as 500 °C. However, after such a treatment the critical temperature does not recover to its original value [15]. This fact shows that not only oxygen defects, but also the cation sublattice disorder has an important effect on the T_c degradation.

We calculated critical temperatures similarly to our earlier work [13] for a 100 nm YBaCuO film irradiated with 200 keV oxygen ions. For this energy the projected range of the ions is larger then the film thickness and therefore only the effects of produced defects are significant. Additionally, the critical temperature depth profile is nearly uniform and one can make straightforward comparison of calculated and measured critical temperatures. The results of these calculations are presented in table 1. In the second column data are given for calculation using the total energy losses of the ions and in third column assuming that oxygen defects are completely annealed out. The calculated critical temperatures, presented in table 1, were averaged over the film thickness.

The measured T_c after a 500 °C thermal treatment [15] (last column in table 1) is in good agreement with the value

Table 2. Parameters of the Gaussian fits of the curves from figure 1.

	Total	Y	Ba	Cu	O
y_0	0.295	0.018	0.096	0.063	0.263
x_c	1.70	1.21	1.55	1.79	2.25
2σ	16.30	16.85	16.35	16.48	15.72
A	618.9	56.6	93.4	175.3	294.7

Table 3. Diffusion coefficients of the YBaCuO components.

	D ($cm^2\ s^{-1}$) at 780 °C	Reference
O	10^{-8}–10^{-10}	[16-18]
Cu	10^{-13}	[19]
Ba	10^{-20}	[20]
Y	10^{-33}	[20]

calculated using only Y, Ba and Cu defects. Obviously the cation disorder causes about one half of the critical temperature reduction and remains the main reason for the T_c reduction even after a 500 °C anneal. These results encourage us to consider also the case of interface-engineered junctions.

All curves shown in figure 1 can be fitted quite well with a Gaussian function

$$F(x) = y_0 + \frac{A}{\sqrt{2\pi}\sigma} \exp\left[\frac{-(x - x_0)^2}{2\sigma^2}\right]. \qquad (1)$$

Here y_0 is the baseline offset, A is the total area under the curve, x_c is the centre of the peak and σ is the standard deviation. Table 2 shows the parameters of the curves from figure 1.

During the thermal treatment of the base electrode and during the deposition of the counter-electrode a thermal diffusion occurs. For a Gaussian distribution the analytical solution of the diffusion equation is:

$$F_a(x) = \frac{A}{\sqrt{1 + 2Dt/\sigma^2}} \exp\left[\frac{-(x - x_0)^2}{2\sigma^2 + 4Dt}\right] \qquad (2)$$

where D is the diffusion coefficient and t is the annealing time. Obviously an annealing takes place when $Dt \geqslant \sigma^2$. For ions with energy of 500 eV the standard deviation σ for all curves from figure 1 is about 0.8 nm for argon ions and about 1.1 nm for similar curves calculated for oxygen ions. Using $t \sim 10^3$ s as a typical time for the counter-electrode deposition, one obtains that the diffusion coefficient has to be greater then 10^{-17} $cm^2\ s^{-1}$ in order for created defects to anneal out completely.

Table 3 summarizes the diffusion coefficients found in the literature for oxygen [16–18] and copper [19] at temperature $T \cong 780\,^{\circ}C$. The data for Ba and Y are available in the literature [20] for a different temperature interval and were extrapolated for 780 °C using the Arrenius relation.

Obviously at 780 °C for oxygen and copper $Dt \gg \sigma^2$ and the ion-induced defects will be almost completely annealed out. Since the heat treatment at this temperature and for the same deposition time is not sufficient to cause changes in the disordered Ba and Y sublattices, their amount is likely to be the factor controlling for YBaCuO interface modification. On the basis of this result, we can conclude that the remaining Ba and Y sublattice displacements, which cannot be removed during the counterelectrode deposition at 780 °C, are responsible for the suppression of T_c and thus for the Josephson effect observed in these junctions. They can be misinterpreted in TEM investigations as a new (cubic) phase [2, 11] of YBaCuO or as an a-axis-oriented YBaCuO [21]. Probably similar is the mechanism of operation of the sandwich junctions YBCO/PBCO/YBCO [22] made by planarization of the base electrode by an Ar ion beam at 700 eV.

The remaining defects after such a thermal treatment are about 25% of the total defect amount (see figure 1). Because the critical temperature reduction is proportional to the average number of defects, this means that for the parameters of the fabrication process [1] an apparent ion dose will be about 2.4×10^{18} ions cm^{-2} at its maximum. For such a high dose this part of the barrier should be in an insulator state. The number of created defects drops rapidly inside the film and reaches a level equivalent the dose $\sim 6 \times 10^{13}$ ions cm^{-2}, which is needed to reduce the critical temperature to zero without annealing, at a depth of about 4 nm. This depth will be actually an effective barrier length of the junction. Deeper in the film a gradual transition from an insulator through a normal conductor to a superconductor with reduced critical temperature occurs. Hence, the nature of the barrier in these devices is likely to be very complicated, probably 'insulator–normal conductor–superconductor with reduced critical temperature' and the Josephson junctions can be described as S–I–N–S′–S. By choosing the appropriate ion energy and annealing conditions, it is possible to fabricate high-T_c Josephson junctions with a wide range of barriers ranging from almost S–N–S junctions to cases where the S–I–S mechanism is dominant.

Acknowledgments

This work was supported by the project F-561 of the National Science Fund of the Ministry of Education, Science and Technology of Bulgaria. I thank Dr A Veneva for providing the papers [19, 20], with data for Cu, Ba and Y diffusion coefficients.

References

[1] Moeckly B H and Char K 1997 *Appl. Phys. Lett.* **71** 2526
[2] Moeckly B H, Char K, Huang Y and Merkle K 1998 *Applied Superconductivity Conf. (Palm Desert, CA, September 13–18 1998) Preprint*
[3] Hunt B D, Forrester M G, Talvacchio J and Young R M 1998 *Applied Superconductivity Conf. (1998) Preprint*
[4] Dittmann R, Heinsohn J K, Braginski A I and Jia C I 1998 *Applied Superconductivity Conf. (Palm Desert, CA, September 13–18 1998) Preprint*
[5] Tinchev S S and Alexandrova S 1998 *Appl. Phys. Lett.* **73** 1745
[6] Tinchev S S 1990 *Supercond. Sci. Technol.* **3** 500
[7] Tinchev S S 1993 *IEEE Trans. Appl. Supercond.* **3** 28
[8] Tinchev S S 1994 *Physica* C **222** 173
[9] Tinchev S S 1994 *Proc. 7th Int. Symp. on Weak Superconductivity (Smolenice Castle, June 6–10 1994)* (Bratislava) p 312
[10] Tinchev S S 1996 *Physica* C **256** 191
[11] Moeckly B H and Char K 1998 *Appl. Phys. Lett.* **73** 1747
[12] Ziegler J and Biersack P 1985 *The Stopping and Range of Ions in Solids* (New York: Pergamon)
[13] Tinchev S S 1995 *J. Appl. Phys.* **78** 5851
[14] Summers G P, Burke E A, Chrisey D B, Nastasi M and Tesmer J R 1989 *Appl. Phys. Lett.* **55** 1469
[15] Kahlmann F 1998 *PhD Thesis* Koln University
[16] Lee S H, Bae S C, Ku J K and Shin H J 1992 *Phys. Rev.* B **46** 9142
[17] Li Y, Kilner J A, Tate T J, Lee M J, Chater R J, Fox H, De Souza R A and Quincey P G 1995 *Phys. Rev.* B **51** 8498
[18] Michaelis A, Irene E A, Auciello O and Krauss A R 1998 *J. Appl. Phys.* **83** 7736
[19] Routbort J L, Rothman S J, Chen N, Mundy J N and Baker J E 1991 *Phys. Rev.* B **43** 5489
[20] Chen N, Rothman S J, Routbort J I and Goretta K C 1992 *J. Mater. Res.* **7** 2328
[21] Li Y, Linsen S, Machalet F, Schmidl F and Seidel P 1995 *Physica* C **243** 294
[22] Maruyama M, Yoshida K, Horibe M, Fujimaki A and Hayakawa H *Applied Superconductivity Conf. (Palm Desert, CA, September 13–18 1998)* Preprint at press

ELSEVIER

Physica C 366 (2001) 51–56

PHYSICA C

www.elsevier.com/locate/physc

Structural variation of the interface-engineered layers in $YBa_2Cu_3O_{7-\delta}$ thin films

Y. Wu *, Y. Ishimaru, K. Tanabe

Superconductivity Research Laboratory, ISTEC, 1-10-13 Shinonome, Koto-ku 135-0062, Tokyo, Japan

Received 2 April 2001; received in revised form 16 April 2001; accepted 2 May 2001

Abstract

The atomic structures of interface-engineered $YBa_2Cu_3O_{7-\delta}$ (YBCO)/plasma-treated YBCO/*a*-axis YBCO 'trilayer' samples have been observed by transmission electron microscopy. The microstructures are compared by changing the plasma treatment conditions. The detailed structure of the interface or the barrier layer varies both from sample to sample and from place to place in the same sample. It is found that the interface structure depends on both the accelerating voltage and the atmosphere for the plasma treatment. The interfaces under high accelerating voltages (700 and 500 V) are strained, while strain-free barriers with different crystal structures are formed by the treatment under lower accelerating voltages (350 and 200 V). In the sample prepared in the mixed atmosphere of argon and oxygen, a kind of cubic structure is found at the interface, while in the sample fabricated in pure argon, besides the cubic structure, $BaCuO_2$ and Y_2O_3 are also observed in the interface.

PACS: 74.80.Dm; 74.72.Bk; 61.16.Bg

Keywords: Microstructure; $YBa_2Cu_3O_{7-\delta}$ multilayers; Plasma treatment; Transmission electron microscopy

1. Introduction

Fabrication of superconductor–normal–superconductor (SNS) or superconductor–insulator–superconductor (SIS) Josephson junctions has been an attractive topic since the discovery of high T_c superconductors [1–4]. No matter the junctions are in the form of trilayers or edge designs using various normal materials as barriers, to make a thin (typically less than 10 nm), uniform barrier is the most difficult step in the fabrication.

Recently, Moeckly et al. have developed an interface-engineered junction (IEJ), in which no barrier deposition is involved [5,6]. IEJ barriers are fabricated from an amorphous layer that is made by an ion bombardment process. Radio frequency (RF) plasma discharge, Ar ion milling or electron cyclotron resonance (ECR) ion etching is usually used to make an amorphous layer, which is changed to a barrier layer through appropriate annealing and upper $YBa_2Cu_3O_{7-\delta}$, (YBCO) deposition processes [7], however, ion bombardment and recrystallization processes are quite complex. In particular, the latter process is closely related with disordered arrangement of cations, which depends on the former process. Thus, it is worthwhile clarifying the factors governing the

* Corresponding author. Tel.: +81-3-3536-5709; fax: +81-3-3536-5705.

E-mail address: wy@istec.or.jp (Y. Wu).

0921-4534/01/$ - see front matter
PII: S0921-4534(01)00785-7

recrystallization process. Huang et al. concluded that the interface barrier is cubic or pseudocubic YBCO-variant with a lattice parameter of 0.51 nm in *c*-YBCO/plasma-treated-YBCO/*c*-YBCO structure [8], while Wen et al. proposed that the modified interface in YBCO ramp-edge junctions has a kind of Ba-based perovskite-like structure, $(Y_{1-x}Cu_x)$-BaO_y with $x < 0.5$ [7]. This suggests that, under different experimental conditions and geometry of the samples, the structures of the interface barriers are likely different.

In order to develop more reliable fabrication procedures, it is necessary to study how the microstructure of the barrier varies with the experimental conditions such as the ion accelerating voltage and the atmosphere. Recently, Ishimaru et al., found a variation in RHEED patterns from the recrystallized *a*-axis YBCO interface, which was plasma-treated under different conditions. The results suggest a significant change in the microstructure of the recrystallized interface. In this paper, we report the detailed results on microstructural study of YBCO/plasma-treated YBCO/*a*-axis YBCO trilayer samples by transmission electron microscopy (TEM).

2. Experimental

a-axis oriented YBCO thin films were prepared on $SrTiO_3$ (100) substrate by pulsed laser deposition. A KrF excimer laser ($\lambda = 248$ nm) with a power density of about 2 J/cm^2 on a stoichiometric high-density target and a repetition rate of 5 Hz was used. About 200 nm thick films were grown in an oxygen pressure of 200 mTorr at a substrate temperature of 580°C. Fig. 1 illustrates the fabrication conditions of the four samples studied in this paper. The experimental details were described in Ref. [9]. Briefly, an ECR source with a grid was

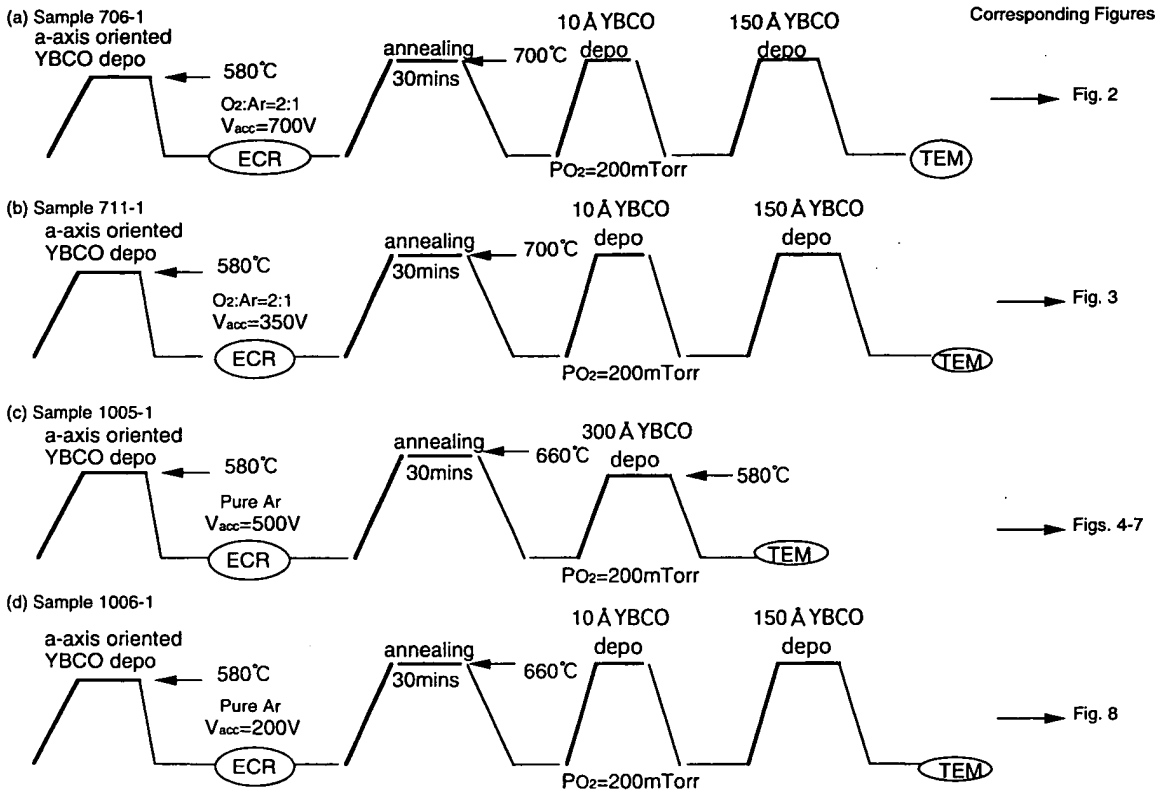

Fig. 1. Illustrations of the experimental procedures for the four samples examined.

used to modify the surfaces of *a*-axis YBCO films. Either pure Ar or Ar and O_2 mixed gas was employed and the accelerating voltage was varied between 200 and 700 V. In samples 706-1, 711-1 and 1006-1, we selected 700°C and 660°C as annealing temperatures and upper YBCO thin film deposition temperatures, respectively, because they were close to the temperature for making interface-modified barrier ramp-edge Josephson junctions in our group. In sample 1005-1, the upper YBCO thin film was deposited at a lower temperature (580°C) in order to avoid the presence of *c*-axis YBCO grains.

In order to protect the termination of the upper layer, which is easily damaged during the TEM preparation process, a layer of gold was deposited on the samples. Cross-section specimens for TEM were prepared by a standard method including mechanical grinding and ion-milling. TEM observation was carried out in a JEOL-4000EX operated at an accelerating voltage of 400 kV.

3. Results and discussion

Fig. 2 shows the cross-sectional TEM image of sample 706-1. The geometry of the sandwich structure is not what was intended: the upper YBCO layer consists of both *a*- and *c*-axis oriented YBCO. It results from the high deposition temperature (700°C) for the upper YBCO film. No clear barrier material is observed between the upper and lower layer of YBCO, however, there is a 1–2 atom thick strained trace at the interface between the upper and lower *a*-axis YBCO, as indicated by black arrows in the inset, which is the enlarged image of the framed area. The difference in contrast around the interface area indicates the existence of strain field. The absence of secondary phases is consistent with the RHEED results reported in Ref. [9].

The detailed geometry of sample 711-1 is shown in Fig. 3(a). In some regions, a clear secondary phase – barrier layer is observed, as indicated by the arrows. The barrier layer grows on the *a*-axis YBCO with a cube-on-cube orientation relationship and is flat, uniform, strain-free, and thinner than 0.5 nm. Under the image condition employed, the Cu–O planes appear as white lines. It is evident that the Cu–O planes are interrupted by the thin barrier layer. However, the barrier layer did not cover the whole area of the lower YBCO, resulting in the connection of Cu–O planes in some other regions. The surface of *a*-axis film is not an ideally flat plane as well known and the thickness of recrystallized layer is less than 1 nm. Therefore, it is rather difficult to distinguish the intermediate layer from the lower and upper YBCO even in

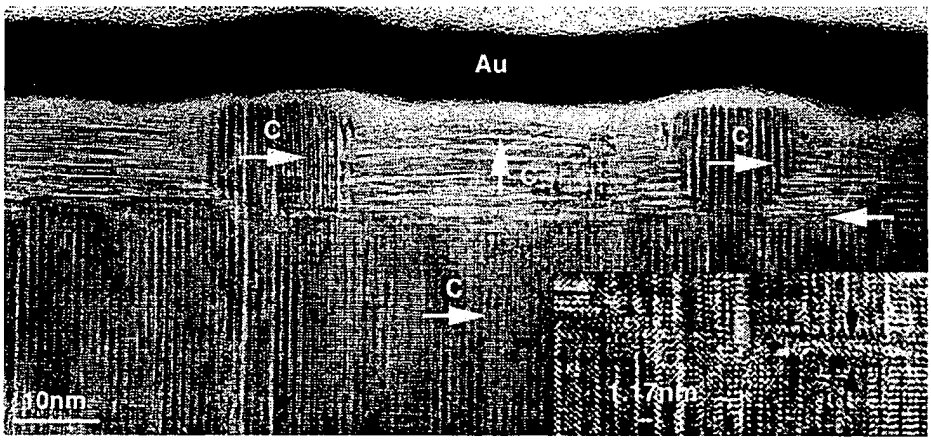

Fig. 2. Cross-section TEM image of a YBCO/plasma-treated YBCO/*a*-YBCO sample 706-1 which was treated under 700 V accelerating ion voltage and atmosphere of O_2:Ar = 2:1. The interface between the lower YBCO and the upper YBCO is indicated by the arrow. The enlarged image of the area in the frame are displayed in the inset.

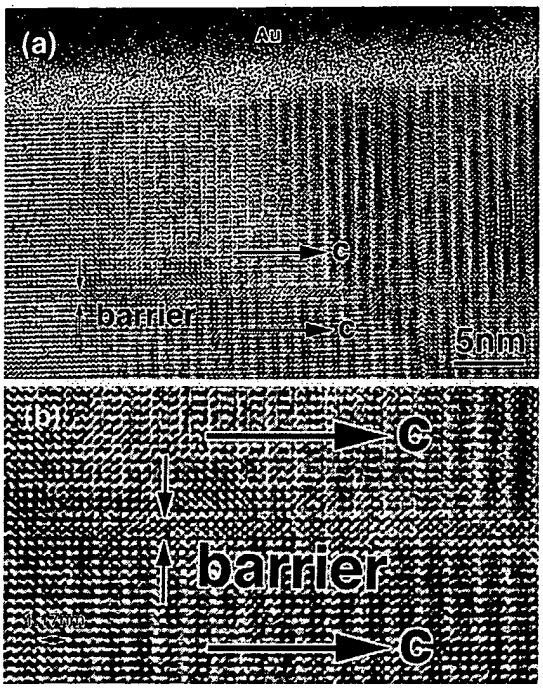

Fig. 3. (a) High resolution image of a YBCO/plasma-treated YBCO/*a*-YBCO sample 711-1 which was treated under a 350 V accelerating voltage and O_2:Ar = 2:1 annealing atmosphere. The interface between the lower YBCO and the upper YBCO is indicated by the arrow. (b) An enlarged image of the interface area in (a).

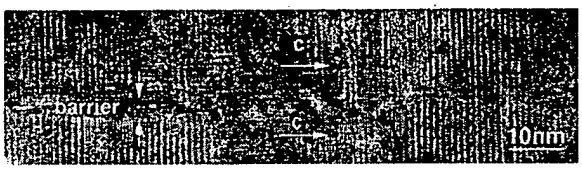

Fig. 4. Cross-section TEM image of sample 1005-1, in which the interface was formed by ECR treatment under a 500 V accelerating voltage in pure Ar annealing atmosphere and a lower deposition temperature for the upper YBCO layer.

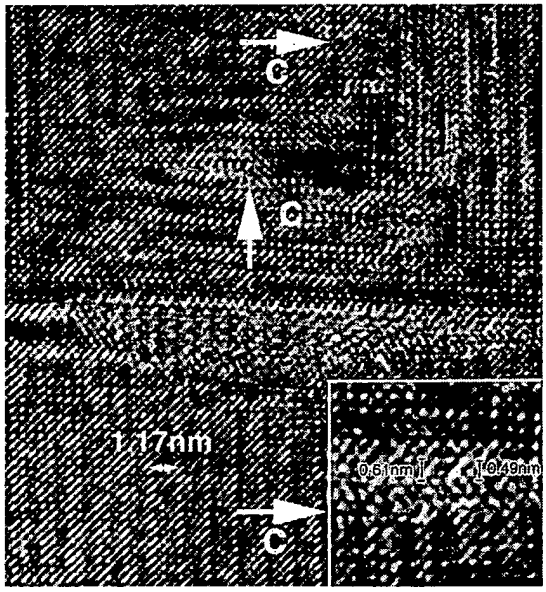

Fig. 5. High resolution image of one area of sample 1005-1 with an atomic configuration consisting of rectangles, in which the width is about 0.74 nm and length is about 0.52 nm. The inset is an enlarged image of the right side of the area.

an enlarged image shown in Fig. 3(b). However, a careful examination revealed a very small thickness variation of the barrier layer. Using the known *a*-axis YBCO lattice as a reference, the lattice parameter along the *c*-axis of the upper YBCO film is estimated to be 0.39 nm, while the lattice parameter along the *a*-axis ranged from 0.38 to 0.41 nm from place to place. This is in good agreement with the result reported in Ref. [8]. It suggests that there may be a slight composition variation in the barrier.

Fig. 4 shows a low magnification image of sample 1005-1. The barrier layer is clearly observed due to the existence of the strain contrast. Three kinds of microstructures of the ECR-treated interface layers were observed in the same specimen. HRTEM image in Fig. 5 shows that barrier layer can be about 2 nm thick. It is difficult to determine the composition of the barrier layer by EDX because a sufficiently strong signal could not be obtained. However, *d*-spacings can be measured directly from the images using the adjacent YBCO fringes as a reference and identification of the phases in the barrier layer was made tentatively. The image configuration consists of rectangles, in which the length is about 0.74 nm and the width is about 0.53 nm. A careful checking of the X-ray database for all the compounds of Y, Ba, Cu and O reveals that the only possibility for the appearance of such atomic configuration is $BaCuO_2$, of which $d_{\{211\}} = 0.75$ nm, and $d_{\{222\}} = 0.53$ nm, respectively. The material on the left side of the barrier layer is so heavily strained that the atomic

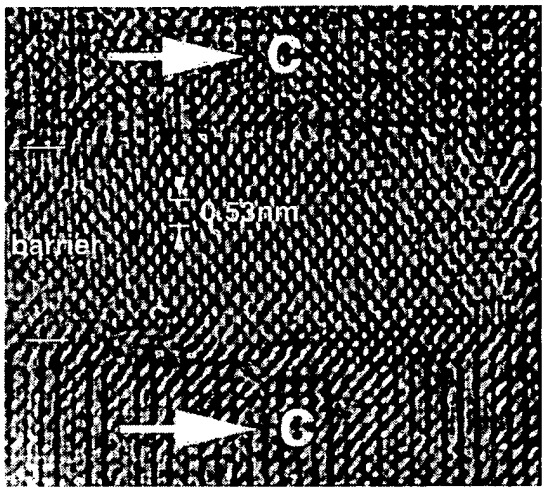

Fig. 6. High resolution image of another area of sample 1005-1. Here, the interface layer is about 4.5 nm thick and the atomic configuration consists of centered rectangles with the length of about 0.53 nm and the ratio of length to width ratio of about 1.4.

configuration is invisible, while that on its right side is composed of centered rectangles with various lengths along the *a–b* planes, as shown in the enlarged image in the inset.

Another type of interface layer is shown in Fig. 6. The lattice image is similar to that reported by Huang et al. [7]. The image is considered to be taken from the [1 1 0] direction of cubic or pseudo-cubic structure, since the ratio of the length to the width of the centered rectangles in the image is approximately 1.4 and its lattice parameter is calculated to be about 0.53 nm. According to the X-ray database for the compounds consisting of Y, Ba, Cu and O, only Y_2O_3, of which the crystal structure is cubic with the lattice parameter $a =$ 1.06 nm and the space group of Ia3, can give rise to such an atomic arrangement as shown in Fig. 6.

In the same specimen, a different atomic configuration was observed as shown in Fig. 7. This configuration appears to be similar to that shown in Fig. 3. Recently, Rutherford backscattering spectrometry (RBS) results indicated that the surfaces of the YBCO films, fabricated under the accelerating voltage of 350 V, are more Y-rich than those of the films treated under the accelerating voltage of 700 V [10], which is probably favorable for the formation of pseudo-cubic phases.

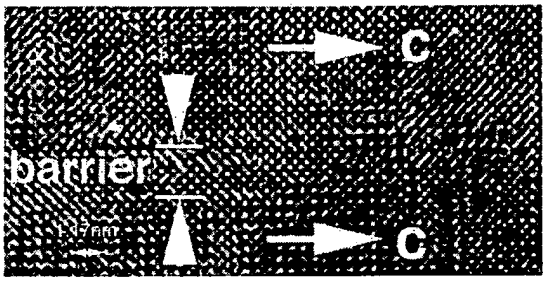

Fig. 7. High resolution image of the other area of sample 1005-1, showing an about 1 nm thick cubic structure similar to the one observed in Fig. 3.

However, in pure Ar, the decomposition of YBCO may occur to some extent, which leads to the complicated structure of the interface.

In order to further clarify the effects of the accelerating voltage and the atmosphere on the microstructure of the interface, we investigated another sample1006-1, as shown in Fig. 8. On the right side of the image, we observed two kinds of atomic configurations. It was found that one is the same as that in Fig. 5, i.e., $BaCuO_2$, and the other is the same as that in Fig. 6, i.e., Y_2O_3. Though the secondary phases are the same as those found in sample 1005-1, the interface layer in sample 1006-1 is strain-free. Both samples 1005-1 and 1006-1 were treated in Pure Ar, but at different accelerating voltages. This confirms that strain-free interfaces are formed at lower accelerating voltages.

None of the four samples examined displays full-coverage by the barrier materials. This may be due to both the large lattice mismatch between YBCO and the barrier layer, which leads to

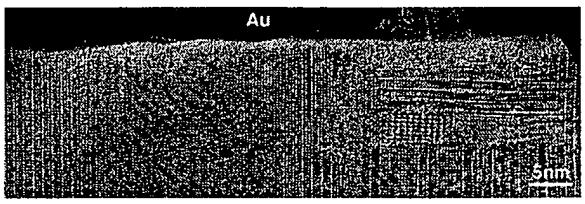

Fig. 8. TEM image of sample 1006-1, in which the interface was formed by ECR treatment under a 200 V accelerating ion voltage in pure Ar annealing atmosphere and lower deposition temperature for the upper YBCO. The presence of $BaCuO_2$ and Y_2O_3 is noticed along the interface at the right side of the image.

island-growth mode of the barrier layer during the initial growth stage, and the atomic-scale steps at the surface of the lower YBCO.

4. Conclusions

a-YBCO/plasma-treated-YBCO/*a*-YBCO 'tri-layer' thin films fabricated under different plasma-treatment conditions have been observed by TEM. The results show that

1. The interface under high accelerating voltage (700 or 500 V) is a strained one, while strain-free interfaces are formed under lower accelerating voltage (350 or 200 V).
2. A cubic barrier material with $a = 0.38$–0.41 nm and $c = 0.39$ nm is formed at the interface under the accelerating voltage lower than 500 V, while no secondary phase is observed under 700 V.
3. Plasma-treatment in pure Ar may result in the decomposition of YBCO to form Y_2O_3 and $BaCuO_2$ to some extent, while the treatment in Ar and O_2 mixture seems to suppress the decomposition.

Acknowledgements

This work was supported by the New Energy and Industrial Technology Development Organization (NEDO) as collaborative Research and Development of Fundamental Technologies for Superconductivity Applications.

References

[1] J.G. Wen, S. Mahajan, T. Morishita, N. Koshizuka, Physica C 266 (1996) 320.
[2] J.B. Barner, C.T. Rogers, A. Inam, R. Ramesh, S. Bersey, Appl. Phys. Lett. 59 (1991) 742.
[3] C.L. Jia, M.I. Faley, U. Poppe, K. Urban, Appl. Phys. Lett. 67 (1995) 3635.
[4] E. Olsson, K. Char, Appl. Phys. Lett. 64 (1994) 1292.
[5] B.H. Moeckly, K. Char, Appl. Phys. Lett. 71 (1997) 2526.
[6] B.H. Moeckly, K. Char, Y. Huang, K.L. Merkle, IEEE Trans. Appl. Supercond. 9 (1999) 3358.
[7] Y. Huang, K.L. Merkle, B.H. Moeckly, K. Char, Physica C 314 (1999) 36.
[8] J.G. Wen, N. Koshizuka, S. Tanaka, T. Satoh, M. Hidaka, S. Tahara, Appl. Phys. Lett. 75 (1999) 2470.
[9] Y. Ishimaru, Y. Wu, O. Horibe, Y. Tarutani, K. Tanabe, Physica C 357–360 (2001) 1432.
[10] Y. Ishii, H. Zama, T. Morishita, unpublished.

Current transport in ramp-type junctions with engineered interface

J.-K. Heinsohn, R. Dittmann,[a] J. Rodríguez Contreras, J. Scherbel, A. Klushin, and M. Siegel
Institut für Schicht- und Ionentechnik, Forschungszentrum Jülich GmbH, 52425 Jülich, Germany

C. L. Jia
Institut für Festkörperforschung, Forschungszentrum Jülich GmbH, 52425 Jülich, Germany

S. Golubov
Department of Applied Physics, University of Twente, Enschede, The Netherlands

M. Yu. Kupryanov
Institute of Nuclear Physics, Moscow State University, Moscow, Russia

(Received 27 September 2000; accepted for publication 21 December 2000)

The transport properties of "interface-engineered" edge-type $YBa_2Cu_3O_7$ Josephson junctions are investigated in detail. We have investigated the dependence of the current–voltage characteristics on external magnetic field, temperature, and microwave irradiation and compare them to the resistively shunted junction model. The temperature dependence of the critical current and the normal resistance allows us to draw conclusions to the transport of quasiparticles and Cooper pairs in the investigated "interface-engineered" junctions. We have studied the properties of junctions for which La doped $YBa_2Cu_3O_7$ is used for the superconducting electrodes. We will propose a model for the undoped and the La doped case which takes into account a barrier which consists of a series connection of a normal conducting layer and an insulator, containing superconducting microconstrictions. © *2001 American Institute of Physics.* [DOI: 10.1063/1.1351056]

I. INTRODUCTION

Interface-engineered junctions (IEJs) are an interesting approach for the realization of reliable, controllable, high-temperature superconducting (HTS) Josephson junctions. The idea of fabricating a barrier by interface treatments instead of using an epitaxially grown nonsuperconducting thin film was first suggested by Moeckly *et al.*[1] At present, several groups are employing IEJs by using different approaches for the interface treatment.[2–7] All approaches have in common an ion treatment of the surface of the base electrode in the ramp area and a subsequent annealing step, but the methods for the generation of the ions and the process parameters differ strongly from group to group. However, each group claims that the junctions are much more reliable than ramp-type junctions with epitaxially deposited barrier layers, previously fabricated in their laboratories.

Since IEJs are resistively shunted junctions the most suitable model to describe their transport properties is the resistively and capacitively shunted junction (RCSJ) model.[8] For most cryoelectronic applications, e.g., superconducting quantum interference devices, digital circuits, or voltage calibrators, RSCJ-like junctions are required. Nevertheless, no detailed comparisons of the static and dynamic properties of IEJs to the RCSJ model at different temperatures have been published up to now.

The current transport and the nature of the barrier are still open questions since the results of microstructural investigations differ from group to group. Whereas some groups observe the formation of a cation disordered (pseudo) cubic $YBa_2Cu_3O_7$(YBCO) phase,[9,10] Wen *et al.*[11] report on the formation of a Cu deficient YBCO phase $Y_{1-x}BaCu_xO_y$. There exists no consistent picture for the current transport. The published current densities, the normal resistances, and the suggested transport mechanisms differ for the junctions fabricated in different ways. Some groups observe properties of an insulating barrier containing localized states[4,5] whereas previous results of our group hint on a metallic behavior of the barrier material.[6]

The presence of La either in the superconducting electrodes or in the insulator strongly influences the properties of the junctions. Hunt *et al.* observed a strong increase of the normal resistance and a decrease of the critical current by using La doped YBCO for the bottom electrode.[2] Satoh *et al.* observed RCSJ-like current–voltage ($I-V$) characteristics only if La is present in the near area of the ramp.[5]

We will present detailed measurements of the transport properties of IEJs with $YBa_2Cu_3O_7$ (undoped junctions) as well as $YBa_{1.95}La_{0.05}Cu_3O_7$ electrodes [La(5%) doped junctions]. The $I-V$ characteristics as well as the dependence of the critical current I_C on external magnetic field, $I_C(H)$, were investigated for the whole temperature range below the superconducting transition temperature T_C. The $I-V$ characteristics and their response to microwave irradiation will be compared with the RCSJ model and the deviations will be discussed. We will propose a model to explain the transport of quasiparticles and Cooper pairs in undoped and La(5%) doped junctions and draw conclusions to the nature of the barrier.

[a]Author to whom correspondence should be addressed; phone: +49-2461-612357, fax: +49-2461-612940, electronic mail: r.dittmann@fz-juelich.de

II. JUNCTION PREPARATION

The junction preparation process can be divided into the deposition of a YBCO–$SrTiO_3$ bilayer, the ramp fabrication process, the interface engineering, and the deposition of the counterelectrode.

First, a bilayer consisting of a 120 nm thick YBCO or $YBa_{1.95}La_{0.05}Cu_3O_7$ [La(5%) doped YBCO] film and a 220 nm thick $SrTiO_3$(STO) film is deposited *in situ* by pulsed laser deposition. We employed STO as well as $LaAlO_3$ as substrate materials and did not observe any influence on the film quality or junction properties. The YBCO films are deposited at a substrate temperature of $T=805\,°C$, an oxygen pressure $p=60\,Pa$, an energy density of 2 J/cm^2, and a laser frequency of 10 Hz. The STO films deposited *in situ* on top of the YBCO films are fabricated at $T=760\,°C$, $p=15\,Pa$, with the same energy density and frequency as for YBCO. Further details can be extracted from Ref. 12.

For the fabrication of the ramps, the bilayers are patterned by conventional photolithography. The STO film is Ar-ion-beam milled in a Kaufmann-type source using a current density of 0.25 mA/cm^2 and an energy of 250 eV. The sample is tilted 30° to the substrate normal and rotates during the etching process. The sample is cooled down to $-15\,°C$ during ion beam etching. The photoresist is then removed in an oxygen plasma. Subsequently, using the STO ramp as an etching mask, the YBCO ramps are ion-beam milled at the same etching parameters. This process results in ramps with edge angles of 20° for STO and 30° for YBCO. The thickness of the STO layer is reduced to 20–50 nm during the ion milling of the YBCO ramp. A more detailed description of the ramp fabrication process can be found in Refs. 12 and 13.

The interface engineering consists of a short *ex situ* ion-milling step at higher voltages and an annealing step in the deposition chamber. We investigated the parameters for these steps in combination with the deposition temperature of the counterelectrode using statistical methods.[12] In summary, we found out that the homogeneity of the junctions can be improved by using higher etching voltages and lower annealing temperatures whereas the critical currents of the junctions are mainly determined by the deposition temperature of the counterelectrode. Optimal junction properties are achieved by using a 5 min annealing step at 1200 V, a 30 min annealing step at 500 °C at the deposition pressure of 60 Pa O_2, and a deposition temperature of 760 °C for the counterelectrode.

The junctions with bridge widths between 1 and 8 μm are patterned by conventional photolithography and Ar-ion-beam milling. Finally, a 200 nm thick gold layer is evaporated and patterned by a lift-off process to provide electrical contacts.

Several undoped and La(5%) doped junctions were investigated by transmission electron microscopy (TEM) and no significant difference between the microstructure of the junctions was observed. The TEM micrograph of a La(5%) doped junction is shown in Fig. 1. At the interface between the bottom YBCO electrode and the counterelectrode a region with a slightly different contrast can be identified. However, in higher resolution, as shown in the inset of Fig. 1, no interface layer with a different crystalline structure can be observed. This is in contradiction to the observations published in Refs. 9 and 11, where a 2 to 3 nm thin interface layer with a clearly different crystal structure was detected.

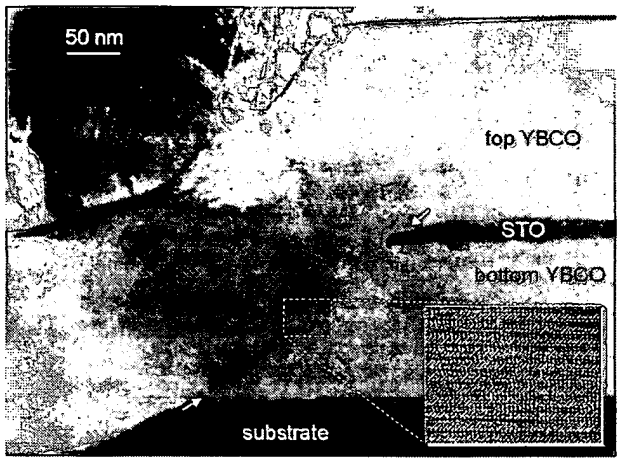

FIG. 1. TEM micrograph of the junction area. The arrows indicate the interface between the top and bottom electrode, which can be identified by a region with different contrast. The inset shows a high resolution image of the interface region. The thickness of the STO film is reduced to about 20 nm during the ion milling of the YBCO ramp.

Cation disorder in the interface region due to the Ar-ion treatment could lead to local strain which may become visible in TEM as a region with different contrast. So the TEM investigations of our junctions are consistent with an interface layer where the orthorhombic crystal structure of YBCO is maintained, but in which some cation disorder is present.

III. STATIONARY PROPERTIES

The chip layout used for our investigations contains 40 junctions with 2–4 μm junction width. We investigated about ten chips with undoped junctions and about ten chips with La doped junctions with different La content. Since our process ensures the reliable fabrication of Josephson junctions, the measurements presented in this article are representative of our IEJs. The Josephson junctions are measured in the standard four-point geometry. A coil situated in our probe enables us to measure the $I-V$ characteristics in magnetic fields up to 3 mT. Trapping of flux is a crucial point in ramp-type junctions. Marx *et al.* showed by low-temperature-scanning-electron microscopy that magnetic flux is trapped in the YBCO film covering the ramp edge.[14] Therefore the junctions are shielded against external magnetic fields by Cryoperm shielding. Since self-generated fields also induce trapped magnetic flux in the junctions, the maximum critical current is often obtained at nonzero magnetic fields. Therefore we adjusted the magnetic field towards the maximum of the critical current before we recorded the $I-V$ characteristics. A detailed investigation of the magnetic-field dependence of the $I-V$ characteristics of our junctions will be published elsewhere.

The normal resistance R_N is determined by the slope of the linear part of the $I-V$ characteristics at high bias currents where $V \gg I_C R_N$.

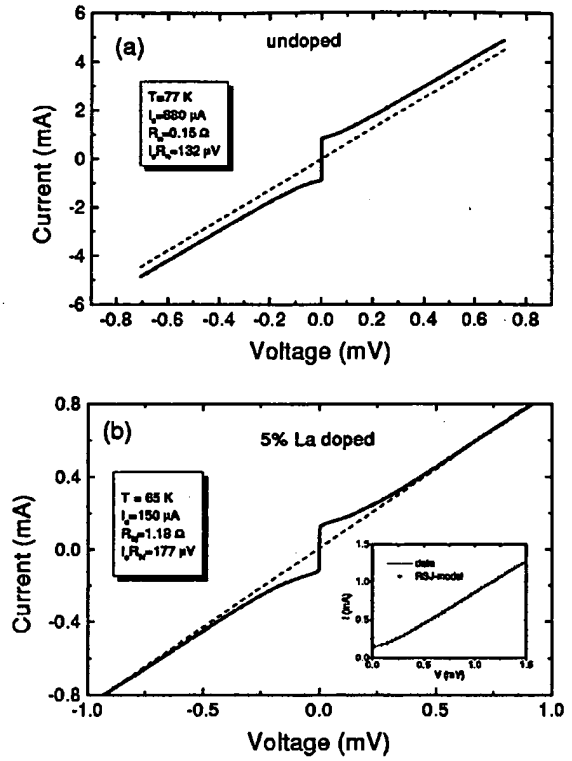

FIG. 2. (a) $I-V$ characteristic of a 4 μm wide undoped junction at 77 K. (b) $I-V$ characteristic of a 3 μm wide La(5%) doped junction at 65 K.

A. Influence of La doping on the junction properties

Figure 2(a) shows a typical $I-V$ characteristic of an undoped junction at 77 K. The parameters can be extracted from Table I. The shape of the $I-V$ characteristic is RCSJ-like but approximates at high bias current a straight line with a positive offset relative to the $I-V$ characteristic of an ohmic resistor [see the dashed line in Fig. 2(a)]. This offset corresponds to an excess current of about 500 μA.

For La(5%) doped junctions, supercurrents become detectable between 75 and 80 K although the critical temperatures of the La(5%) doped YBCO films are only slightly suppressed (at most 1 to 2 K). Figure 2(b) shows a typical $I-V$ characteristic of a La(5%) doped junction at 65 K. The shape can be well-described by the RCSJ model with neglected capacitance as can be seen in the inset of the figure.

The parameters of the undoped and the La(5%) doped junctions presented in Fig. 2 are summarized in Table I. It shows that the critical current density j_C of the La(5%) doped junctions is about one order of magnitude lower and the R_NA is about one order of magnitude higher than that for undoped junctions. Similar results have been obtained by other groups.[2]

TABLE I. Summary of the junction parameters of the junctions in Fig. 2 (j_C: critical current density; R_NA: normal resistance times junction area; and T: measurement temperature).

Sample No.	La concentration	T(K)	j_C (A cm^{-2})	R_NA (Ω cm^2)	I_CR_N(μV)
1	0%	77	1.8×10^5	7.2×10^{-10}	132
1	0%	65	2.5×10^5	6.2×10^{-10}	155
2	5%	65	4.2×10^4	4.2×10^{-9}	177

Since a high concentration of La reduces the T_C of YBCO,[15] a possible explanation for the difference between undoped and La(5%) doped junctions could be that La diffuses into the ramp area and this agglomeration of La results in an interface layer with reduced T_C forming an additional barrier.

From this point of view, it seems possible to adjust the junction parameters by the La content. Therefore we investigated junctions fabricated with electrodes of doping levels from 0% to 7%. We identified two groups of junctions: For La(5%) and La(7%) doped junctions, the critical currents are about one order of magnitude lower and the normal resistances are about one order of magnitude higher than for the La(3%) doped and undoped junctions. This means that a threshold La content is needed to change the junction parameters, but it is impossible to continuously adjust the junction parameters. Due to these results, it seems unlikely that the La content itself determines the electrical properties of the barrier. However, La is prerequisite for the modification of the barrier layer.

To further investigate the role of La in the preparation process, we fabricated junctions where La(5%) doped YBCO was used either only for the base electrode or only for the counterelectrode. The junctions with La(5%) doped YBCO bottom electrodes behave like junctions in which both electrodes consist of La(5%) doped YBCO. The junctions with La(5%) doped YBCO top electrodes behave like undoped junctions. This shows that the interdiffusion of La is not the most important mechanism for the barrier formation in the La(5%) doped junctions because interdiffusion would as well occur during the fabrication of the counterelectrode. We conclude that La has to be present during etching and annealing to influence the formation of the barrier.

Hunt *et al.*[2] suggest that during the treatment of the ramp, the La atoms interchange in the interface region with a much higher probability with Y than Ba atoms, because the atomic radius of La is more similar to Y as the atomic radius of Ba. Wen *et al.* observed by TEM that if they utilize the La containing insulator $(La_{0.3}Sr_{0.7})(Al_{0.65}Ta_{0.35})O_3$ the barrier is continuous whereas for $SrTiO_3$ a high number density of pinholes is observed.[11]

We did not observe a difference between undoped and La(5%) doped junctions by TEM. The nature of the barrier for the different types of junctions will be discussed in the context of the transport properties of our junctions in Sec. V.

B. Behavior of the junctions in different current density regions

Due to the increase of the critical current with decreasing temperature the short-junction limit where self-field effects of the critical current can be neglected may be exceeded at lower temperatures. Therefore we measured $I-V$ characteristics and $I_C(H)$ patterns for several samples for different temperatures below T_C. To check the role of self-field effects due to Joseph-son currents in our junctions, we regard the relation of the junction width w to the Josephson penetra-

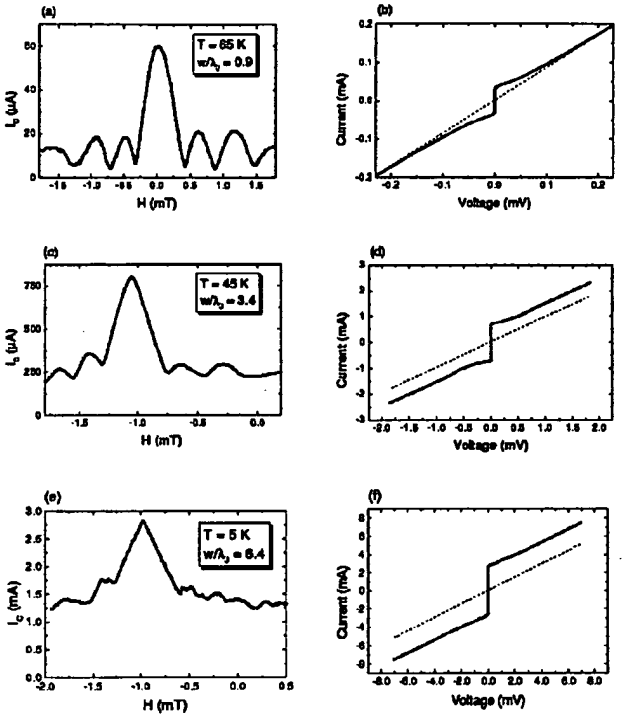

FIG. 3. $I_C(H)$ patterns and $I-V$ characteristics of a 3 μm wide La(5%) doped junction at different temperatures: (a) and (b): 65 K; (c) and (d): 45 K; (e) and (f): 5 K. The dashed lines correspond to the Ohmic law with the respective R_N of the junction.

tion depth $\lambda_J=\sqrt{\hbar/2e\mu_0 d' j_C}$, with $d'=d+2\lambda_L$ (see, e.g., Ref. 16). We used $d'=2\lambda_{L,ab}=300\,\text{nm}$ because supercurrents flow in the *ab* planes and the thickness of our barrier layer can be neglected ($\lambda_L/d \gg 1$ in any case).

Figure 3 shows the $I_C(H)$ patterns with corresponding $I-V$ characteristics of a 3 μm La(5%) doped junction at different current density regions. At 65 K, the critical current density is $j_C=8.5\times10^3$ A/cm^2 corresponding to $w/\lambda_J=0.9$. Therefore the junction is clearly in the short-junction limit. The $I_C(H)$ curve is very similar to the Fraunhofer pattern [see Fig. 3(a)]. Deviations from the ideal Fraunhofer pattern may be attributed to barrier inhomogeneities. The $I-V$ characteristic can be well-described by the RCSJ model and no significant amount of excess current is observed [see Fig. 3(b)].

At 45 K, the critical current density is $j_C=1.1\times10^5$ A/cm^2 corresponding to $w/\lambda_J=3.4$ which means that the junction is in the transition to the long-junction regime. There appears an excess current in the $I-V$ characteristics [see Fig. 3(d)] and the influence of self-field effects can be seen in the $I_C(H)$ curves: the second maxima are suppressed and the central maximum approaches a triangular shape [see Fig. 3(c)].

At 5 K, the current density is $j_C=3.9\times10^5$ A/cm^2 corresponding to $w/\lambda_J=6.4$. The long-junction characteristics are obvious in Figs. 3(e) and 3(f). The $I_C(H)$ characteristic is triangular, the second maxima are nearly completely suppressed as expected for a long junction.[16] Furthermore, there is almost 100% excess current in the $I-V$ characteristic [Fig. 3(f)]. The RCSJ model is not valid anymore.

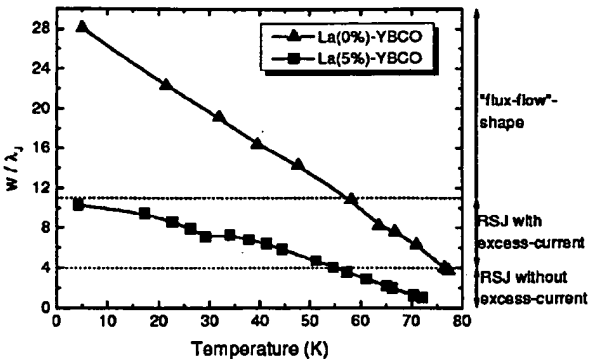

FIG. 4. Temperature dependences of w/λ_J for a 4 μm wide undoped junction and a 3 μm wide La(5%) doped junction. The dotted horizontal lines indicate the w/λ_J ranges where different shapes of the $I-V$ characteristics are observed in the junctions.

Since barrier inhomogeneities may cause additional deviations from a homogeneous current distribution, there is no strict value of w/λ_J for which junctions switch from short junction to long junction behavior. Furthermore, although the ramp geometry is very similar to an overlap junction configuration, the electrodes are in the same plane and the boundary conditions may be different. Therefore a quantitative comparison of our $I_C(H)$ curves to existing calculations is not reasonable.

Nethertheless, some features of the junctions demonstrated in Fig. 3 are typical for all our junctions in the different j_C regions. At $w/\lambda_J\approx4$, excess current becomes significant in the $I-V$ characteristics. Since undoped junctions and La(5%) doped junctions have different current densities, $w/\lambda_J=4$ is obtained at different temperatures. To illustrate this effect, Fig. 4 shows the temperature dependence of w/λ_J for an undoped junction and a La(5%) doped junction. The temperature range can be divided into three regions of w/λ_J. For $w/\lambda_J>4$, excess current becomes significant in the $I-V$ characteristics. For $w/\lambda_J>11$, the $I-V$ characteristics have a positive curvature like flux-flow $I-V$ characteristics. In the case of La(5%) doped junctions, the junctions are RCSJ-like in the whole temperature range, but start to have a significant amount of excess current at 50 K. In the case of undoped junctions, the $I-V$ characteristics show ideal RCSJ behavior only in the vicinity of T_C. Below 55 K, the $I-V$ characteristics are already flux-flow-like. Therefore undoped junctions are not suitable for applications where ideal RCSJ behavior is needed at temperatures below 77 K.

Waldram *et al.* showed that for $w/\lambda_J>4$ a dc supercurrent persists up to large voltages.[17] This supercurrent can be identified with our excess current I_{ex} because the voltage regime where the supercurrent should disappear is not obtained in the $I-V$ characteristics before dissipation in the superconducting electrodes leads to a positive curvature. The amount of additional supercurrent is expected to increase with increasing w/λ_J as experimentally observed in low-temperature-superconductor junctions.[17] Therefore it is reasonable to attribute the increase of the excess current in our junctions with w/λ_J to self-field effects. This is in agreement

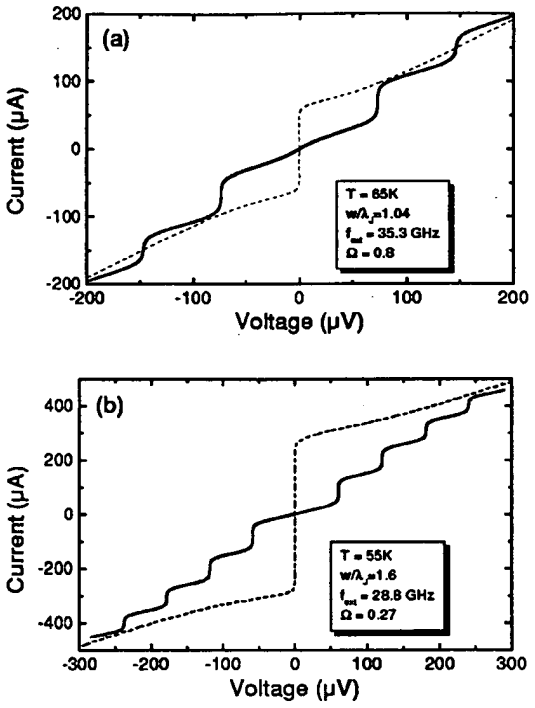

FIG. 5. $I-V$ characteristics of a 3 μm wide La(5%) doped junction (a) at 65 K and (b) at 55 K. The dashed lines are the $I-V$ characteristics without microwave irradiation. The continuous lines correspond to the $I-V$ characteristics at (a) 35.3 GHz and (b) 28.8 GHz.

with the increase of I_{ex}/I_C with decreasing temperature which is observed in our junctions.

Concerning the observation of flux-flow-like $I-V$ characteristics at high current densities ($w/\lambda_J > 11$), heating effects as well as dissipation in the electrodes may be an explanation, especially at high temperatures. Furthermore, the T_C of a possible interlayer with reduced critical temperature may be exceeded in the corresponding temperature regime. However, it is not unreasonable to explain the observation of flux-flow-like $I-V$ characteristics with the dissipation of Josephson vortices in the junctions.

IV. DYNAMIC PROPERTIES

To compare the dynamic properties of our junctions with the RCSJ model at different characteristic frequencies $2eI_CR_N/h$, we investigated the $I-V$ characteristics of our junctions under microwave irradiation at two different temperatures. Since the La(5%) doped junctions are in the short-junction limit for a broader temperature range than the undoped junctions, we measured the microwave response of a La(5%) doped junction at 65 and 55 K.

Figure 5(a) shows the $I-V$ characteristics of a 3 μm wide junction with and without microwave irradiation at 65 K. With $w/\lambda_J = 1.04$, the junction is clearly in the short-junction regime and no significant excess current is visible. The $I-V$ characteristic exhibits well-defined Shapiro steps under microwave irradiation with a frequency f_{ext}. The characteristic voltage I_CR_N is 92 μV which results at $f_{ext} = 35.5$ GHz in a normalized frequency of $\Omega = hf_{ext}/2eI_CR_N = 0.8$.

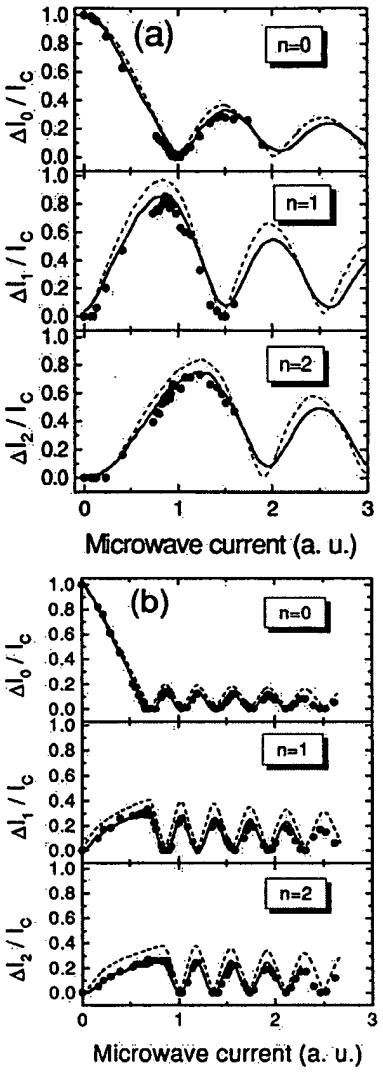

FIG. 6. Dependence of the Shapiro-step heights on the microwave current for $n = 0,1,2$ of the junction shown in Fig. 4. (a) $T = 65$ K and $f_{ext} = 35.3$ GHz. The dashed line shows the simulation without noise for $\Omega = 0.79$ and $\beta_C = 0.1$; the continuous line shows the simulation with noise parameter $\Gamma = 0.036$. (b) $T = 55$ K and $f_{ext} = 28.8$ GHz. The dashed line shows the simulation without noise for $\Omega = 0.23$ and $\beta_C = 0.1$; the continuous line shows the simulation with noise parameter $\Gamma = 0.016$.

Figure 5(b) shows the $I-V$ characteristic of the junction with and without Shapiro steps at 55 K. With $w/\lambda_J = 1.6$, the junction is still in the short-junction regime, but some contribution of excess current to the critical current exists. The characteristic voltage I_CR_N is 270 μV which results at $f_{ext} = 28.8$ GHz in $\Omega = 0.27$.

Figure 6 shows the dependence of the heights of the Shapiro steps on the microwave current at 65 and 55 K. Additionally, in Fig. 6(a) the results of simulations with the RCSJ model with $\Omega = 0.79$ and $\beta_C = 2eI_CR_N^2C/\hbar = 0.1$ (C is the capacitance of the junction) without noise (dashed line) and with the influence of noise (straight line) are plotted. With a noise parameter $\Gamma = 0.036$, the data at 65 K can be well-described with the RCSJ model. At 65 K, the values for Ω and Γ correspond exactly to the values calculated from the

measured $I_C R_N$ product and from thermal fluctuations, $\Gamma = 2ek_BT/\hbar I_C$, respectively.

In Fig. 6(b) the results of simulations with the RCSJ model with $\Omega = 0.23$ and $\beta_c = 0.1$ without noise (dashed line) and with the influence of thermal noise (straight line) are plotted. With a noise parameter $\Gamma = 0.016$, the data can be well-described with the RCSJ model. This value is higher than the noise parameter calculated from thermal fluctuations, $\Gamma = 0.009$, at 55 K. There is also a discrepancy between the $\Omega = 0.27$ determined from the static $I-V$ characteristics and the $\Omega = 0.23$ used for the simulation of the Shapiro steps at 55 K. Therefore at lower temperatures, the values for I_C and R_N determined from the static $I-V$ characteristics are not exactly suitable for the description of the dynamics of the junctions. A possible explanation is that with decreasing temperature additional transport channels influence I_C and R_N but do not contribute to the dynamics of the junctions.

For both investigated internal frequencies, corresponding to temperatures where the junction is in the short-junction regime, the dynamic properties qualitatively can be described with the RCSJ model. For lower temperatures, for which $w/\lambda_J > 4$, we observe subharmonic steps in the $I-V$ characteristics of this junction as predicted for Josephson junctions in the long-junction regime.[17]

V. CURRENT TRANSPORT PROPERTIES

The temperature dependencies of R_N and I_C allow one to draw conclusions to the transport of quasiparticles and Cooper pairs. Therefore we measured $R_N(T)$ and $I_C(T)$ for several undoped and La(5%) doped samples. In Sec. V A we present typical measurements of each junction type. In Sec. V B we propose a model which consistently explains the experimental results.

A. Temperature dependence of I_C and R_N

An important means to draw conclusions to the transport of quasiparticles is to investigate the temperature dependence of the normal resistance of the junctions. Figure 7(a) shows a typical temperature dependence of R_N for a 4 μm wide undoped junction. The resistance decreases with decreasing temperature from T_C to about 40 K as could be expected for a metallic barrier. Below 40 K, the resistance is temperature independent.

The typical temperature dependence of R_N of a La(5%) doped junction can be seen in Fig. 7(b). Similar to the case of undoped junctions, the resistance decreases with decreasing temperature for $T > 50$ K. Below 50 K, there is a striking difference to the undoped junctions, since R_N increases with decreasing temperature.

We analyzed the temperature dependence in the low-temperature regime in more detail. The temperature dependent contribution to the conductivity $\sigma(T) = 1/R_N(T) - 1/R_N(0\ \mathrm{K})$ against the temperature T in a double logarithmic plot can be seen in Fig. 8. In the temperature range from 0 to 50 K, the data points are on a line with the slope 4/3, resulting in

$$\sigma(T)(\Omega^{-1}) = 1/1.38 + 8.1\times 10^{-4}\, T^{4/3}.$$

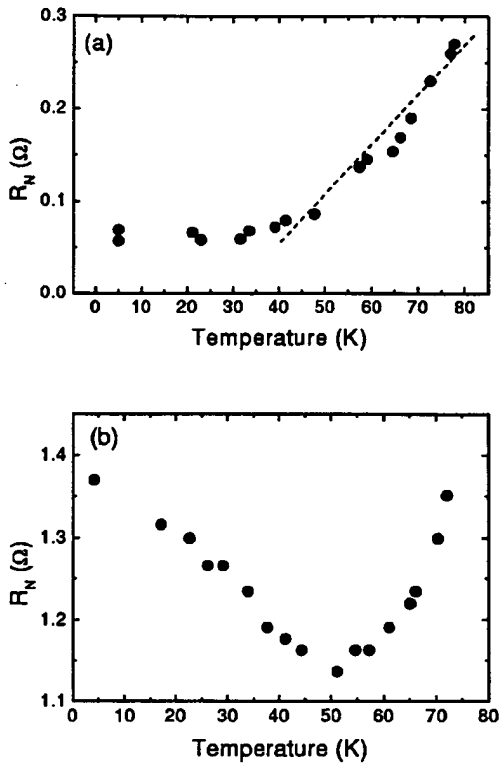

FIG. 7. Temperature dependence of the normal resistance (a) for a 4 μm wide undoped junction and (b) for a 3 μm wide La(5%) doped junction. The dashed line in (a) sketches the linear dependence of R_N between 80 and 40 K.

This behavior can be explained by the Glazman–Matveev theory.[18] Resonant tunneling via one and two localized states leads to the following dependence of I on V:

$$I = [\langle G_1\rangle + \langle G_2(T,0)\rangle + \langle G_2(0,V)\rangle]\cdot V, \tag{1}$$

$$\langle G_2(T,0)\rangle = A\, T^{4/3} \quad \text{for } \mathrm{eV} \ll k_BT, \tag{2}$$

$$\langle G_2(0,V)\rangle = B\, V^{4/3} \quad \text{for } k_BT \ll \mathrm{eV}. \tag{3}$$

The temperature and voltage independent part of the conductivity, G_1, contains the contributions from direct tunneling and tunneling via one localized state. The temperature

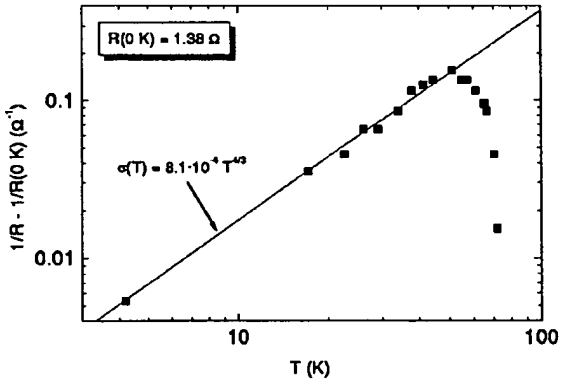

FIG. 8. Temperature dependent contribution to the conductivity of a 3 μm wide La(5%) doped junction in a double logarithmic scale. Straight line: Result of the linear regression of the data points from 0 to 50 K.

and voltage dependent parts, $\langle G_2(T,0)\rangle$ and $\langle G_2(0,V)\rangle$, respectively, are contributions from resonant tunneling via two localized states. These voltage and temperature dependences have been observed for HTS junctions with different barrier materials, e.g., $PrBa_2Cu_3O_7$ (Refs. 19 and 20) and $SrRuO_3$.[21]

The voltage dependence of the normal resistance due to resonant tunneling via two localized states is expected to become visible for $eV>k_BT$ [see Eq. (3)]. In the case of junctions with $PrBa_2Cu_3O_7$ barriers, the voltage dependence was fitted to the Glazman–Matveev theory between 25 and 60 mV at 4.2 K.[20] In the case of our IEJs with a typical R_N of 1 Ω, this corresponds to currents of 25–60 mA, which are in the order of the current densities of the YBCO electrodes. Therefore for high bias currents we observe an increase of the resistivity due to dissipation in the electrodes which dominates a possible decreasing resistivity due to resonant tunneling via two localized states.

Summarizing, the normal resistances of undoped junctions decrease until they saturate at about 40 K. The normal resistances of La(5%) doped junctions as well decrease with decreasing temperature down to 50 K but start to increase with decreasing temperature below 40 K. The temperature dependence of R_N below 40 K can be explained by resonant tunneling via two localized states.

In order to draw conclusions to the transport of Cooper pairs we analyzed the temperature dependence of the critical current. Figure 9 shows typical $I_C(T)$ curves for an undoped [Fig. 9(a)] and a La(5%) doped junction [Fig. 9(b)]. The shapes of the curves are almost linear with an increase of the slope for low temperatures and near T_C. The characteristics cannot be fitted by an exponential law as expected for a superconductor–normal metal–superconductor (SNS) junction[22,23] and do not saturate at low temperatures as expected for a tunnel junction.[24] A so called "quasilinear" temperature dependence of the critical current, similar to our data, was observed for many HTS junctions.[25] For example, the $I_C(T)$ dependences of HTS junctions with Au interlayers were fitted to a superconductor–constriction–superconductor (ScS) model.[26]

For the undoped junctions, the interpretation of the $I_C(T)$ data is difficult because the $I-V$ characteristics are flux-flow-like below 60 K (see Fig. 4). Therefore for the main part of the temperature region below T_C, the critical current may be correlated with the pinning force of vortices and not with the Josephson-coupling energy. Due to these considerations, it is not reasonable to compare the $I_C(T)$ data of the undoped junctions with existing theories for Josephson junctions. Therefore for further analysis we regard only $I_C(T)$ curves of La(5%) junctions.

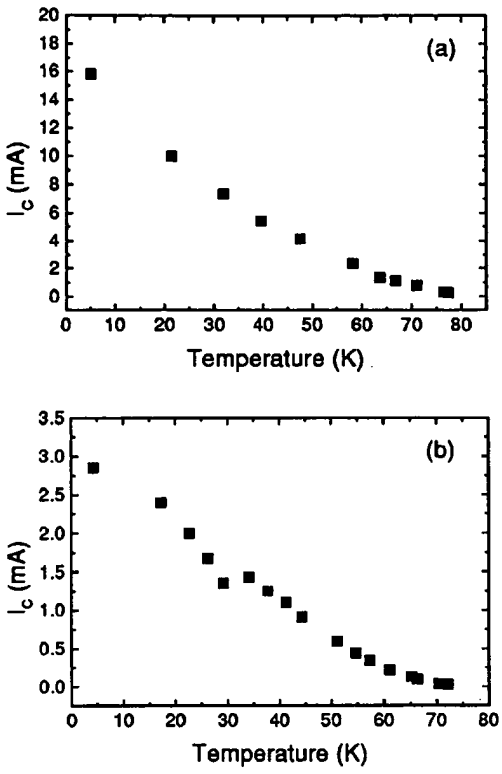

FIG. 9. Temperature dependence of the critical current (a) for a 4 μm wide undoped junction and (b) for a 3 μm wide La(5%) doped junction.

B. Model for the current transport

The temperature dependences of I_C and R_N of undoped and La(5%) doped junctions described in the previous section lead us to a consistent picture of the barrier for both types of junctions which is shown in Fig. 10. The barrier consists of a series connection of an insulator with pinholes (constrictions) and a superconductor with reduced $T_C(S')$. In the equivalent scheme in Fig. 10, it can be seen that there exist several channels in parallel in the insulating region (R_0–R_2 and R_{const}) and one metallic channel (R_{metal}) in the S' layer. The dominant channel in the insulating region depends on the density of constrictions, their diameter, the electrical properties, and the thickness of the insulator. Direct tunneling as well as resonant tunneling are transport mechanisms for the quasiparticles if the insulator contains localized states. Concerning the supercurrent, it is still an open question whether Cooper-pair transport via localized states is possible in HTS junctions or if pair breaking due to Coulomb

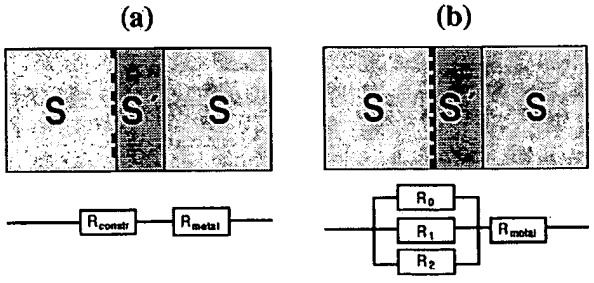

FIG. 10. Scheme of the barrier in the IEJs and equivalent scheme of the quasiparticle conductivity (a) for undoped junctions and (b) La(5%) doped junctions. The barrier consists of an insulator (black area) with pinholes (constrictions) and an S' layer. R_0: resistivity due to direct tunneling; R_1: resistivity due to resonant tunneling via one localized state; R_2: resistivity due to resonant tunneling via two localized states; R_{const}: boundary resistance in the constriction; and R_{metal}: resistivity of the S' layer above its T_C.

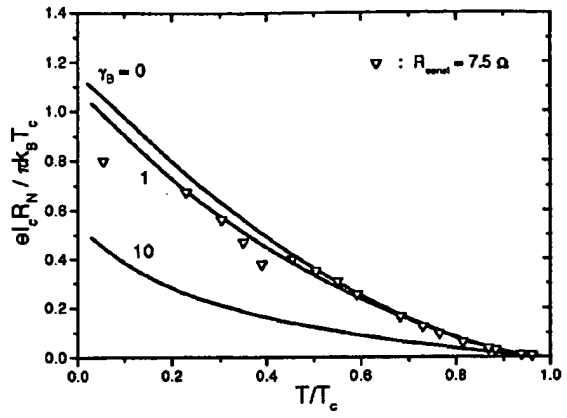

FIG. 11. Comparison of the $I_C(T)$ data of a 3 μm wide La(5%) doped junction with the ScNS model (Ref. 28) Straight lines: Calculation of the normalized I_CR_N in the ScNS model for $D=1$, $d_N/\xi=1$, $\gamma=1$, and $\gamma_B=0,1,10$. ▽: Normalized $I_C(T)R_N$ data with $R_{const}=5.7\,\Omega$ and $T_C=75$ K.

repulsion makes it impossible.[27] In our junctions, it is reasonable to assume that the Cooper-pair transport occurs via the constrictions in the insulator.

For the undoped junctions, no contribution from resonant tunneling via two localized states was observed. Therefore it is reasonable to assume that the density and the diameter of the constrictions allow Cooper-pair as well as quasiparticle transport through the constrictions. The resistivity of the constrictions is so low ($R_{const} \ll R_{0,1,2}$) that the current transport through the insulator can be neglected. At high temperatures, the normal resistance is determined by the resistivity of the S' layer, R_{metal}. Below 40 K, R_{const} exceeds R_{metal} and R_N is determined by the temperature independent interface resistance of the constrictions.

In the case of La(5%) doped junctions, the contribution from resonant tunneling via localized states to the quasiparticle transport can be observed in the temperature dependence of R_N (Fig. 8). This means that the diameter and the density of the constrictions are so small that the resistance of the constriction channels always exceeds the resistivity of the resonant-tunneling channels ($R_{const} \gg R_{0,1,2}$) [Fig. 11(b)].

The Cooper-pair transport occurs only via the constrictions. This enables us to compare the $I_C(T)$ data to calculations of a simplified model which describes the current transport through a series connection of a normal conducting N layer and a constriction (ScNS model).[28] Within this model, the NS sandwich is characterized by the suppression parameters γ, γ_B.[29] These parameters describe the proximity effect in the NS bilayer and are defined as

$$\gamma_B = \frac{R_B}{\rho_N \xi_N}, \quad \gamma = \frac{\rho_S \xi_S}{\rho_N \xi_N},$$

where R_B is the specific resistance of the NS interface, $\rho_{N,S}$ are the normal-state resistivities, and $\xi_{N,S}$ are the coherence lengths of the N and S materials, respectively. These parameters can be understood as follows: The parameter γ_B describes the effect of the boundary transparency between these layers. γ is a measure of the strength of the proximity effect between the N and S metals, i.e., it describes the diffusion of Cooper pairs from S into N across the interface. In our junctions, a nonzero γ also describes that we do not have a sharp NS interface because the ion induced defects will decrease continuously in the superconductor at the interface which leads to a gradually increased order parameter. The constriction is characterized by the transmission coefficient D which accounts for the scattering of Cooper pairs in the constriction.

Figure 11 shows the normalized I_CR_N product calculated for $\gamma=1$ and different values of γ_B. The transparency D is assumed to be $D=1$ because for $D<1$ the curves saturate at low temperatures what is not observed for our data. The shape is similar to the $I_C(T)$ curve of the La(5%) junction in Fig. 9(b). In order to compare our data quantitatively to the model, we would have to take the resistance of the constriction, R_{const}, which we are not able to extract from our experimental $R_N(T)$ data due to the existence of parallel conducting channels.

The open triangles in Fig. 11 show the normalized I_CR_N product of the La(5%) doped junction if we choose $R_{const}=5.7\,\Omega$. The data fit well to the curve corresponding to $\gamma=1$ and $\gamma_B=1$. Similar agreement of our data could be obtained by comparing it to calculations with higher values of γ and γ_B which reduce the normalized I_CR_N product. Because of the ambiguity of estimating R_{const} and the abovementioned fact that the ScNS model only describes a sharp NS interface, it is not reasonable to make a quantitative fit and draw conclusions from the parameters. However, a qualitative agreement of our data to the ScNS model is obtained.

Furthermore, the ScNS model predicts an excess current in the $I-V$ characteristics due to Andreev reflections at the interfaces.[28] As mentioned in Sec. III B, due to self-field effects, a dc supercurrent exists which cannot be discriminated from an excess current due to Andreev reflections. Therefore it is not reasonable to discuss the existence of excess currents in terms of the ScNS model.

In summary, the model for our barrier sketched in Fig. 10 qualitatively describes the $R_N(T)$ dependence and the $I_C(T)$ dependence of the undoped and La(5%) doped junctions. Since we did not observe a material with different lattice constants at the interface in TEM studies, the layers with different electrical properties have to be identified with orthorhombic YBCO with different levels of damage. The fact that the properties of our junctions are stable in time and against O_2-annealing treatments suggests cation disorder instead of disorder in the oxygen sublattice to be the main lattice defect. Especially, the constrictions have to be identified with small areas with undisturbed YBCO in a cation disordered YBCO matrix.

It is difficult to distinguish between an N layer and an S' layer if an additional interface resistance is present, but it is more likely to attribute the metallic properties to an S' layer because YBCO becomes a disordered hopping insulator as soon as T_C is completely suppressed by the presence of defects. This would lead to a strong increase of R_N at low temperatures.

According to our model, the presence of La reduces the density and the diameter of the constrictions. That means that La homogenizes the engineered interface. This is partly

in agreement with the TEM investigations of Wen *et al.*[11] Although they detected a different barrier layer in their IEJs, they also observed a homogenization of their barrier in the presence of La.

VI. SUMMARY

IEJs have been fabricated by using $YBa_2Cu_3O_7$ as well as $YBa_{2-x}La_xCu_3O_7$ for the superconducting electrodes, and the role of La in our fabrication process has been investigated. The critical currents of the La(5%) doped junctions are about one order of magnitude lower as the critical currents of the undoped junctions, and the normal resistances are about one order of magnitude higher. We investigated different concentrations of La and found out that the properties of the junctions cannot be continuously adjusted by the La content, but there exists a threshold value of about 5% for La to influence the junction properties. This shows that La is prerequisite for the modification of the barrier but does not form the barrier by local doping of the interface.

At current densities where the junctions are in the small junction limit, the static $I-V$ characteristics as well as the $I-V$ characteristics under microwave irradiation can be well described with the RCSJ model. The $I_C(H)$ patterns in this regime are similar to the ideal Fraunhofer pattern. Junctions with w/λ_J in the order of 4 exhibit excess currents which can be attributed to self-field effects. In the case of the undoped junctions, the current densities are so high that ideal RCSJ behavior can only be observed near T_C. The La(5%) doped junctions are small junctions above about 50 K and are therefore more suitable for cryoelectronic applications.

The current transport in our junctions can be explained by a barrier consisting of a series connection of an S' layer and an insulator, containing microshorts (constrictions) and localized states. We suggest these layers and the constrictions to be YBCO with different degrees of cation disorder induced by the ion-milling treatment. For the undoped junctions, the resistance of the constrictions is so low that the quasiparticle transport as well as the Cooper-pair transport occurs via the constrictions in the insulator. The presence of La reduces the number density and the diameter of the constrictions. As a result, the quasiparticle-current transport in the La(5%) doped junctions occurs by resonant tunneling via localized states in the insulating layer. Since the $I_C(T)$ dependence can be fitted to an ScNS model, it is reasonable that the Cooper-pair transport occurs via the constrictions and not by resonant tunneling via localized states across the insulator.

ACKNOWLEDGMENT

The work was supported in part by the German DFG Project No. Si 704/1-1.

[1] B. H. Moeckly and K. Char, Appl. Phys. Lett. **71**, 2526 (1997).
[2] B. D. Hunt, M. G. Forrester, J. Talvacchio, and R. M. Young, IEEE Trans. Appl. Supercond. **9**, 3362 (1999).
[3] Y. Soutome, T. Fukazawa, A. Tsukamoto, Y. Tarutani, and K. Takagi, 1999 International Workshop on Superconductivity, Hawaii, Extended Abstracts (1999), p. 113.
[4] A. Fujimaki, K. Kawai, N. Hayashi, M. Horibe, M. Maruyama, and H. Hayakawa, IEEE Trans. Appl. Supercond. **9**, 3436 (1999).
[5] T. Satoh, M. Hidaka, and S. Tahara, IEEE Trans. Appl. Supercond. **9**, 3141 (1999).
[6] R. Dittmann, J.-K. Heinsohn, A. I. Braginski, and C. L. Jia, IEEE Trans. Appl. Supercond. **9**, 3440 (1999).
[7] T. Satoh, J. G. Wen, M. Hidaka, S. Tahara, N. Koshizuka, and S. Tanaka, International Workshop on Superconductivity, Hawaii, Extended Abstracts (1999), p. 199.
[8] W. C. Steward, Appl. Phys. Lett. **12**, 277 (1968); D. E. McCumber, J. Appl. Phys. **39**, 3113 (1968).
[9] Y. Huang, K. L. Merkle, B. H. Moeckly, and K. Char, Physica C **314**, 36 (1999).
[10] C. L. Jia, M. I. Faley, U. Poppe, and K. Urban, Appl. Phys. Lett. **67**, 3635 (1995).
[11] J. G. Wen, N. Koshizuka, S. Tanaka, T. Satoh, M. Hidaka, and S. Tahara, Appl. Phys. Lett. **75**, 2470 (1999).
[12] J.-K. Heinsohn, R. H. Hadfield, and R. Dittmann, Physica C **326–327**, 157 (1999).
[13] C. Horstmann, P. Leinenbach, A. Engelhardt, R. Gerber, C. L. Jia, R. Dittmann, U. Memmert, U. Hartmann, and A. I. Braginski, Physica C **302**, 176 (1998).
[14] A. Marx, K.-H. Husemann, B. Meyer, T. Nissel, R. Gross, M. A. J. Verhoeven, and G. J. Gerritsma, Appl. Phys. Lett. **64**, 241 (1994).
[15] A. P. B. Sinha, I. S. Mulla, and M. R. Chandrachood, in *Chemical and Structural Aspects of High Temperature Superconductors* (World Scientific, Singapore, 1988).
[16] A. Barone and G. Paternó, *Physics and Applications of the Josephson Effect* (Wiley, New York, 1982).
[17] J. R. Waldram, A. B. Pippard, and J. Clarke, Philos. Trans. R. Soc. London, Ser. A **268**, 265 (1970).
[18] L. I. Glazman and K. A. Matveev, Sov. Phys. JETP **67**, 1276 (1988).
[19] M. A. J. Verhoeven, G. J. Gerritsma, H. Rogalla, and A. A. Golubov, Appl. Phys. Lett. **69**, 848 (1996).
[20] A. Engelhardt, R. Dittmann, and A. I. Braginski, Phys. Rev. B **59**, 3815 (1999).
[21] R. Dömel, C. Horstmann, M. Siegel, A. I. Braginski, and M. Yu. Kupriyanov, Appl. Phys. Lett. **67**, 1775 (1995).
[22] P. G. de Gennes, Rev. Mod. Phys. **36**, 225 (1964).
[23] M. Yu. Kupryanov, Sov. J. Low Temp. Phys. **7**, 342 (1981).
[24] V. Ambegaokar and A. Baratoff, Phys. Rev. Lett. **10**, 486 (1963).
[25] K. A. Delin and A. W. Kleinsasser, Supercond. Sci. Technol. **9**, 227 (1996).
[26] M. Bode, M. Grove, M. Siegel, and A. I. Braginski, J. Appl. Phys. **80**, 6378 (1996).
[27] L. I. Glazman and K. A. Matveev, JETP Lett. **49**, 659 (1989).
[28] A. A. Golubov, V. M. Krasnov, and M. Yu. Kupryanov, J. Low Temp. Phys. **106**, 249 (1997).
[29] M. Yu. Kupryanov and V. F. Lukichev, Sov. Phys. JETP **67**, 1163 (1988).

INVITED PAPER Special Issue on Superconductive Devices and Systems

Recent Progress of High-Temperature Superconductor Josephson Junction Technology for Digital Circuit Applications

Jiro YOSHIDA† a), *Member*

SUMMARY Recent progress of high-temperature superconductor Josephson junction technology is reviewed in the light of the future application to digital circuits. Among various types of Josephson junctions so far developed, ramp-edge-type junctions with a barrier layer composed of oxide materials in the vicinity of metal-insulator transition seem to offer a unique opportunity to fulfill all the requirements for digital circuit applications by virtue of their small junction dimensions, overdamped properties and relatively high I_cR_n product values at the temperature of around 30–40 K. Recently developed interface engineered junctions can be classified as junctions of this type. These junctions also raise an interesting problem in physics concerning the possibility of resonant tunneling of Cooper pairs via localized states in the barrier. From the viewpoint of practical applications, the improvement of the spread of the junction parameters is still a serious challenge to the present fabrication technology. Although interface engineered junctions seem to be most promising in this regard at present, 1σ spread of around 8% in the present fabrication technology is far from satisfactory for the fabrication of large-scale integrated circuits. The detailed understanding of the barrier formation mechanism in the interface engineered junction is indispensable not only for advancing this particular fabrication technology but also for improving other junction technology utilizing ramp-edge structures.

key words: *high-temperature superconductors, Josephson junction, SFQ circuit, ramp-edge-type structure, resonant tunneling*

1. Introduction

The development of superior-quality Josephson junctions with high I_cR_n product values is still one of the most important research issues relating to the electronics applications of high-temperature superconductors (HTS). Josephson junctions without hysteresis in their current-voltage characteristics are of particular importance in the construction of ultra-fast digital circuits utilizing a single flux quantum (SFQ) as an information carrier [1]. Among various types of Josephson junctions so far developed, ramp-edge type junctions with an artificial barrier layer schematically shown in Fig. 1 seem to be the most promising candidates for digital circuit applications because of their small dimensions, the potential controllability of junction critical current (I_c) and junction resistance (R_n) values, and the ease of superconducting wiring.

The operation of SFQ logic circuit is based on the transmission and storage of a single flux quantum by superconducting loops which are connected either in series or in parallel. This operation principle results in the inductance L of the superconducting loops in SFQ circuits being restricted according to the inequality $0.5\Phi_0 < LI_c < 1.5\Phi_0$, where Φ_0 denotes the flux quantum ($=h/2e$), and this limits the maximum I_c of Josephson junctions in practical circuits. Even if we adopt a superconducting ground plane technique utilizing c-axis oriented $YBa_2Cu_3O_{7-x}$ (YBCO) films with the London penetration depth of 0.2 μm, it would be difficult to reduce the inductance per unit square L_{sq} of a superconducting microstrip line to less than 0.6 pH. Since the minimum inductance of a practical loop in SFQ circuits is around 3–4 times L_{sq}, the maximum I_c value of a Josephson junction in the circuit should be less than 0.4–0.5 mA. On the other hand, for the reliable operation of an SFQ circuit, I_c must be sufficiently large compared with thermal and quantum fluctuation currents I_T and I_Q, where the fluctuation currents are defined as $I_T=(2\pi/\Phi_0)k_BT$ and $I_Q=(2\pi/\Phi_0)eI_cR_n$, respectively [2]. Thus the requirement that $I_c>>I_T, I_Q$ restricts the maximum operation temperature of SFQ circuits as well as the maximum I_cR_n product value of Josephson junctions usable in a practical circuit.

Another restriction on the maximum I_cR_n product values of Josephson junctions in SFQ circuits arises from the fact that the McCumber-Stewart parameter β_c of a junction should be less than 1 to maintain overdamped characteristics [3]. The condition that $\beta_c<1$ is rewritten as $I_cR_n < \sqrt{\hbar/2eC^{-1/2}}I_c^{1/2}$, where C is the junction capacitance. This relationship is usually fulfilled automatically in junctions with a metallic barrier owing to its inherently small capacitance values. Unfortunately, however, it has been clarified that a high I_cR_n value cannot be expected for such junctions due to their extremely low junction resistance, as is discussed in the later section. Instead, recent interest has fo-

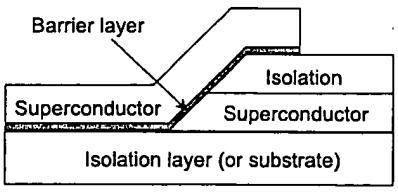

Fig. 1 Schematic representation of ramp-edge-type Josephson junction structure.

Manuscript received June 2, 1999.
Manuscript revised July 19, 1999.

† The authors are with Advanced Materials and Devices Laboratory, Research and Development Center, Toshiba Corporation, Kawasaki-shi, 210-8582 Japan.
a) E-mail: jiro-yoshida@arl.rdc.toshiba.co.jp

cused on junctions with an insulative barrier made of materials in the close vicinity of metal-insulator transition. In such junctions, resonant tunneling via localized states in the barrier is believed to play an important role in determining the junction characteristics [4]. However, the physical nature of the localized states in the barrier and its relevance to Josephson coupling have not been fully understood. Furthermore, there has been growing evidence that the charge transport across interfaces between electrodes and a barrier in a wide variety of junctions suffers from the localized states inevitably formed at the interfaces [5]–[8]. Proper understanding of the mechanism of current transport across a semi-insulative barrier has been one of key issues in the recent development of HTS Josephson junctions.

Another major challenge to HTS Josephson junctions is the uniformity of junction characteristics in a wafer and the reproducibility among wafers. The fabrication of SFQ circuits with reasonable yield requires a strict control of I_c values, say, less than 5% in the standard deviation of I_c for LSIs containing 1000 junctions [9]. Recently, some encouraging results, though not sufficient yet, have been reported for "interface engineered junctions" [10].

The intention of this paper is to review the recent progress of HTS Josephson junction technology for the future application to SFQ circuits operating at an elevated temperature. In this context, I focus on Josephson junctions with an artificial barrier layer and little discussion is given for grain boundary junctions in spite of their practical importance in SQUID applications and many common aspects of underlying junction physics [11].

2. Classification of HTS Josephson Junctions

In the past decade, a wide variety of materials with a resistivity ranging from 10^{-6} to 10^{6} Ωcm have been tested as possible candidates for the barrier layer of HTS Josephson junctions, as shown in Fig. 2. It is known that a material can be classified either as a metal or an insulator depending on whether the material has a finite conductivity at zero temperature or not. The boundary between a metal and an insulator is given by the so-called "minimum metallic conductivity" σ_{min} [12].

In junctions with a metallic barrier, Josephson coupling between two superconducting electrodes originates from the penetration of Cooper pairs into the energy band of the barrier metal, which is known as the proximity effect [13]. Cooper pairs which penetrate into a normal metal can conserve their original phase in the superconducting electrode during the time interval given by $\tau \approx \hbar / k_B T$. Hence, the characteristic length scale ξ_n (normal coherence length) over which an appreciable amount of Cooper pairs exists is given either as $\xi_n = v_F \tau = \hbar v_F / k_B T$ (clean limit) or $\xi_n = \sqrt{D\tau} = \sqrt{\hbar D / k_B T}$ (dirty limit) depending on the electron mean-free-path in the normal metal, where v_F is the Fermi velocity and D denotes the electron diffusion constant. Due to the proximity effect, if the metal barrier thickness does not exceed several ξ_n, a finite number of Cooper pairs exist throughout the barrier, resulting in a supercurrent flow between electrodes. ξ_n in Au at 4.2 K amounts to 100 nm whereas it decreases to less than 10 nm in Co-doped YBCO and in $(Sr,Ca)RuO_3$ at 70 K [14], [15]. Junctions which utilize the proximity effect to create a weak superconducting contact between electrodes are classified as SNS (Superconductor-Normal metal-Superconductor) junctions.

In junctions with a barrier having a resistivity larger than $1/\sigma_{min}$, Cooper pairs can transfer only by tunneling processes. In this sense, it is appropriate to classify all of these junctions as SIS (Superconductor-Insulator-Superconductor) junctions. The Josephson characteristics of an "ideal" SIS junction with a negligible amount of localized states in the barrier are fully understood. The weak superconducting contact in such a junction is established by direct tunneling of Cooper pairs between electrodes. The length scale which characterizes the barrier layer thickness to obtain a useful supercurrent density is determined by the penetration depth a of electron wave functions into the potential barrier, and is given as $a \approx \hbar / \sqrt{2mE_0}$ where m and E_0 are the electron effective mass and the potential barrier height, respectively. In the field of HTS junctions, $NdGaO_3$ and $PrGaO_3$ are thought to be promising candidates for the barrier layer in the "ideal" SIS junction because of their close lattice matching to YBCO [16], [17].

Insulators having a resistivity in the vicinity of $1/\sigma_{min}$ contain a large number of localized states in their bandgap and usually exhibit the variable range hopping conduction at low temperatures [12]. SIS junctions utilizing such a "dirty" insulator barrier show a complex behavior in their transport properties because not only direct tunneling but also resonant tunneling and hopping conduction via a finite number of localized states take place in the barrier layer [18]. The relative importance of each process depends on the barrier thickness, the radius and the density of the localized states, the temperature and the voltage across the electrodes. $PrBa_2Cu_3O_{7-x}$ (PBCO) and doped PBCO are typical examples of this type of barrier material [4], [19]–[22].

Further importance of the "dirty" insulator barrier in the field of HTS Josephson junction technology comes from the fact that high-temperature superconductors themselves lie in the close vicinity of the metal-insulator transition. This implies that an oxygen disorder, cation substitution, lattice dis-

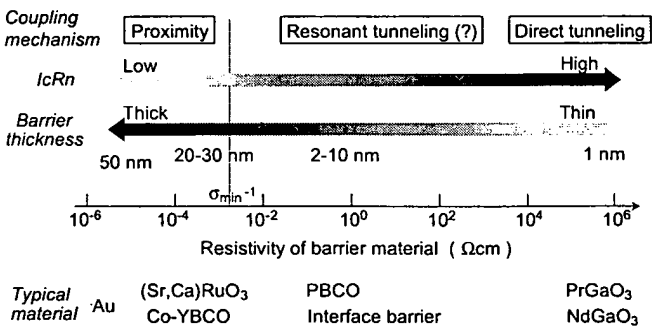

Fig. 2 Classification of high-temperature superconductor Josephson junctions from the viewpoint of the resistivity of the barrier material.

tortion due to stress and strain, or even a disruption of periodic lattice may result in the formation of a thin dirty insulator layer in high-temperature superconductors [6]. It is not difficult to suppose that such an insulator layer is apt to be formed at junction interfaces unless some care is taken to avoid it. In the rather early stage of HTS Josephson junction development, Gross has pointed out that the barrier in grain boundary junctions has the nature of a dirty insulator [23]. Since then, there has been growing evidence that most of the HTS SNS junction characteristics suffer from the unintentional incorporation of an interface layer [7], [8].

In the following sections, we take a brief look at the representative junction characteristics of each type of HTS Josephson junction.

3. Josephson Junctions with a Metallic Oxide Barrier

The Josephson characteristics of an ideal SNS junction can be described by either the Eilenberger equations or the Usadel equations depending on whether the barrier material lies in the clean limit or in the dirty limit [13]. Although these equations can be solved numerically under appropriate boundary conditions which define the actual junction structure, it is not convenient to apply them directly to the analysis of experimental results. Fortunately, simple analytical formulae which describe I_c as functions of the barrier layer thickness and the temperature are known in some cases. In the case of an SNS junction in dirty limit, I_c at the temperature T not far from the critical temperature T_c of the superconducting electrodes can be described as

$$I_c = \frac{1}{R_n}\frac{\pi\Delta^2}{4ek_BT}\sum_{n\geq 0}\frac{8}{\pi^2(2n+1)^2}\frac{\ell_n}{\sinh \ell_n},$$

$$\ell_n = (2n+1)^{1/2}\frac{d}{\xi_n(T)}, \qquad (1)$$

where d is the barrier layer thickness, Δ is the order parameter at the junction interface and ξ_n is the normal coherence length [13]. Equation (1) can be simplified further if the condition that $d >> \xi_n(T)$ is fulfilled as

$$I_c = \frac{1}{R_n}\frac{4\Delta^2}{\pi ek_BT}\frac{d}{\xi_n}\exp\left(-\frac{d}{\xi_n}\right). \qquad (2)$$

Equations (1) and (2) indicate that I_c of an ideal SNS Josephson junction in the dirty limit should exhibit a nearly exponential dependence on both the square root of temperature and the barrier layer thickness in a relatively wide range of temperature. Another feature of SNS junctions is that their normal resistance values are determined simply by the resistivity and the thickness of the barrier. Recently, Delin and Kleinsasser have pointed out that most of the HTS SNS Josephson junctions so far reported do not exhibit the temperature dependence of I_c predicted by the conventional proximity effect theory [24]. The only exceptions are junctions with Ca-doped YBCO [25] or Co-doped YBCO [14] barriers. Other junctions with a barrier material including Au [26], $(La,Sr)CoO_3$ [6], $CaRuO_3$ [27] and $SrRuO_3$ [7], [15] exhibit a quasi-linear temperature dependence of I_c and an anomalously large R_n value, which are apparently beyond the scope of the proximity effect theory. These junction characteristics resemble those of grain boundary junctions, suggesting that some interface layer which governs the junction properties is formed in the junctions.

Char and coworkers have argued that the interface layer originates from the oxygen disorder at the YBCO electrode surface due to stress created by the thermal expansion mismatch between YBCO and the barrier [6]. It is not difficult to suppose that a certain amount of oxygen disorder in YBCO leads to the localization of electrons, resulting in the formation of an insulative barrier. However, it should be pointed out that a thin insulator layer which gives a resistance of as low as 10^{-8} Ωcm^2, that is, the typical value of the resistance observed for the "anomalous SNS junctions," suppresses the proximity effect between the electrode and the metal barrier almost completely [5]. Therefore, if a junction with a metal barrier of around 10 nm in thickness contains such interface layers on both sides of the barrier, we can hardly expect any observable Josephson current to flow across the junction. It is highly probable that the interface layer in the actual "anomalous SNS junctions" is formed only at the interface of one side. This may require another explanation for the formation mechanism of the interface barrier.

The proper proximity effect has been observed for junctions with either a Ca-doped YBCO or Co-doped YBCO barrier [14], [25]. In these junctions, the junction resistance showed a reasonable agreement with the value calculated from the bulk resistivity of the barrier material and the junction geometry. Furthermore, the junction critical current was confirmed to be described well by Eq. (3).

$$I_c = \frac{1}{R_n}\frac{\pi\Delta(0)^2}{4ek_BT_c}\left(1-\frac{T}{T_c}\right)^2\frac{d/\xi_n(T)}{\sinh\left(d/\xi_n(T)\right)}, \qquad (3)$$

where $\Delta(0)$ is the BCS order parameter in YBCO electrodes at 0 K. Equation (3) is an approximation of Eq. (1) under the assumption that the superconductive wave function and its derivative are continuous at the electrode-barrier interfaces [28]. Based on the detailed comparison between the experiment and the theory, Antognazza et al. have derived the conclusion that junctions with a 14% Co-doped YBCO barrier can be classified as SNS junctions in the dirty limit and that the electron diffusion constant in the barrier is D=6.6 cm^2/sec [14]. The consistency of experimental data for Co-doped YBCO barriers with lower doping level as well as for 30% Ca-doped YBCO barrier was less satisfactory . The reason has been ascribed to the erroneous application of the dirty limit theory to these junctions [25].

The work by Antognazza et al. has demonstrated that the Josephson characteristics of HTS SNS junctions without an interface layer can be described quantitatively by the conventional proximity effect theory. At the same time, this clarifies the limitation of HTS SNS junctions for SFQ circuit ap-

plications. It is straightforward to calculate I_cR_n values using Eq. (3) together with the expression for the normal coherence length ξ_n in the dirty limit. The junction resistance in unit area is expressed by

$$R_n = \frac{d}{2e^2N(0)D}, \tag{4}$$

where $N(0)$ is the density of state per spin for electrons at the Fermi energy in the barrier. By choosing $N(0)$ and D to be 1×10^{21} $eV^{-1}cm^{-3}$ and 6.6 cm^2/sec, Eq. (4) gives an R_n value close to those actually observed for 14% Co-doped YBCO barrier junctions.

Table 1 summarizes the calculated I_cR_n and R_n values. Some junctions seem to exhibit a high I_cR_n product value at low temperatures. However, when we look at the R_n values of these junctions, it becomes obvious that we cannot expect such high I_cR_n values for SNS junctions. For example, if we use a 5-nm thick barrier, R_n is of the order of 10^{-10} Ωcm^2. In order to attain an I_cR_n product of 1 mV, the junction critical current density J_c must be of the order of 10^7 A/cm^2, which is close to the critical current density of bulk superconductors. It is highly questionable that a junction with such a high critical current density maintains a sinusoidal current-phase relationship required for proper Josephson characteristics. Furthermore, for HTS SFQ circuit applications, the allowable maximum I_c of the junction is limited to below 0.4–0.5 mA. Even if we adopt a ramp-edge-type geometry, the area of a practical junction would amount to 2×10^{-9} cm^2 (1 μm in junction width and 200 nm in electrode thickness). These restrictions limit the J_c of a junction to less than $2–2.5\times10^5$ A/cm^2. When we apply this criterion to the data listed in Table 1, only the hatched region remains. This simple consideration leads to the conclusion that we cannot expect I_cR_n product values exceeding, say, 0.5 mV for ideal SNS junctions.

A possible way to overcome the low-resistance problem in SNS junctions might be an intentional incorporation of an insulative interface layer in the junctions. In this case, the metallic barrier layer is utilized only as a means to create the interface layer and as long as the barrier layer is thinner than the normal coherence length, it does not play an important role in determining the Junction characteristics except for reducing the order parameter at the interface. Hunt et al. have demonstrated this type of junction by replacing the YBCO base electrode material in 5-nm thick Co-doped YBCO barrier junctions with La-doped YBCO [29]. The average I_cR_n product of 0.3 mV has been attained at 65 K. The spread of I_c in a chip was 13%, which was comparable to the value reported for the low-resistance junctions with a Co-doped YBCO barrier [30].

Table 1 I_cR_n product values (in mV) as a function of barrier thickness (d) and operation temperature (T) expected for HTS SNS Josephson junctions with an ideal junction interface.

d (nm)	T=10 K	T=30 K	T=45 K	T=60 K	T=70 K	R_n (Ωcm^2)
5	14.5	8.0	4.5	2.0	0.9	2.4×10^{-10}
10	14.1	7.5	4.0	1.7	0.7	4.7×10^{-10}
15	13.6	6.6	3.4	1.4	0.6	7.1×10^{-10}
20	12.9	5.7	2.7	1.0	0.4	9.5×10^{-10}
25	12.0	4.7	2.1	0.7	0.3	1.2×10^{-9}
30	11.0	3.8	1.5	0.5	0.2	1.4×10^{-9}

4. Josephson Junctions with an Insulative Barrier Close to the Metal-Insulator Transition

The absence of superconductivity and nonmetallic behavior in $PrBa_2Cu_3O_{7-x}$ (PBCO) make the material an attractive candidate for a barrier in Josephson junctions with YBCO electrodes. Pioneering work on Josephson junctions with a PBCO barrier was first reported by Barner et al. [31] Since then, a considerable number of attempts have been made to create reliable YBCO/PBCO/YBCO Josephson junctions as well as to understand the mechanism of Josephson coupling in them [19]–[22], [32]–[36]. In the early stage of the development, junctions with a PBCO barrier had often been regarded as SNS junctions and analyses based on the proximity effect theory were made to explain the mechanism of Josephson coupling through the relatively thick PBCO barrier layers amounting to several tens of nm [32], [34], [35]. These attempts, however, failed to provide a reasonable explanation, though there still remains some possibility that one-dimensional metallic path along the Cu-O chains or even a superconducting pocket might exist locally in some of the PBCO barriers [37], [38].

The possibility of resonant tunneling of Cooper pairs via localized states with an attractive interaction between electrons in a barrier was first pointed out by Halbritter as an alternative explanation for Josephson coupling in YBCO/PBCO/YBCO junctions [39]. This idea has been extended by Devyatov and Kupriyanov to the theoretical conclusion that the Josephson critical current due to resonant tunneling via localized states with negligible Coulomb repulsion should exhibit the barrier thickness dependence of $\exp(-2d/a)$ as long as the barrier thickness d is far larger than the decay length a of wave function (=the radius of the localized states) in the barrier [40]. Since the junction resistance due to resonant tunneling of quasiparticles obeys the relation $\exp(-d/a)$, this model can give a reasonable explanation for the scaling behavior of I_cR_n with the square root of I_c, which has been observed generally for PBCO barrier junctions [41]. Unfortunately, however, the relation that $I_c \propto \exp(-2d/a)$ is exactly the same as that for Josephson current due to direct tunneling of Cooper pairs. Furthermore, Glazman and Matveev have shown that a similar relation is also valid for resonant tunneling of Cooper pairs via localized states with an infinite Coulomb repulsion energy [42]. Thus the Josephson coupling mechanism in YBCO/PBCO/YBCO junctions has not been fully identified and is often discussed rather controversially. Nevertheless, experimental evidence is accumulating that

YBCO/PBCO/YBCO junction characteristics are governed completely by the charge transport via localized states in the barrier [19]–[22], [33], [36]. In the following, this problem is discussed in detail based on our own experimental results.

We have fabricated YBCO/7% Co-doped PBCO/YBCO junctions with a ramp-edge geometry. The ramp-edge structure was produced using a photoresist mask reflowed after patterning together with Ar ion milling with substrate rotation during etching. The resultant ramp edges had a taper of 20° independently of the edge orientation in a wafer. After etching, the samples were heated to the temperature for the barrier layer deposition by sputtering. An activated oxygen flux from an ECR plasma source was supplied during the heating process. The junction properties were extremely sensitive to a variation in the substrate temperature and the power supplied to the ECR plasma source. We found that junctions fabricated at relatively low temperatures of around 700°C exhibited clear Josephson characteristics even without the deposition of a Co-doped PBCO barrier, indicating that an interface barrier layer was formed naturally during the annealing process. The problem posed by this interface barrier is discussed in Sect. 6 in detail.

In contrast, junctions fabricated at temperatures of around 750°C under a high oxygen flux exhibited Josephson characteristics only when a Co-doped PBCO barrier ranging from 6 to 11 nm in thickness was inserted between two YBCO electrodes. Junctions with a thinner barrier showed flux-flow dominated behavior, which is probably due to the presence of microshorts within the barrier.

Figure 3 shows a set of current-voltage characteristics observed for a junction with a 7.5-nm thick barrier at various temperatures. The junction exhibited RSJ-like characteristics with a small excess current below 50 K, and weak hysteretic behavior was seen at low temperatures (≤10 K). The critical current (I_c) and the junction conductance (G_n) observed at 4.2 K for junctions of 4 μm in width are depicted in Figs. 4 and 5 as functions of the barrier layer thickness. Both I_c and G_n exhibited a nearly exponential dependence on the barrier layer thickness, and the decay parameters determined from the linear regression lines in the figures were 0.59 and 0.96 nm, respectively. The experimental fact that the decay parameter for G_n is almost twice as large as that for I_c can be more clearly seen in the I_cR_n versus I_c plot in Fig. 6. Although the spread of data is still large, an overall tendency can be observed for the I_cR_n values to scale with the square root of I_c.

In order to obtain further insights into the transport processes in our junctions, we measured the temperature dependence of G_n with the barrier layer thickness as a parameter. The results are shown by open squares in Fig. 7. We found that the temperature dependence could be modeled closely

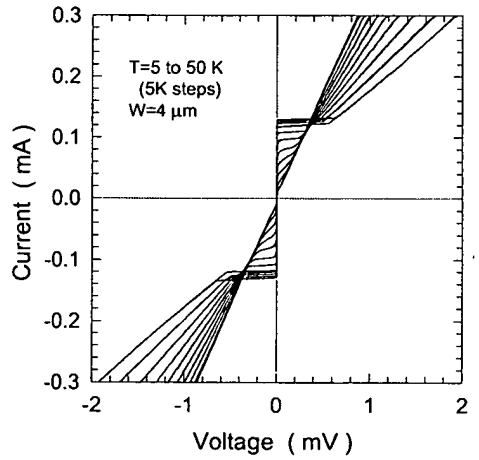

Fig. 3 Current-voltage characteristics observed for a ramp-edge-type Josephson junction with a 7.5-nm thick Co-doped PBCO barrier at various temperatures ranging from 5 to 50 K.

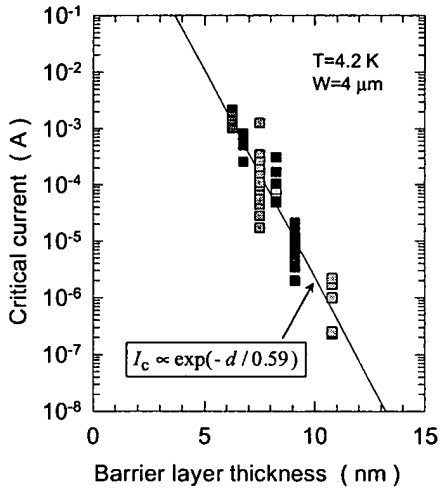

Fig. 4 Critical current versus barrier thickness observed for ramp-edge junctions with a Co-doped PBCO barrier. The decay parameter was estimated to be 0.59 nm from the linear regression line in the figure.

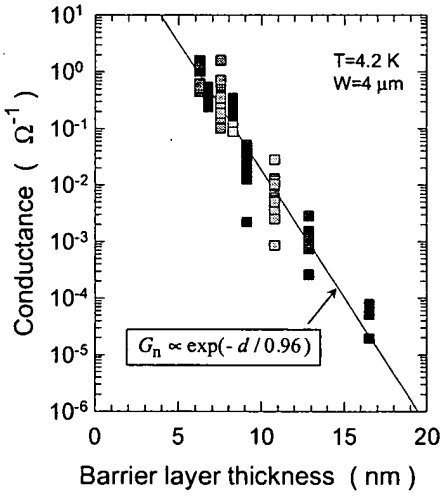

Fig. 5 Junction conductance versus barrier thickness observed for ramp-edge junctions with a Co-doped PBCO barrier. The decay parameter estimated from the linear regression line in the figure is 0.96 nm.

by the following formula:

$$G_n = G_0 + \alpha T^{4/3} + \beta T^{5/2} + \frac{\sigma_0}{d}\exp\left(-\left(\frac{T_0}{T}\right)^{1/4}\right) \quad (5)$$

where T is the temperature, d is the barrier thickness, and other symbols are fitting parameters. The first term in Eq. (5) represents the contribution of tunneling, whereas the second and the third terms correspond to hopping conduction through two and three localized states [18]. The last term denotes variable range hopping process via a large number of localized states. The solid lines in Fig. 7 represent the least-squares fit of the experimental data by Eq. (5). The agreement between the experiment and the calculation is satisfactory. From the fitting, we determined G_0 and α in Eq. (5) to be functions of d. We confirmed that α/d varied exponentially with d with a decay parameter of 1.4 nm. Theoretically, α/d is given as

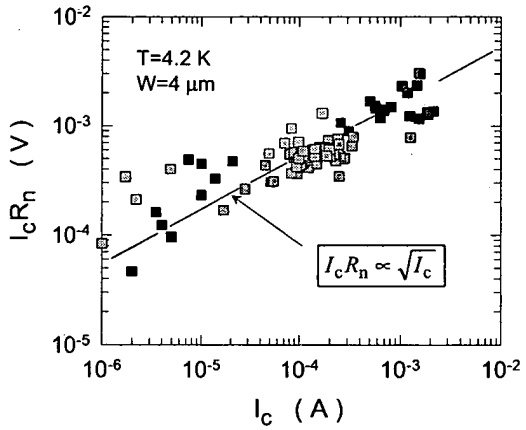

Fig. 6 I_cR_n product versus critical current for junctions with a Co-doped PBCO barrier. The experimental data exhibit an overall tendency for the I_cR_n values to scale with the square root of I_c.

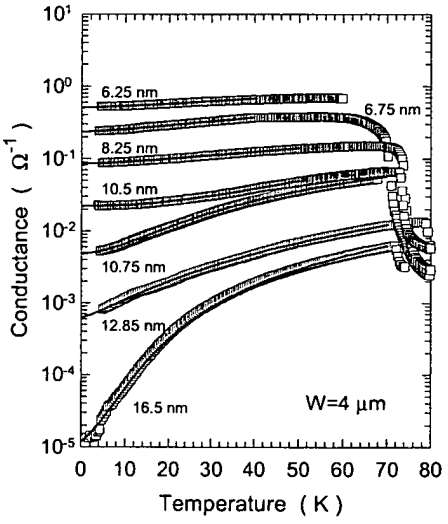

Fig. 7 Temperature dependence of junction conductance observed for junctions with a Co-doped PBCO barrier ranging from 6.25 nm to 16.5 nm. The solid lines are the least-squares fit by Eq. (5).

$$\alpha/d \propto \exp(-2d/3a) \quad (6)$$

where a is the radius of the localized states. The experimental result indicates that a is 0.93 nm. This value is very close to the decay parameter for G_0, indicating that G_0 in our junction is really dominated by resonant tunneling.

The experimental data suggest that the localized states in our Co-doped PBCO barrier is around 1 nm. This implies that the barrier height E_0 is about 38 meV. According to the recent study by Kakinuma and Fueki, high-temperature superconductors can be regarded as a kind of semiconductor doped with impurity, and the gap ΔE between the acceptor level and the top of the valence band becomes zero in YBCO with an oxygen content exceeding 6.5, whereas it remains finite in PBCO [43]. ΔE in PBCO is reported to range from 20 to 120 meV at 100 K depending on the oxygen content. These values are in reasonable agreement with our E_0.

The remaining problem is whether the Josephson current in our junction is consistent with the model based on resonant tunneling of Cooper pairs or not. Since the Coulomb repulsion energy between electrons at a localized states is expressed as $U \approx e^2/\varepsilon_r\varepsilon_0 a$, the value exceeds 160 meV even if we assume a large relative dielectric constant ε_r amounting to 100 in our Co-doped PBCO barrier. This value is far larger than any other energy scales relating to the resonant tunneling phenomenon in our junctions. Therefore, we adopted the theory given by Glazman and Matveev [42].

According to their theory, the possibility of resonant tunneling of Cooper pairs varies with the relation between two time scales: electron tunneling time $\tau_T = \hbar/\Gamma$ ($\Gamma = E_0\exp(-d/a)$) and the correlation time of the electrons in a Cooper pair $\tau_C = \hbar/k_B T_c$, where T_c denotes the transition temperature of superconductive electrodes. In the case of $\tau_T >> \tau_C$, Coulomb repulsion U at the localized states results in a strong suppression of resonant Josephson current. The Josephson critical current at low temperatures under the condition of extremely large U is given as

$$I_c \approx (G_r/\pi e)E_0\left(d/a - \ln(E_0/\Delta)\right)\exp(-d/a) \quad (7)$$

where G_r is the junction conductance due to resonant tunneling and Δ is the superconducting gap energy. We calculated I_c as a function of d based on Eq. (7) by assuming that G_n in Fig. 5 was entirely due to resonant tunneling. The result corresponding to the regression line in Fig. 4 is shown in Fig. 8 together with the prediction by the direct tunneling model. The resonant tunneling model gives a satisfactory agreement with the experimental data. One difficulty in this model, however, is that we have to assume an extremely high density of localized states exceeding 10^{22} eV^{-1} cm^{-3} in order to account for the experimental G_n values. We have not found a reasonable solution to this problem, though the difference between the nominal and the actual barrier layer thickness due to the non-uniform growth of the barrier layer may be a possible explanation. At all events, it should be emphasized that our analysis is based on the theory which takes the large Coulomb repulsion at the localized states into account. We have

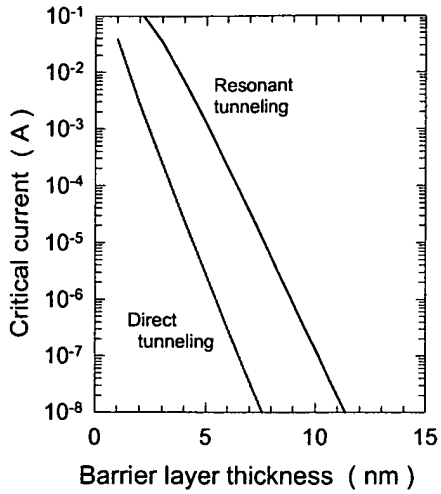

Fig. 8 Theoretical calculation of resonant Josephson current using Eq. (7) under the assumption that the experimental junction conductance shown in Fig. 5 is entirely due to resonant tunneling. The calculated result coincides well with the experimental I_c values shown in Fig. 4.

not found any experimental evidence that the localized states in PBCO possess an anomalous feature like a negative-U center as discussed by Halbritter [39].

The spread of I_c in our present Co-doped PBCO junctions is rather large: amounting to 35% in a chip. Though there is confidential evidence that we can reduce the value at least down to 10% by refining the process conditions [44], it is not clear whether we will be able to find a method to reduce the I_c spread further, say, down to a few % by the simple extension of the present technology. A serious challenge would be a complete step-flow growth of the barrier layer on the ramp edges to guarantee the uniformity in the barrier layer thickness.

5. Josephson Junctions with a Highly Resistive Barrier

The most successful Josephson junction technology in the field of low temperature superconductors is that based on Nb films and an AlO_x tunnel barrier of 1–1.5 nm in thickness. There are a few attempts to create SIS junctions similar to Nb/AlO_x/Nb junctions in the field of HTS. The major difficulty with this approach lies in the fact that it requires an extremely thin barrier layer together with atomically smooth interfaces. Earlier attempts to use MgO [45] and $SrTiO_3$ [46] as the barrier were of limited success and recent interest seems to focus on other perovskite materials such as $NdGaO_3$ and $PrGaO_3$.

Grundler et al. have succeeded in fabricating YBCO ramp-edge-type Josephson junctions with a $NdGaO_3$ barrier layer having a nominal thickness of 2 nm [16]. The junctions exhibited current-voltage characteristics approximately coinciding with the resistively-shunted-junction (RSJ) model. Although the maximum I_cR_n product value of about 5 mV was attained at 4.2 K, the McCumber-Stewart parameter β_c of the junction was rather small at around 13 at the critical current density of the order of 10^4 A/cm^2. The junction capacitance estimated from β_c was 0.15 μF/cm^2, which was more than one order of magnitude smaller than that expected for the 2-nm thick $NdGaO_3$ barrier layer. This small capacitance value together with the low junction resistance of around 3×10^{-7} Ωcm^2 cast a doubt as to whether we can really classify this junction as an SIS junction like a Nb/AlO_x/Nb junction. There remains a possibility that the junction characteristics were not governed by the $NdGaO_3$ barrier itself but by some interface barrier which was formed unintentionally at the junction interface during the fabrication of the ramp-edge structure.

In order to remove the ambiguity concerning the junction interface, which arises more or less inherently in any ramp-edge-type junctions with an ion-milled surface, Tsuchiya et al. have developed YBCO/$PrGaO_3$/YBCO trilayer junctions with a sandwich structure based on precisely controlled *a*-axis oriented YBCO films [17]. The junction with a 2.4 nm thick $PrGaO_3$ barrier exhibited a weakly hysteretic current-voltage characteristic (β_c=3) at 4.2 K and the critical current density and the normal resistance were 8×10^3 A/cm^2 and 3.5×10^{-7} Ωcm^2, respectively. These junction characteristics are similar to those observed for the ramp-edge-type junction with a $NdGaO_3$ barrier. It is difficult to imagine that an insulator such as $NdGaO_3$ or $PrGaO_3$ contains a high density of localized states as is definitely the case with PBCO. Apart from the fact that no indication of superconducting gap has ever been observed for these SIS junctions, which might be ascribed to the unconventional symmetry of order parameters in HTS, we have to seek a reasonable explanation for the low β_c values of the junctions originating from the anomalously low junction resistance and junction capacitance values.

6. Interface Engineered Junctions

A completely new approach to create an artificial barrier layer in ramp-edge-type junctions without the deposition of any barrier materials has recently been demonstrated by Moeckly and Char [10]. The basic idea is to create a thin layer of high-resistivity material on ramp edges by altering the structure or chemistry of the YBCO base electrodes only at the surfaces, which is a loose analogy of the tunnel barrier in Nb/AlO_x/Nb junctions formed by oxidation.

The process to form an interface barrier originated by Moeckly and Char utilizes low-temperature annealing of YBCO ramp edges at 400–600°C in vacuum for 30 minutes followed by plasma treatment of the surface for several minutes in 10–100 mTorr Ar/O_2 mixture gas. The counter YBCO electrode is then deposited by laser ablation without breaking vacuum. Junctions fabricated by this rather simple process have exhibited clear Josephson characteristics coinciding well with the RSJ model, and the junction characteristics have been confirmed to be adjustable by varying the gas pressure and rf power during the plasma treatment. I_cR_n values ranging from 0.5 to 3 mV with corresponding R_n values of 6×10^{-8}–1.2×10^{-9} Ωcm^2 at 20 K have been reported. The most

significant feature of such interface engineered junctions is that they display a good uniformity in junction characteristics in spite of their relatively early stage of development. The 1σ spread in I_c of 7.8% and a spread in R_n of 3.5% over 10 junctions in a chip are far superior to those reported for any other junctions with an artificial barrier [47].

The high uniformity of the interface engineered junctions has been verified further by the subsequent work by Satoh and his co-workers [48], though the detail of their fabrication process differs considerably from that developed by Moeckly and Char. Satoh and his co-workers employed $(La_{0.3}Sr_{0.7})(Al_{0.65}Ta_{0.35})O_3$ (LSAT) as the substrate and the interlayer isolation material in the ramp-edge-type junctions. They found that a conventional ion-milling process to form the ramp-edge structure alone was sufficient to create an interface layer which acts as a barrier in Josephson junctions. A puzzling fact is that the junctions fabricated by the same process using $SrTiO_3$ as the substrate and the isolation layer material have not displayed Josephson characteristics. This experimental fact led them to the conclusion that a slight inclusion of La atoms at the interface during the ion-milling process enhanced the formation of the interface barrier layers. No evidence of this, however, has been verified yet. The spread in I_c of this new type of interface engineered junction is as low as 1σ=8% for 100-junction array in a chip at 4.2 K.

The structure and the chemical composition of the barrier at the interface are still the subjects of intensive investigations [49]. Transmission electron microscopy (TEM) and microanalysis have revealed that a well-crystallized material with cubic or pseudo-cubic symmetry of around 2–3 nm in thickness covers the ramp-edge surfaces continuously without any detectable pinholes. The lattice parameter of the cubic or pseudo-cubic material, however, differs between junctions; it is 0.51 nm for the junctions by Moeckly and Char and 0.41–0.43 nm for the junctions by Satoh et al. [50]. Both of these lattice parameters are different from that of YBCO

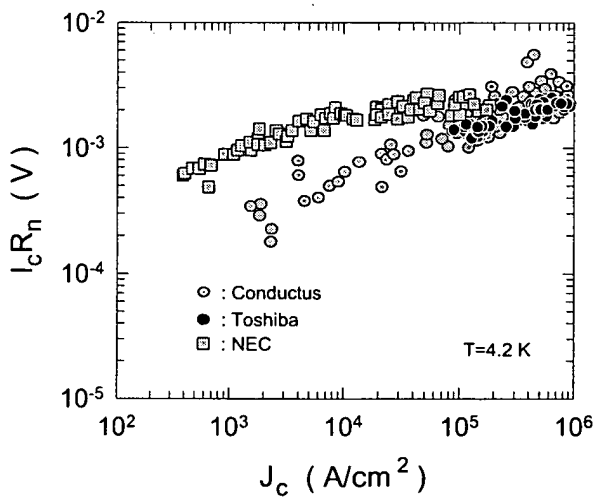

Fig. 9 I_cR_n product values of interface engineered junctions as a function of the critical current density observed by three independent research groups.

with cubic symmetry which has previously been discovered to be formed on an ion-milled YBCO film surface after annealing [51]. Furthermore, it has been becoming evident that the chemical composition of the interface barrier layer differs considerably from that of stoichiometric YBCO [50]. Further investigation is definitely required to clarify the barrier layer formation mechanism.

Interface engineered junctions with a relatively large R_n value have exhibited a slight increase in R_n with decreasing temperature as well as a nonlinear behavior in their current-voltage characteristics at high voltages [10]. These features are similar to those observed for Josephson junctions with a PBCO barrier, indicating that the localized states in the barrier play some role in determining the junction properties. Figure 9 summarizes I_cR_n values of interface engineered junctions as functions of J_c reported by three independent research groups [47], [52], [53]. We can see an overall tendency that the I_cR_n values gradually increase with an increase in J_c at the region of relatively low J_c and then saturate at 2–3 mV in higher J_c. We can conceive two plausible explanations for such a behavior in the I_cR_n versus I_c characteristic.

One possibility is that the charge transport in the interface engineered junctions is governed entirely by resonant tunneling. In this case, as long as the barrier thickness is sufficiently large compared with the radius of the localized states, I_cR_n values vary with the square root of I_c, as discussed in Sect. 4. However, if the barrier thickness becomes sufficiently small to satisfy the condition τ_T (electron tunneling time) << τ_C (correlation time of a Cooper pair), the probability that two electrons in a Cooper pair can tunnel through the barrier separately in time without the loss of the pair correlation increases [42]. In such a case, the Josephson current does not suffer a suppression due to the Coulomb repulsion, and the critical current can be expressed as

$$I_c = (\pi\Delta / 2e)G_r \ . \tag{8}$$

Comparison of Eqs. (7) and (8) shows that the relationship that $I_cR_n \propto \sqrt{I_c}$ changes to a new one in which I_cR_n=constant with decreasing the barrier layer thickness. The saturation behavior seen in the I_cR_n versus J_c plot may be an indication of this crossover in the barrier thickness dependence of resonant Josephson current.

An alternative explanation may be a crossover of transport mechanism from resonant tunneling to direct tunneling with a decrease in the barrier layer thickness. This type of crossover should accompany the change in the barrier thickness dependence of the junction conductance. Unfortunately, we do not have data to correlate the J_c and R_n values with the thickness of the interface barrier layer at present. In either case, we have to assume a reduced order parameter value at the junction interface in order to account for the experimental I_cR_n values.

7. Conclusion

Recent progress in the fabrication technology and understand-

ing of junction physics has made it possible to design a realistic specification of HTS Josephson junctions for SFQ circuit applications. In HTS SFQ circuits, the maximum I_c value of the Josephson junction is restricted to around 0.4 mA. This corresponds to J_c of 2×10^5 A/cm^2 for 1-μm wide ramp-edge-type junctions with 200-nm thick superconducting electrodes. Such a J_c value has already been obtained in junctions with a PBCO barrier of around 6 nm in thickness as well as in interface engineered junctions, at least at 4.2 K. It is feasible to attain the same J_c value at higher temperatures, say, at 30–40 K, which may be a reasonable upper limit for operating SFQ circuits without a significant increase in the probability of thermally-induced bit errors.

The capacitance C in ramp-edge-type Josephson junctions has not been analyzed as fully as other device parameters such as J_c and R_n. For bulk PBCO, a relative dielectric constant of around 20 seems to be a good estimate [54]. If we adopt this value as a typical one in insulative oxides with a high density of localized states, the capacitance of a 5-nm thick PBCO barrier junction and that of an interface engineered junction with a 2-nm thick barrier are calculated to be 3.5×10^{-6} F/cm^2 and 8.7×10^{-6} F/cm^2, respectively. Only those junctions which fulfill the condition that the McCumber-Stewart parameter is less than one can be utilized in the construction of an SFQ circuit. This condition together with the J_c and C values estimated above determines the maximum I_cR_n product of HTS Josephson junctions for SFQ circuit applications to be 2.7–4.3 mV. The performance of some interface engineered junctions has already been approaching these specifications.

The improvement of the spread of the junction parameters is a serious challenge to the present fabrication technology. Although interface engineered junctions seem to be most promising also in this regard, 1σ spread of around 8% in the present fabrication technology is still far from satisfactory for realizing HTS SFQ LSIs. The identification of the material composing the interface barrier and understanding of its formation mechanism are the most important issues and need to be addressed urgently.

The integration of Josephson junctions into SFQ circuits requires a multilayer process which can incorporate a superconducting ground plane to minimize circuit inductances. Several attempts have already been made to establish such a process and promising results indicating that the incorporation of a ground plane either underneath or over a Josephson junction does not affect the junction characteristics have been reported [55]–[58]. Further efforts, however, are definitely required to reduce the defects in the multilayers significantly compared with those at the present technological level in order to fabricate HTS SFQ LSIs with a reasonable yield.

Acknowledgment

A part of this work was supported by the New Energy and Industrial Technology Development Organization (NEDO) as a part of its Research and Development of Fundamental Technologies for Superconductor Applications Project under the New Sunshine Program administered by the Agency of Industrial Science and Technologies of the Ministry of International Trade and Industry (M.I.T.I.) of Japan through International Superconductivity Technology Center (ISTEC).

References

[1] K.K.Likharev and V.K.Semenov, "RSFQ logic/memory family: A new Josephson-junction technology for sub-terahertz-clock-frequency digital systems," IEEE Trans Appl. Supercond., vol.1, no.1, pp.3-28, March 1991.

[2] V.K.Semenov, T.V.Filippov, Yu.A.Polyakov, and K.K.Likharev, "SFQ balanced comparators at a finite sampling rate," IEEE Trans. Appl. Supercond., vol.7, no.2, pp.3617-3621, June 1997.

[3] T.Van Duzer and C.W.Turner, Principles of Superconductive Devices and Circuits, Chapt. 5, Elsevier North Holland, New York, 1981.

[4] J.Yoshida and T.Nagano, "Tunneling and hopping conduction via localized states in thin $PrBa_2Cu_3O_{7-x}$ barriers," Phys. Rev. B, vol.55, no.17, pp.11860-11871, May 1997.

[5] J.Yoshida, T.Hashimoto, S.Inoue, Y.Mizutani, M.Sagoi, and K.Mizushima, "Josephson effect in $YBa_2Cu_3O_7$/Au-Ag/Pb junctions," Jpn. J. Appl. Phys., vol.31, no.6A, pp.1771-1777, June 1992.

[6] K.Char, L.Antognazza, and T.H.Geballe, "Study of interface resistances in epitaxial $YBa_2Cu_3O_{7-x}$/barrier/$YBa_2Cu_3O_{7-x}$ junctions," Appl. Phys. Lett., vol.63, no.17, pp.2420-2422, Oct. 1993.

[7] R.Domel, C.Horstmann, M.Siegel, A.I.Braginski, and M.Y.Kupriyanov, "Resonant tunneling transport across $YBa_2Cu_3O_7$-$SrRuO_3$ interfaces," Appl. Phys. Lett., vol.67, no.12, pp.1775-1777, Sept. 1995.

[8] L.Antognazza, K.Char, and T.H.Geballe, "Conductance-voltage characteristics of interface between $YBa_2Cu_3O_7$ and metallic oxides," Appl. Phys. Lett., vol.68, no.7, pp.1009-1011, Feb. 1996.

[9] D.L.Miller, J.X.Przybysz, and J.H.Kang, "Margins and yields of SFQ circuits in HTS materials," IEEE Trans. Appl. Supercond., vol.3, no.1, pp.2728-2731, March 1993.

[10] B.H.Moeckly and K.Char, "Properties of interface-engineered high T_c Josephson junction," Appl. Phys. Lett., vol.71, no.17, pp.2526-2528, Oct. 1997.

[11] R.Gross, L.Alff, A.Beck, O.M.Froehlich, D.Koelle, and A.Marx, "Physics and technology of high temperature superconducting Josephson junctions," IEEE Trans. Appl. Supercond., vol.7, no.2, pp.2929-2935, June 1997.

[12] N.F.Mott, Metal-insulator transitions, Chapt. 1, Tayler & Francis LTD, London, 1974.

[13] K.K.Likharev, "Superconducting weak links," Rev. Mod. Phys., vol.51, no.1, pp.101-159, Jan. 1979.

[14] L.Antognazza, S.J.Berkowitz, T.H.Geballe, and K.Char, "Proximity effect in $YBa_2Cu_3O_{7-\delta}$/$YBa_2(Cu_{1-x}Co_x)_3O_{7-\delta}$/$YBa_2Cu_3O_{7-\delta}$ junctions: From the clean limit to the dirty limit with pair breaking," Phys. Rev. B, vol.51, no.13, pp.8560-8563, April 1995.

[15] L.Antognazza, K.Char, T.H.Geballe, L.L.H.King, and W.Sleight, "Josephson coupling of $YBa_2Cu_3O_{7-x}$ through a ferromagnetic barrier $SrRuO_3$," Appl. Phys. Lett., vol.63, no.7, pp.1005-1007, Aug. 1993.

[16] D.Grundler, J.P.Krumme, B.David, and O.Dossel, "$YBa_2Cu_3O_7$ ramp-type junctions and superconducting quantum interference devices with an ultra thin barrier of $NdGaO_3$," Appl. Phys. Lett., vol.65, no.14, pp.1841-1843, Oct. 1994.

[17] R.Tsuchiya, M.Kawasaki, H.Kubota, J.Nishino, H.Sato, H.Akoh, and H.Koinuma, "$YBa_2Cu_3O_{7-\delta}$ trilayer junctions with nm thick $PrGaO_3$ barrier," Appl. Phys. Lett., vol.71, no.11, pp.1570-1572, Sept. 1997.

[18] L.I.Glazman and K.A.Matveev, "Inelastic tunneling across thin

amorphous films," Sov. Phys. JETP, vol.67, no.6, pp.1276-1282, June 1998.

[19] T.Satoh, M.Yu.Kupriyanov, J.S.Tsai, M.Hidaka, and T.Tsuge, "Resonant tunneling transport in YBaCuO/PrBaCuO/YBaCuO edge-type Josephson junctions," IEEE Trans. Appl. Supercond., vol.5, no.2, pp.2612-2615, June 1995.

[20] M.A.J.Verhoeven, G.J.Gerritsma, H.Rogalla, and A.A.Golubov, "Ramp-type junction parameter control by Ga doping of $PrBa_2Cu_3O_{7-\delta}$ barriers," Appl. Phys. Lett., vol.69, no.6, pp.848-850, Aug. 1996.

[21] J.Yoshida, T.Nagano, and T.Hashimoto, "Current transport and electronic states in *a,b*-axis-oriented $YBa_2Cu_3O_7/PrBa_2Cu_3O_7/YBa_2Cu_3O_7$ sandwich-type junctions," Phys. Rev. B, vol.53, no.13, pp.8623-8631, April 1996.

[22] M.Horibe, N.Hayashi, K.Kawai, M.Maruyama, A.Fujimaki, and H.Hayakawa, "Systematic investigations of ramp edge junction using Ca-doped and Ga-doped PBCO barrier," to be published in IEEE Trans. Appl. Supercond.

[23] R.Gross and B.Mayer, "Transport processes and noise in $YBa_2Cu_3O_{7-\delta}$ grain boundary junctions," Physica C, vol.180, no.1-4, pp.235-241, Sept. 1991.

[24] K.A.Delin and A.W.Kleinsasser, "Comparative study of the stationary properties of high-T_c proximity-coupled Josephson junctions," IEEE Trans. Appl. Supercond., vol.5, no.2, pp.2976-2979, June 1995.

[25] L.Antognazza, B.H.Moeckly, T.H.Geballe, and K.Char, "Properties of high-T_c Josephson junctions with $Y_{0.7}Ca_{0.3}Ba_2Cu_3O_{7-\delta}$ barrier layers," Phys. Rev. B, vol.52, no.6, pp.4559-4567, Aug. 1995.

[26] R.H.Ono, J.A.Beall, M.W.Cromer, T.E.Harvey, M.E.Johansson, C.Reintsema, and D.A.Rudman, "High-T_c superconductor-normal metal-superconductor Josephson microbridges with high-resistance normal metal links," Appl. Phys. Lett., vol.59, no.9, pp.1126-1128, Aug. 1991.

[27] K.Char, M.S.Colclough, T.H.Geballe, and K.E.Myers, "High T_c superconductor-normal-superconductor Josephson junctions using $CaRuO_3$ as the metallic barrier," Appl. Phys. Lett., vol.62, no.2, pp.196-198, Jan. 1993.

[28] P.G.DeGennes, "Boundary effects in superconductors," Rev. Mod. Phys., vol.36, no.1, pp.225-237, Jan. 1964.

[29] B.D.Hunt, M.G.Forrester, J.Talvacchio, and R.M.Young, "High-resistance SNS edge junctions," Ext. Abst. 6th Int. Superconductive Electronics Conference, vol.2, pp.64-66, Berlin, Germany, June 1997.

[30] B.D.Hunt, M.G.Forrester, J.Talvacchio, R.M.Young, and J.D.McCambridge, "High-T_c SNS edge junctions with integrated $YBa_2Cu_3O_x$ groundplanes," IEEE Trans. Appl. Supercond., vol.7, no.2, pp.2936-2939, June 1997.

[31] J.B.Barner, C.T.Rogers, A.Inam, R.Ramesh, and S.Bersey, "All a-axis oriented $YBa_2Cu_3O_{7-x}$-$PrBa_2Cu_3O_{7-z}$-$YBa_2Cu_3O_{7-y}$ Josephson devices operating at 80 K," Appl. Phys. Lett., vol.59, no.6, pp.742-744, Aug. 1991.

[32] T.Hashimoto, M.Sagoi, Y.Mizutani, J.Yoshida, and K.Mizushima, "Josephson characteristics in a-axis oriented $YBa_2Cu_3O_{7-\delta}/PrBa_2Cu_3O_{7-\delta}/YBa_2Cu_3O_{7-\delta}$ junctions," Appl. Phys. Lett., vol.60, no.14, pp.1756-1758, April 1992.

[33] Yu.Boguslavskij, J.Gao, A.J.H.M.Rijnders, D.Terpstra, G.J.Gerritsma, and H.Rogalla, "Transport processes in $YBa_2Cu_3O_x/PrBa_2Cu_3O_x/YBa_2Cu_3O_x$ ramp type Josephson junctions," Physica C, vol.194, no.3, 4, pp.268-276, May 1992.

[34] T.Umezawa, D.J.Lew, S.K.Streiffer, and M.R.Beasley, "Josephson coupling in a-axis $YBa_2Cu_3O_{7-\delta}/Pr_{1-x}Y_xBa_2Cu_3O_{7-\delta}/YBa_2Cu_3O_{7-\delta}$ sandwich-type junctions," Appl. Phys. Lett., vol.63, no.23, pp.3221-3223, Dec. 1993.

[35] H.Sato, H.Akoh, and S.Takada, "Anisotropic Josephson effect in all (103)-oriented $YBa_2Cu_3O_{7-\delta}/PrBa_2Cu_3O_{7-\delta}/YBa_2Cu_3O_{7-\delta}$ junction," Appl. Phys. Lett., vol.64, no.10, pp.1286-1288, March 1994.

[36] Y.Sawada, H.Terai, A.Fujimaki, Y.Takai, and H.Hayakawa, "Transport properties of YBCO/PBCO/YBCO junctions," IEEE Trans. Appl. Supercond., vol.5, no.2, pp.2099-2102, June 1995.

[37] M.Lee, Y.Suzuki, and T.H.Geballe, "Coexistence of metallic and nonmetallic charge transport in $PrBa_2Cu_3O_7$," Phys. Rev. B, vol.51, no.21, pp.15619-16662, June 1995.

[38] H.A.Blackstead, J.D.Dow, D.B.Chrsey, J.S.Horwitz, M.A.Black, P.J.McGinn, A.Klunzinger, and D.B.Pulling, "Observation of superconductivity in $PrBa_2Cu_3O_7$," Phys. Rev. B, vol.54, no.9, pp.6122-6125, Sept. 1996.

[39] J.Halbritter, "Pair weakening and tunnel channels at cuprate interfaces," Phys. Rev. B, vol.46, no.22, pp.14861-14871, Dec. 1992.

[40] I.A.Devyatov and M.Y.Kupriyanov, "Resonant tunneling and long-range proximity effect," JETP Lett., vol.59, no.3, pp.200-205, Feb. 1994.

[41] H.Akoh, H.Sato, N.Nakamura, and S.Takada, "Scaling behavior of YBaCuO/PrBaCuO/YBaCuO trilayer Josephson junctions," Jpn. J. Appl. Phys., vol.33, no.6A, pp.L766-L768, June 1994.

[42] L.I.Glazman and K.A.Matveev, "Resonant Josephson current through Kondo impurities in a tunnel barrier," JETP Lett., vol.49, no.10, pp.659-662, May 1989.

[43] K.Kakinuma and K.Fueki, "Electronic structure of $Pr_{1-x}Y_xBa_2Cu_3O_y$ (x=0, 0.5, and 1.0)," Phys. Rev. B, vol.56, no.6, pp.3494-3507, Aug. 1997.

[44] T.Satoh, M.Hidaka, and S.Tahara, "Fabrication process for high-T_c superconducting integrated circuits based on edge-type Josephson junctions," IEICE Trans. Electron., vol.E81-C, no.10, pp.1532-1539, Oct. 1998.

[45] R.R.Robertazzi, R.H.Koch, R.B.Laibowitz, and W.J.Gallagher, "$Y_1Ba_2Cu_3O_7/MgO/Y_1Ba_2Cu_3O_7$ edge Josephson junctions," Appl. Phys. Lett., vol.61, no.6, pp.711-713, Aug. 1992.

[46] R.B.Laibowitz, J.Z.Sun, V.Foglietti, W.J.Gallagher, and R.H.Koch, "High-T_c multilevel edge junction superconducting quantum interference devices with $SrTiO_3$ barriers operating at 77 K," Appl. Phys. Lett., vol.64, no.2, pp.247-249, Jan. 1994.

[47] B.H.Moeckly and K.Char, "Interface engineered high-T_c Josephson junctions," Ext. abst. 6th International Superconductive Electronics Conference, vol.1, pp.8-10, Berlin, Germany, June 1997.

[48] T.Satoh, M.Hidaka, and S.Tahara, "High-temperature superconducting edge-type Josephson junctions with modified interfaces," IEEE Trans. Appl. Supercond., vol.9, no.2, pp.3141-3144, June 1999.

[49] Y.Huang, K.L.Merkle, B.H.Moeckly, and K.Char, "The effect of microstructure on the electrical properties of YBCO interface-engineered Josephson junctions," Physica C, vol.314, no.1, 2, pp.36-42, March 1999.

[50] J.G.Wen, T.Satoh, M.Hidaka, S.Tahara, and N.Koshizuka, unpublished.

[51] C.L.Jia, M.I.Faley, U.Poppe, and K.Urban, "Effect of chemical and ion-beam etching on the atomic structure of interfaces in $YBa_2Cu_3O_7/PrBa_2Cu_3O_7$ Josephson junctions," Appl. Phys. Lett., vol.67, no.24, pp.3635-3637, Dec. 1995.

[52] T.Satoh, M.Hidaka, and S.Tahara, unpublished.

[53] S.Inoue, T.Nagano, H.Sugiyama, and J.Yoshida, unpublished.

[54] F.M.Saba, T.Utagawa, K.Tanabe, and Y.Enomoto, "Temperature-dependent dielectric properties of $PrBa_2Cu_3O_{7-\delta}$ films," Advances in superconductivity, eds. X, K. Osamura and I. Hirabayashi, vol.2, pp.1069-1072, Springer-Verlag, Tokyo, 1998.

[55] B.D.Hunt, M.G.Forrester, J.Talvacchio, J.D.McCambridge, and R.M.Young, "High-T_c SNS edge junctions and SQUIDs with integrated groundplanes," Appl. Phys. Lett., vol.68, no.26, pp.3805-3807, June 1996.

[56] W.H.Mallison, S.J.Berkowitz, A.S.Hirahara, M.J.Neal, and K.Char, "A multilayer $YBa_2Cu_3O_x$ Josephson junction process for digital circuit applications," Appl. Phys. Lett., vol.68, no.26, pp.3808-3810, June 1996.

[57] H.Terai, M.Hidaka, T.Satoh, and S.Tahara, "Direct injection high-T_c dc-SQUID with an upper $YBa_2Cu_3O_{7-x}$ groundplane," Appl. Phys. Lett., vol.70, no.20, pp.2690-2692, May 1997.

[58] T.Hashimoto, S.Inoue, T.Nagano, and J.Yoshida, "Design and fabrication of a voltage divider utilizing high-T_c ramp-edge Josephson junctions with a ground plane," IEEE Trans. Appl. Supercond., vol.9, no.2, pp.3821-3824, June 1999.

Jiro Yoshida received the B.S., M.S. and Dr.Sc. degrees in physics from the University of Tokyo, Tokyo, Japan in 1974, 1976 and 1979, respectively. In 1979, he joined the Research and Development Center, Toshiba Corporation, Kawasaki, Japan, and is currently a Chief Research Scientist at the Advanced Materials and Devices Laboratory. His initial research at Toshiba was to develop novel semiconductor devices based on Si and GaAs technology. He started the research of superconductive devices in 1988. His current research interests center on the fabrication and characterization of high-T_c Josephson junctions and their SFQ circuit applications. Dr. Yoshida is a member of the Japan Society of Applied Physics, the Physical Society of Japan, the Materials Research Society, and the Institute of Electrical and Electronics Engineers.

Atomic structure and composition of the barrier in the modified interface high-T_c Josephson junction studied by transmission electron microscopy

J. G. Wen, N. Koshizuka, and S. Tanaka
Superconductivity Research Laboratory, ISTEC, 1-10-13 Shinonome, Koto-ku 135-0062, Tokyo, Japan

T. Satoh, M. Hidaka, and S. Tahara
Fundamental Research Laboratory, NEC Corporation, 34 Miyukigaoka, Tsukuba, Ibaraki 305-8501, Japan

(Received 14 June 1999; accepted for publication 17 August 1999)

The atomic structure and composition of modified interface junctions which showed reproducible critical current I_c ($I_c 1\sigma < 8\%$ for 100 junctions) are investigated by transmission electron microscopy. Transmission electron microscopic observations show the existence of a thin barrier (1–2 nm) homogeneously covering the ion milled edge of the base $YBa_2Cu_3O_y$ film although there is no barrier deposition and annealing process. High-resolution electron microscopy images and energy dispersive x-ray analysis with a spot size of 1 nm indicates that the barrier is a Ba-based perovskite-like structure, $(Y_{1-x}Cu_x)BaO_y$ with $x<0.5$. A thin amorphous layer whose composition deviates from $YBa_2Cu_3O_y$ is formed due to the preferential sputtering of Cu. The amorphous layer recrystallizes into the nonequilibrium phase $(Y_{1-x}Cu_x)BaO_y$ after heating up to the deposition temperature. © *1999 American Institute of Physics.* [S0003-6951(99)02942-3]

Recently, interface-engineered $YBa_2Cu_3O_y$ (YBCO) junctions (IEJ), developed by Moeckly *et al.*[1,2] attracted much attention since the reproducible and manufacturable process of fabrication is quite suitable for digital circuit applications. In this process, no barrier deposition is carried out: the barrier is formed just by structural modification using ion bombardment and vacuum annealing. Recently, Satoh *et al.*[3] modified the process, in which the edge of the base YBCO film was formed by normal Ar ion milling and then the film was heated to a deposition temperature of about 700 °C in O_2 for a top YBCO layer deposition without being exposed to air. Their modified interface junctions (MIJ) also showed reproducible critical currents I_c, with a 1σ spread in I_c of less than 8% for 100 junctions.

In order to understand the formation mechanism of the barrier in these junctions, it is necessary to study the atomic structure and composition of the barrier by cross-sectional transmission electron microscopy (TEM), in particular, high-resolution electron microscopy (HREM) with nanometer-size element analysis. TEM investigations of Jia *et al.*[4] have shown that a homogeneous layer of a nonsuperconducting, cation-disordered cubic YBCO phase can recrystallize at an interface which is made amorphous by Ar ion-beam etching. Huang *et al.*[5] reported their TEM observations on the microstructures of IEJs and they concluded that the barrier is probably a cubic or pseudocubic YBCO variant. In this letter, the atomic structure and composition of the barrier in the MIJs are studied by TEM. We found that the barrier layer has a Ba-based perovskite-like atomic structure and composition, $(Y_{1-x}Cu_x)BaO_y$ with $x<0.5$.

The base electrode YBCO layer and insulation layer $(La_{0.3}Sr_{0.7})(Al_{0.65}Ta_{0.35})O_y$ (LaSrAlTaO) (or $SrTiO_3$) were deposited on a LaSrAlTaO (or $SrTiO_3$) substrate by KrF pulsed laser deposition (PLD). In order to avoid the ion-milled YBCO edge being exposed to air prior to the top film deposition, the insulation layer was first patterned by photoresist and then the YBCO edge was fabricated using the patterned insulation layer as a mask.[6] The 200 V Ar ion beam had an incidence angle of 30°–45° to the substrate surface. The fabricated edge was directly heated to about 700 °C without breaking vacuum for the further deposition of the top YBCO layer. This fabrication process has been described in detail elsewhere.[3,6] Cross-sectional specimens for TEM are mechanically ground by tripod directly down to a uniform thickness less than 10 μm and followed by an ion milling process. More details of the sample preparation can be found elsewhere.[7] Electron microscopy was performed with JEOL-4000EX and JEOL-2010 electron microscopes equipped with an Oxford energy dispersive x-ray (EDX) analysis system.

Two types of MIJs which exhibited resistively shunted junction (RSJ) and flux-flow (FF) type current–voltage ($I-V$) characteristics were selected to carry out TEM observations. The fabrication processes for these two types of junctions are similar; the only difference is that substrate and insulation layer are LaSrAlTaO for the RSJ type junction and $SrTiO_3$ for the FF type junction. Figure 1 shows a cross-sectional TEM image of a junction exhibiting RSJ $I-V$ characteristics. Although there was no barrier deposited, an interface can be clearly seen as a dark line in the low magnification image in the inset of Fig. 1. The structure of the barrier is different from YBCO, as indicated by white dashed lines in Fig. 1. CuO layers in YBCO films appear as white lines in this image, but these white lines cannot be observed in the barrier. The 2-nm-thick barrier covers the base YBCO edge homogeneously. The barrier consists of many small domains with a size of 2–3 nm. The orientations of different domains are more or less the same.

Figures 2(a) and 2(b) show HREM images of interfaces in MIJs exhibiting RSJ and FF type $I-V$ characteristics, re-

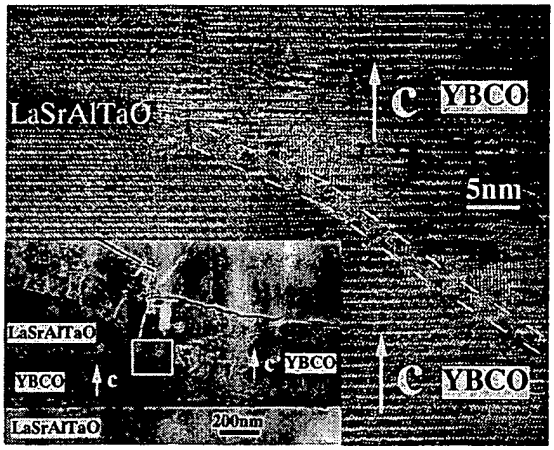

FIG. 1. Cross-sectional TEM image of a MIJ which had an RSJ type $I-V$ characteristic. The barrier (about 2 nm thick) is indicated by the dashed lines. Note the disappearance of CuO lines in the barrier. Inset is the low magnification image of junction.

spectively. In Fig. 2(a), although steps of height of 1.2 nm can be observed on the ion-milled surface, the 2-nm-thick barrier still fully covers the ion-milled surface. In contrast, one can see the continuity of CuO layers across the interface in the upper and lower part of Fig. 2(b). We believe this is the source of the FF type $I-V$ characteristics. The lattice parameters of the barriers in Fig. 2(a) and the circled regions in Fig. 2(b) are estimated to be about 4.1 Å along both the a and c axes of the YBCO film, using the lattice parameters of the YBCO film as an internal standard. In some areas of the barrier, one of lattice parameters along the c axis of the YBCO film is 4.3 Å, while the lattice parameter along the a axis of the YBCO film is still 4.1 Å as is shown in the inset of Fig. 2(a). Due to the slightly larger lattice parameter of the barrier compared to the YBCO films, one can observe misfit dislocations at the interfaces between the YBCO films and the barrier in Figs. 2(a) and 2(b).

High spatial resolution EDX analysis, with a probe size of about 1 nm, showed that the barriers in Figs. 2(a) and 2(b) have the same composition as each other but differ from YBCO, as shown in Fig. 3. The average atomic ratio of Y:Ba:Cu from 20 areas in the junction is 30:43:27. The EDX spectrum of the adjacent YBCO film (with known atomic ratio) was measured under the same conditions for internal calibration by the Cliff–Lorimer technique.[8] Compared to the YBCO film, Cu content is low in the barrier. This can be used to distinguish whether the electron beam is on the barrier or on the adjacent YBCO film by monitoring the intensity of the Cu peak during the EDX measurements. The atomic ratio Y:Ba in the barrier might be even higher, because some x rays from the adjacent YBCO may contribute to the EDX spectrum due to the comparable size of the electron beam and the barrier.

From the above results, one can see that the atomic structure and composition of the barrier material in MIJs exhibiting RSJ and FF type $I-V$ characteristics are similar. The only difference in microstructure is that the barrier fully covers the ion-milled edge in the RSJ type MIJs while the barrier does not fully cover the edge in the FF type MIJs. The RSJ type MIJs were made with LaSrAlTaO substrates and insulators and the existence of a small amount of La in

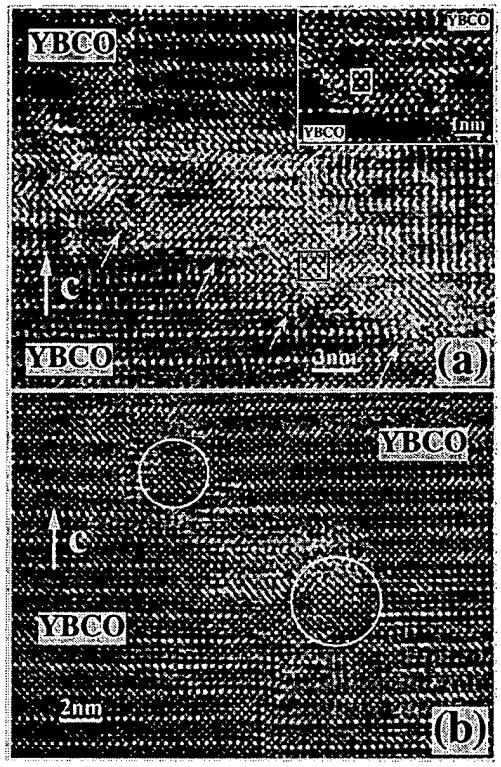

FIG. 2. HREM images of interfaces in MIJs exhibiting (a) RSJ type and (b) FF type $I-V$ characteristics. In most areas the lattice parameters of the barrier are 4.1×4.1 Å, while in some areas, one of lattice parameters along the c axis of YBCO film is 4.3 Å, as shown in the inset of (a). Steps on the bottom YBCO edge are indicated by small arrows in (a). Note that the continuity of CuO layers across the interface can be seen in the upper and lower part of (b).

the barrier due to redeposition during ion milling cannot be excluded. La may influence the coverage of the barrier, however, it was not found by EDX analysis. Another possible reason for the difference is that different substrates may slightly change the effective growth temperature, such that the coverage of the barrier is different. Recent experiments confirm that an RSJ type $I-V$ characteristic can also be obtained on a $SrTiO_3$ substrate with a $SrTiO_3$ insulation layer over a narrow range of deposition temperatures. The coverage of the barrier is more sensitive to the deposition temperature than La impurities.

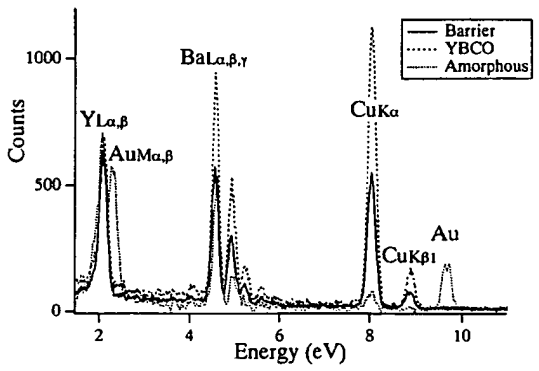

FIG. 3. EDX spectra of the barrier, the adjacent YBCO film, and the amorphous layer at circled regions in the inset of Fig. 4. The average atomic ratio of Y:Ba:Cu from 20 areas of the barrier is 30:43:27. The Cu content in the barrier is lower than that in the YBCO film.

From the HREM images and lattice parameters of the barrier shown in Fig. 2, the structure of the barrier is very possibly perovskite-like. All perovskite-like structures found in the YBCO system can be classified into two types according to the occupation rate at A or B sites in ABO_3. In the first type, Cu-based perovskite-like structures, Cu occupies the B site while Y and Ba occupy the A site. YBCO and cubic YBCO in which Y and Ba randomly occupy the A site are Cu-based perovskite-like structures.[4] The average lattice parameter of the Cu-based perovskite-like structure is about 3.9 Å. In the second type, Ba-based perovskite-like structures, Ba occupies the A site while Y and Cu occupy the B site. $(YCu_3)Ba_4O_y$ and $(Y_3Cu_5)Ba_8O_y$ are Ba-based perovskite-like structures.[9] The average lattice parameter of the Ba-based perovskite-like structure is about 4.1 Å, which is slightly larger than that of the Cu-based-like perovskite structure due to the large ionic radius of Ba. From HREM images, lattice parameters, and EDX analysis, one can conclude that the barrier is not a Cu-based, but a Ba-based perovskite-like structure. In all reported Ba-based perovskite-like phases, Y content is lower than Cu content. In the barrier it is the opposite, therefore, the barrier can be written as $(Y_{1-x}Cu_x)BaO_y$, with $x<0.5$. This phase does not exist in the thermal equilibrium YBCO phase diagram. Kwestroo *et al.*[10] reported a perovskite-like $Y_2Ba_2O_5$ phase with lattice parameters of $a=b=4.37$ Å, and $c=11.85$ Å. The lattice parameters of the primary perovskite-like unit cell are then $a=b=4.37$ Å and $c=3.95$ Å. The barrier which shows lattice parameters of 4.1 Å × 4.3 Å could be a $Y_2Ba_2O_5$ phase, which contains nearly no Cu. Hence, the observation of 4.1 Å × 4.3 Å in some areas may indicate an inhomogeneous distribution of Cu in the barrier. Y_2O_3 phase (face-centered cubic, $a=10.5$ Å) can be ruled out by the lattice parameters and the ratio of lattice parameters along the a and c axes of the YBCO film.[11]

In order to understand the composition change of the barrier which happened during the ion milling or heating process, we covered a freshly milled sample with an *in situ* Au layer. The Au layer was *in situ* deposited at room temperature by (PLD) to protect the surface from chemical or TEM sample preparation damage. Both substrate and insulation layer are $SrTiO_3$. Figure 4 shows a cross-sectional TEM image of the test sample. The thickness of the thin amorphous layer is about 1 nm, which is thinner than the barrier shown in Fig. 2(a). Note that the interface between the YBCO and the amorphous layer is quite smooth, as shown in Fig. 4, while the interface between the crystalline barrier layer and the bottom YBCO film shown in Fig. 2(a) is stepped. Both indicate a possible reaction might have occurred between the amorphous layer and the surface of the crystalline YBCO film during the heating process. EDX analysis on the amorphous layer shows a composition similar to the crystallized barrier, i.e., the Cu content is low. However, the exact composition is extremely difficult to estimate because x-ray scattering from the adjacent crystalline YBCO film cannot be avoided. At the bottom of the ion-milled edge, there is a small area in which only amorphous material exists between the Au and the $SrTiO_3$ substrate, shown in the inset of Fig. 4. EDX analysis at the spots indicated by circles in the inset of Fig. 4 shows that the atomic ratio of Y to Ba is close to 1, and the Cu content is nearly zero. So, we conclude that the composition deviation from YBCO is due to the preferential sputtering of Cu. This is consistent with the reported results that the sputtering yield of Y is about three times of that of Cu.[12–14]

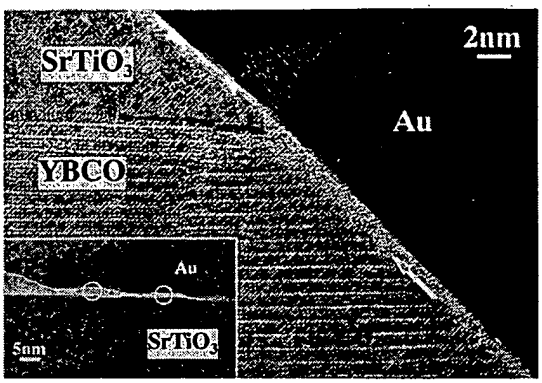

FIG. 4. Cross-sectional TEM image of a test sample in which the fresh ion-milled edge was covered *in situ* by an Au layer. A thin amorphous layer of about 1 nm can be seen on the YBCO edge. EDX measurements at the bottom of the ramp (circled regions) show that the Cu content in the amorphous region is nearly zero.

In summary, we propose a formation mechanism of the barrier in the modified interface junctions which have no intentional barrier deposition or annealing process. A thin amorphous layer is formed on the edge of the ion-milled YBCO film whose composition deviates from YBCO due to the preferential sputtering of Cu. The barrier recrystallizes during the heating of the sample to the deposition temperature. The crystalline barrier is identified as a Ba-based perovskite-like structure, $(Y_{1-x}Cu_x)BaO_y$ with $x<0.5$.

This work was supported by the New Energy and Industrial Technology Development Organization (NEDO).

[1] B. H. Moeckly and K. Char, Appl. Phys. Lett. **71**, 2526 (1997).
[2] B. H. Moeckly, K. Char, Y. Huang, and K. L. Merkle, IEEE Trans. Appl. Supercond. (to be published).
[3] T. Satoh, M. Hidaka, and S. Tahara, IEEE Trans. Appl. Supercond. (to be published).
[4] C. L. Jia, M. I. Faley, U. Poppe, and K. Urban, Appl. Phys. Lett. **67**, 3635 (1995).
[5] Y. Huang, K. L. Merkle, B. M. Moeckly, and K. Char, Physica C **314**, 36 (1999).
[6] T. Satoh, M. Hidaka, and S. Tahara, IEEE Trans. Appl. Supercond. **7**, 3001 (1997).
[7] J. G. Wen, in *From the Macroscopic to the Atomic Scale: Characterization of High-T_c Superconductors by Electron Microscopy*, edited by S. J. Pennycook and N. B. Browning (Cambridge University Press, Cambridge).
[8] J. I. Goldstein, in *Introduction to Analytical Electron Microscopy*, edited by J. J. Hren, J. I. Goldstein, and D. C. Joy (New York, 1979).
[9] D. M. De Leeuw, C. A. H. A. Mutsaers, C. Langereis, H. C. A. Smoorenburg, and P. J. Rommers, Physica C **152**, 39 (1988).
[10] W. Kwestroo, H. A. M. van Hal, and C. Langereis, Mater. Res. Bull. **9**, 1631 (1974).
[11] A. Catana, R. F. Broom, J. G. Bendnorz, J. Mannhart, and D. G. Schlom, Appl. Phys. Lett. **60**, 1016 (1992).
[12] G. Carter and J. S. Colligon, in *Ion Bombardment of Solids* (Heinemann, London, 1968).
[13] N. Laegreid and G. K. Wehner, J. Appl. Phys. **32**, 365 (1961).
[14] D. Rosenburg and G. K. Wehner, J. Appl. Phys. **33**, 1842 (1962).